# ATP-driven Spatial Organization of a Carbon-fixing Organelle in Cyanobacteria

by

Pusparanee Binti Hakim

A dissertation submitted in partial fulfillment
of the requirements for the degree of
Doctor of Philosophy
(Molecular, Cellular and Developmental Biology)
in The University of Michigan
2022

Doctoral Committee:

Assistant Professor Anthony G. Vecchiarelli, Chair
Professor Emeritus Robert A. Bender
Professor Julie S. Biteen
Professor Matthew R. Chapman

Pusparanee binti Hakim

annhakim@umich.edu

ORCID ID: 0000-0002-9018-8179

*To my husband, Hafiz Rothi and our daughters, Iris and Irene.*

*And to the loving memory of my late father, Hakim Ibrahim.*

## ACKNOWLEDGEMENTS

*If I have seen further, it is by standing upon the shoulder of giants* – Sir Isaac Newton

I would like to express my deepest gratitude to my extraordinary mentor, Anthony Vecchiarelli for his unwavering support, thoughtful guidance, and pearls of wisdom from the day I joined his lab. He has inspired me to remain curious, enthusiastic and true to myself during my scientific journey. I will always cherish the time I am fortunate enough to spend under his tutelage. I would also like to thank the best colleagues a Ph. D student can ask for: Lisa Tran, Joshua MacCready, Joe Basalla, Rees Rillema, Chris Azaldegui, Y Hoang, Claudia Mak and everyone else I have had the pleasure to work alongside with in the Vecchiarelli lab. I will always keep you all in my heart. And to current and past members of the Chapman and Miller labs: thank you for being such awesome and helpful science neighbours. Special shoutout to Ann Miller, Maggie Gardner, Neha Jain, Elizabeth Gichana, Janet Price, Hema Swathi, Saranya Varadarajan, Shahana Chumki and Jennifer Landino for being outstanding colleagues and even better friends.

I thank my committee members, Robert Bender, Julie Biteen and Matthew Chapman, for all their helpful advice and critical review of my research and dissertation, as well as the support I needed to make it to the finish line. I want to express my gratitude to all the program and departmental administrators that have always strived to make things easy for us graduate students.

Finally, my most sincere appreciation to all my family and cohort friends, especially Peach Arines, for being the people I can lean on during the ups and downs of my Ph. D journey. To my husband, Hafiz Rothi, and our daughters, Iris Sophia and Irene Nadya: you are the reason I am still standing here when I have every reason to fall apart and crumble. Thank you for being my constant source of strength, joy and love.

## TABLE OF CONTENTS

## LIST OF FIGURES

## LIST OF TABLES

**Table**

## LIST OF ABBREVIATIONS

| | |
|---|---|
| Δ | Deletion |
| ATP | Adenosine-5'-Triphosphate |
| B2H | Bacterial Two-Hybrid Assay |
| BG-11 | Blue-Green Medium |
| BMC | Bacterial microcompartment |
| C-terminal | Carboxy terminal |
| DNA | Deoxyribonucleic acid |
| IPTG | Isopropyl-beta-D-thiogalactopyranoside |
| McdA | Maintenance of Carboxysome Distribution A |
| McdB | Maintenance of Carboxysome Distribution B |
| mNG | monomericNeonGreen |
| mTQ | monomericTurquoise2 |
| N-terminal | Amino terminal |
| ParA | Partitioning protein A |
| ParB | Partitioning protein B |
| PBS | Phosphate-buffered solution |
| PCC | Pearson's Correlation Coefficient |
| SopA | Segregation of Plasmids Protein A |
| SopB | Segregation of Plasmids Protein B |
| SopC | Segregation of Plasmids Protein C |
| TRIFM | Total Internal Reflection Fluorescence Microscopy |

## ABSTRACT

Metabolic compartmentalization contributes to the spatiotemporal modulation of biochemical reactions within eukaryotic and prokaryotic cells. Bacterial microcompartments (BMCs) are widespread, self-assembling proteinaceous organelles that function by physically sequestering key metabolic enzymes essential in carbon source utilization, microbial ecology, and pathogenesis. A well-studied anabolic BMC, called the carboxysome, serves as a critical carbon-fixing organelle in cyanobacteria and many chemoautotrophs. Carboxysomes play a central role in the $CO_2$-concentrating mechanism of these bacteria by compartmentalizing central photosynthetic enzymes, effectively increasing their efficiency, and preventing the occurrence of wasteful side reactions. The basic architecture of carboxysomes consists of multi-protein subunits that form a selectively permeable diffusion barrier, allowing gaseous and metabolic exchanges to take place. While eukaryotic organelles use cytoskeletal highways for their cellular organization, little is known about how bacteria spatially regulate their protein-based organelles for proper segregation, homeostasis, inheritance, and maintenance in a cell population.

Fully assembled, mature carboxysomes are aligned equidistantly along the cell length to ensure faithful inheritance. Previous studies have implicated an important ParA-like protein we termed Maintenance of carboxysome distribution A (McdA) as a critical component in equal spacing of carboxysomes. McdA forms oscillating protein gradients over the nucleoid in response to its carboxysome-localized partner protein, McdB. Prior to my work, the mechanism driving McdA oscillations and carboxysome positioning by the McdAB system was unknown. To address this gap in knowledge I first examined the biochemical interaction between the two-component McdAB system and the nucleoid. I then dissected how the McdA ATPase cycle mediates the protein's dynamic oscillatory patterning and carboxysome positioning. Finally, I demonstrate how multi-generational live-cell imaging of *S. elongatus* can serve as an indispensable tool in studying the mechanistic workings of carboxysome dynamics and inheritance. Together, this thesis work provides the first steps towards an understanding of the ATP-driven molecular mechanisms governing organelle trafficking in bacteria.

# CHAPTER I

# Introduction

## 1.1 Bacterial Microcompartments

### 1.1.1 Compartmentalization in bacteria

Subcellular compartmentalization brings physiological order and efficiency to metabolic reactions in the crowded environment of a cell's cytoplasm. The long-standing perception that bacterial cells are unstructured sacs containing homogenous suspensions of protein and DNA is no longer relevant [1] [2]. Analogous to the membrane-bound organelles of eukaryotes, bacteria have an array of protein-based intracellular compartments that allow for the spatiotemporal regulation of complex and dynamic cellular processes [3].

A major form of compartmentalization in bacteria is through the use of self-assembling protein-based complexes known as bacterial microcompartments (BMCs). Once considered a rarity, BMCs have now been bioinformatically identified across 29 bacterial phyla, through the identification of well-conserved BMC shell protein sequences [4]. BMCs are analogous to eukaryotic organelles; they sequester biochemical reactions in a semipermeable barrier to improve enzymatic efficacy, spatially separate toxic intermediate metabolites, and/or minimize wasteful side reactions. Unlike the phospholipid bilayers that form eukaryotic organelle membrane systems, BMC outer shells consist of homologous protein paralog subunits that self-assemble to form an

icosahedral structure ranging from 100 – 500 nm in size, reminiscent of viral capsids when visualized microscopically [5], [6]. To date, these prokaryotic organelles are implicated in eight catabolic and one anabolic processes [4], [7], [8]. Collectively, BMCs allow for the spatial sequestration of biochemical reactions that would be metabolically expensive or significantly less efficient without compartmentalization.

### 1.1.2 BMCs are functionally diverse

Despite being structurally similar and phylogenetically related, BMCs encapsulate a wide variety of enzymes and subsequently, possess diverse biological functions to enable their bacterial host survival in distinct ecological niches [7]. The first BMC to be identified and characterized is the anabolic carboxysome found in photoautotrophic cyanobacteria and many chemoautotrophs [9], [10]. Catabolic BMCs, also known as metabolosomes, are prevalent in pathogenic and commensal bacteria of the human gut. Metabolosomes act to sequester, degrade and detoxify harmful reactive aldehyde intermediates [11]–[13]. Alternative carbon sources that are oxidized by metabolosomes are ethanolamine [12], propanediol [14]–[16], 1-amino-2-propanol [17], [18], fucose and rhamnose [19], [20] and choline [21], [22]. The discovery of novel and uncharacterized BMCs is rapidly progressing as a result of expanding bacterial genome and metagenome databases over the past decade [4], [7], suggesting the indispensable and robust nature of BMCs in providing a biological advantage to pathogenic bacteria in niche environments [11]. Despite their ubiquity and central roles in bacterial metabolism, it is completely unknown how metabolosomes assemble and spatially organize in the cell.

## 1.2 The Carboxysome: a model for BMC biology

### 1.2.1 The Carboxysome is a Carbon Concentrating Mechanism for Microbes

The carboxysome is the only anabolic BMC identified so far and found across cyanobacteria and many chemoautotrophic bacteria [8], [10], [23]. Two key enzymes in photosynthesis, ribulose-1,5-bisphoshate carboxylase/oxygenase (Rubisco) and carbonic anhydrase (CA) are encapsulated in the carboxysomal lumen as a primary carbon concentrating mechanism (CCM) for these microbes (Fig. 1.1). Rubisco is the most abundant enzyme in nature [24], and when using $CO_2$ as its substrate, Rubisco catalyzes the carbon-fixation step in the Calvin-Benson-Bassham cycle.

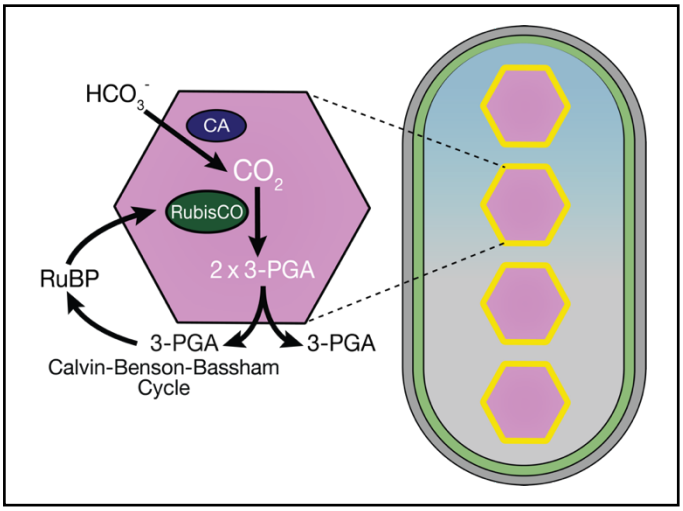


Figure 1.1: **Carboxysomes play a central role in the carbon concentrating mechanism (CCM) of cyanobacteria**. (Left) Schematic of localized enzymatic reactions occurring inside a carboxysome. $HCO_3^-$: bicarbonate ion; $CO_2$: carbon dioxide; RuBP: ribulose-1,5-bisphosphate; PGA: 3-phosphoglycerate. (Right) Carboxysomes are present in cyanobacterial cytoplasmic region.

However, Rubisco is an inefficient enzyme and has the ability to also bind $O_2$. CA catalyzes the conversion of diffuse bicarbonate into $CO_2$. The presence of CA in the vicinity of the kinetically inefficient bacterial Rubisco creates a $CO_2$-rich microenvironment within carboxysomes that ensures carboxylation of Ribulose-1,5-bisphosphate is favored over the

undesired side-reaction called photorespiration when $O_2$ is used as the substrate [25]. With this CCM mechanism, carboxysomes are responsible for almost half of global carbon-fixation through atmospheric $CO_2$ assimilation for photosynthesis and biomass production [26], [27]. Despite the importance of carboxysomes to the global carbon cycle, the mechanisms underlying their subcellular organization remain unclear.

### 1.2.2 There are two structurally- and phyletically-distinct types of carboxysomes

There are two phyletically distinct types of carboxysomes based on the type of Rubisco encapsulated; α-carboxysomes encapsulate Rubisco form 1A while β-carboxysomes possess Rubisco form 1B [28] [29]. Cyanobacteria can harbor either α- or β-carboxysomes, while carbon-fixing proteobacteria and some actinobacteria contain α-carboxysomes exclusively. It is believed that α-carboxysomes in cyanobacteria were initially obtained from proteobacteria via horizontal gene transfer, resulting in two distinct lineages of α-cyanobacteria with α-carboxysomes and β-cyanobacteria with β-carboxysomes [10].

The two evolutionary divergent α- and β-carboxysomes share similar biological functions but distinct genomic and structural assemblies. The obligate photoautotroph *Synechococcus elongatus* PCC 7942 (henceforth, *S. elongatus*) is the long-standing model bacterium for understanding β-carboxysome biology and the chemoautotrophic proteobacterium *Halothiobacillus neapolitanus* c2 (hereafter, *H. neapolitanus*) is the model organism for studying α-carboxysomes. In both cases, the genes encoding for the encapsulated enzymes and carboxysome shell components are generally grouped together in a clustered operon [4]. In *S. elongatus*, the central *ccm* operon encodes the genes encoding carboxysome components CcmK2,

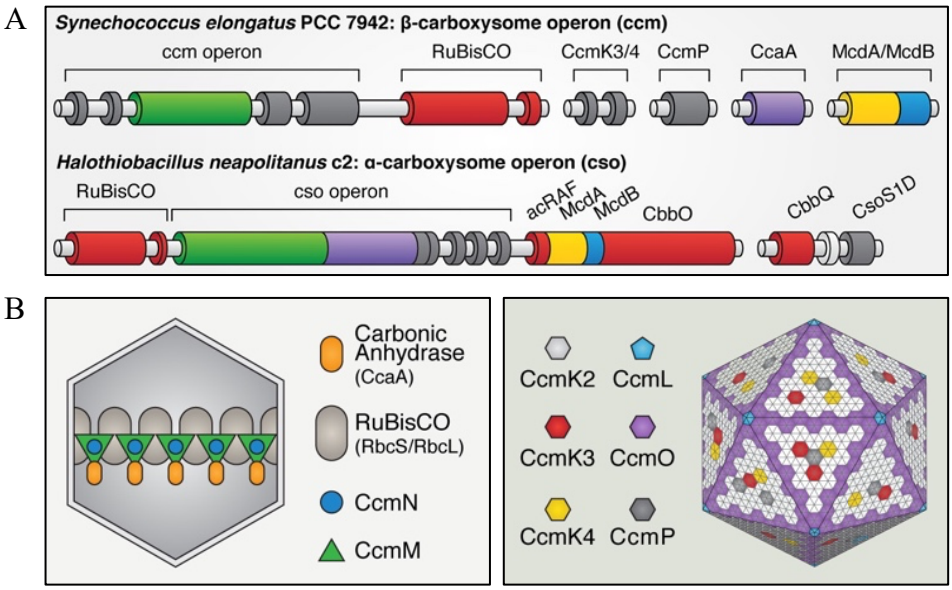


Figure 1.2: **Genomic and structural components of α- and β-carboxysomes.** A. Genomic arrangement of model α- and β-carboxysome operons. Dark gray: shell component; red, Rubisco-related component: green, Rubisco aggregating component: purple, carbonic anhydrase: yellow: McdA; blue: McdB. B. (Left) Schematic depiction of the internal and (right) external shell components of the cyanobacterial β-carboxysome in *S. elongatus*. Panel A from [30] and B from [31] (for both: https://creativecommons.org/licenses/by/4.0/).

CcmL, CcmM, CcmN and CcmO. This *ccm* operon is located upstream of the *rbcL* and *rbcS* genes encoding for the large and small units of Rubisco, respectively (Fig 1.2A). Four other distant loci encode for other shell proteins CcmK3, CcmK4, CcmP and the essential carboxysome enzyme carbonic anhydrase. β-carboxysomes have been shown to assemble from the inside-out – with the interior assembly initiated by CcmM-mediated aggregation of Rubisco and CA to form "procarboxysomes" [30], [31]. Next, CcmN interacts with CcmM and functions to recruit the hexameric shell protein CcmK2 to the procarboxysome cluster. CcmK2 forms the major facets of the carboxysome icosahedral shell (Fig. 1.2B) [32], [33]. CcmO has been thought to form flattened trimers arranged in tandem to form "zipperlike" structures interfacing with and sealing the edges of CcmK2 hexameric facets [32]. The pseudohexameric CcmP, along with heterohexamers CcmK3 and CcmK4, are postulated to function in facilitating metabolite movements between the

carboxysome lumen and the cyanobacterial cytoplasm, subsequently altering carboxysome permeability throughout the day [34]–[36]. Finally, the pentagonal pentameric CcmL caps the icosahedral vertices and facilitate budding of new carboxysomes [37]–[39].

Like the β-carboxysome operon, the core α-carboxysome *cso* (CarboxySOme) operon is also arranged adjacent to the large (*cbbL*) and small (*cbbS*) subunits of Rubisco. The seven α-carboxysome genes (*csoS2*, *csoS3*, *csoS4A*, *csoS4B, csoS1A, csoS1B, csoS1C*) are arranged in tandem in this core operon meanwhile two additional satellite genes (*csoS1D* and *cbbQ*) are located elsewhere in the genome (Fig 1.2A). In contrast to β-carboxysomes, the observation of partially assembled α-carboxysomes via electron cryotomography suggests that the encapsulated enzyme and shell proteins can be assembled concomitantly [40]. The shell protein CsoS2 is functionally analogous to CcmM and CcmN where it tethers encapsulated Rubisco and *csoS3*-encoded carbonic anhydrase to the rest of the assembled α-carboxysome shell [41], [42]. The hexameric shell proteins CsoS1A, CsoS1B and CsoS1C assemble to form icosahedral facets that interact with CsoS2, akin to the roles played by CcmK2 in β-carboxysomes [42]–[44]. Lastly, Cso1D assembles into two trimer subunits that form gated pores, analogous to CcmP in β-carboxysomes [45]. Overall, although phyletically distinct, both α- and β-carboxysomes share a high degree of similarity in their structural assembly and function, which is maximizing the carbon fixation rate of Rubisco through reaction encapsulation.

### 1.2.3 *S. elongatus* is the model organism for the study of β-carboxysomes

Cyanobacteria are the only group of prokaryotes capable of performing oxygenic photosynthesis and were proposed to be the main drivers of arguably the most pivotal biological occurrence in Earth's history, the Great Oxidation Event, that took place around 2.4 billion years

ago [46]. Along with other biogeochemical processes, oxygenic photosynthesis led to the rapid increase in atmospheric and surface-ocean oxygen levels during this period, causing permanent biospheric changes that allowed for the emergence and evolution of complex life forms [47]–[49]. In present day, cyanobacteria are responsible for roughly a third of global oceanic carbon fixation [50].

The model cyanobacterium *S. elongatus* is a rod-shaped, freshwater-dwelling obligate photoautotroph that has been the extensively studied as a model organism for the processes of carbon fixation and photosynthesis, as well as prokaryotic circadian rhythm research. Due to its relatively large cellular size and its distinctive ordered positioning of carboxysomes in the cell, *S. elongatus* is an excellent subject for microscopic investigations into the subcellular organization of carboxysomes [51]–[53]. Its genetic tractability and natural competence for exogenous DNA uptake allow for relatively simple genomic manipulation and mutagenesis [54]. Finally, *S. elongatus* has the most comprehensive and well-established gene and protein information databases relative to other cyanobacteria, making it an attractive model organism for the study of carboxysomes.

### 1.2.4 Carboxysomes for synthetic biology engineering and applications

Due to its versatility, modularity, and catalytic efficiency, carboxysomes have inspired synthetic biologists to emulate their design for carbon assimilation bioengineering into faster-growing non-photosynthetic bacteria and terrestrial plants. Successful reconstitution of *H. neapolitanus* carbon concentrating machinery and mechanism in *E. coli* signifies a breakthrough in the ongoing effort to introduce carboxysomes into tractable heterologous hosts [55]. Earlier attempts to introduce

similar synthetic carboxysome operons in the biotechnological workhorse Gram-positive *Corynebacterium glutamicum* resulted in functional but structurally altered carboxysomes [56].

As β-carboxysomes encapsulate Rubisco that is more biologically similar to the ones found in terrestrial plants, many groups have focused on introducing β-carboxysomes into plant chloroplasts to enhance crop yields [57]. Indeed, cyanobacterial Rubisco expressed in tobacco chloroplasts appear to be encapsulated in carboxysome-like structures and retained their high carbon-fixation activities [57]–[59]. But the engineered plants displayed severe growth deficiencies and a high carbon dioxide requirement. Intriguingly, electron micrographs found carboxysomes aggregated together in only a subset of chloroplasts, whereas in their original host, *S. elongatus*, carboxysomes are faithfully distributed down the cell length. This underscores the many challenges researchers are still overcoming to successfully employ cyanobacterial Rubisco to supercharge photosynthesis in crop plants [5].

To maximize the functionality of heterologous carboxysomes introduced in terrestrial chloroplasts, one would have to design vectors that would express the multi-operon carboxysomal genes at the correct stoichiometry without compromising shell protein assembly and/or ultrastructure as well as Rubisco loading into the engineered carboxysome shells [60]. Additionally, faithful inheritance and maintenance of carboxysomes when expressed in heterologous hosts has not been achieved. To date, all heterologously expressed carboxysomes form aggregates or clusters in the stroma of chloroplasts, and therefore, are not distributed and inherited equally during plastid division. The key to overcoming these challenges in heterologous carboxysome engineering necessitate a more thorough understanding of carboxysome assembly, stoichiometry, trafficking and positioning within their native hosts.

## 1.3 Subcellular organization and positioning of carboxysomes

In *S. elongatus*, β-carboxysomes are first assembled at the cell pole when shell proteins encapsulate a cluster of soluble Rubisco to form the procarboxysome [31]. Fully assembled, mature β-carboxysomes bud off this polar cluster and move down the cell length; an event that has been proposed to take place to ensure faithful inheritance of these organelles [10], [23], [52]. Depending on the maturity of a cyanobacterial cell, between 3-6 β-carboxysomes are aligned equidistant along the cell length (Fig. 1.3A, second panel). This spatial arrangement, as well as carboxysome size, composition, and cellular dynamics, is delicately modulated by variations in $CO_2$ levels, environmental temperature, and light intensity and wavelength that a growing cyanobacterial cell is subjected to during growth [61]–[63]. The mechanism behind how these external cues regulate β-carboxysome homeostasis remains undetermined. In contrast to *S. elongatus* cells, *H. neapolitanus* cells harbor anywhere from 4 to 18 α-carboxysomes based on observations via electron microscopy [9], [10], [64]–[66]. Despite the amount of carboxysomes a small *H. neapolitanus* cell can carry in its cytoplasmic space, these α-carboxysomes are also found to distribute down the cell length (Fig. 1.3B) [40], [67], [68]. These observations suggest that these protein-based organelles are being actively positioned in the cell.

The uniform cellular distribution of carboxysomes is reminiscent of the reported arrangement bacterial plasmids assume when being actively partitioned by ParA family of ATPases [69]. A member of the protein family, termed Maintenance of carboxysome distribution protein A (McdA), has been implicated in spatially organizing both α- [67] and β-carboxysomes [51], [52]. ParA ATPases employ a deviant Walker A box motif as an ATP-binding pocket and have been extensively studied for their roles in segregating and positioning genetic cargos, such as bacterial chromosomes and plasmids [70], [71]. Additionally, ParA family members have been

implicated in positioning functionally diverse protein assemblies, such as the divisome [72]–[74], flagella [75], [76] and chemotaxis cluster [77], [78]. Collectively, these ParA family ATPases play significant roles in the organization and maintenance of cellular components involved in various biological processes. Further investigations into how this newly identified ParA family ATPase member confer proper carboxysome positioning and distribution will provide a basis for mechanistic understanding on how metabolic processes are spatially regulated within a bacterial cell.

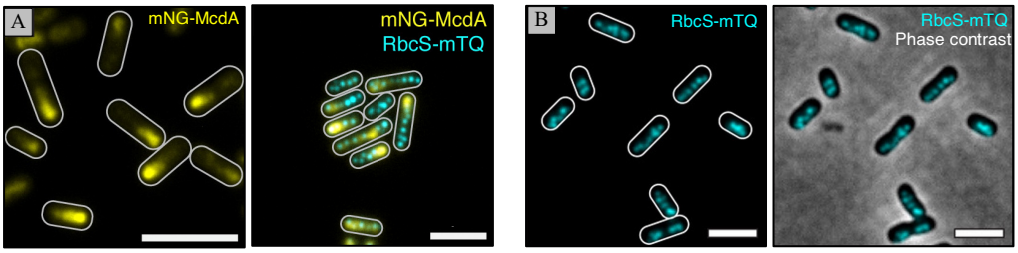


Figure 1.3: **α- and β-carboxysomes are distributed along the cell length**. Fluorescent β-carboxysomes (A) and α-carboxysomes (B) can be observed to be linearly arranged down the longitudinal axis of *S. elongatus* and *H. neapolitanus* cells, respectively. Scale bars in panel A: 5 µm. Scale bars in panel B: 2 µm. Panel A from [31] and B from [68] (for both: https://creativecommons.org/licenses/by/4.0/).

### 1.3.1 Par system

To ensure faithful genetic inheritance, bacteria must properly segregate their genetic materials prior to cytokinesis. In prokaryotes, most chromosomes and low-copy plasmids are actively segregated by the ubiquitous Par (partition) system. Despite being the most prevalent and well-studied DNA segregation system in bacteria, the mechanism remains a much-debated topic.

Partition systems consist of two proteins, one of which is a member of the ParA/MinD family of ATPases called ParA. ParA ATPases use ATP-hydrolysis to drive the segregation, transport, and positioning of replicated copies of chromosomes or low-copy plasmids to opposite cell halves, thus ensuring faithful inheritance of these genetic cargos after cell division [70], [71], [79]. Cytoplasmic ParA monomers bind ATP and form the ATP-sandwich dimer [80], [81]. The

ParA dimer then undergoes an ATP-specific conformational change that licenses binding to nonspecific DNA (nsDNA) *in vitro*, which equates to binding the bacterial nucleoid *in vivo* [82]–[84]. In its DNA-binding form, ParA can robustly interact with its partner protein, partition protein B (ParB) [85]. ParB dimers site-specifically load onto the plasmid, or chromosome, to be partitioned via specific binding to a centromere-like site, typically called *parS* [70], [79]. ParB dimers spread from *parS* onto flanking DNA to form a massive multimeric nucleoprotein complex [86], [87]. This ParB-*parS* complex can interact with ParA dimers and stimulate its ATPase activity, which is coupled to ParA release from the nucleoid [88]–[90]. The resulting ParA depletion zone that forms around the ParB-*parS* [85]complex also provides a ParA concentration gradient on the nucleoid. In this Brownian-ratchet mechanism, ParB-*parS* complexes on newly replicated chromosomes or plasmids are bidirectionally segregated to opposing cell-halves as they chase higher concentrations of ParA along the nucleoid in opposing directions [84], [91]. The emergent ParA oscillatory dynamics can be observed as plasmids are transported, or surf along the nucleoid towards the quarter regions of the cells.

Early reports of cellular ParA dynamics described the protein as a nucleoid-spanning cytoskeletal filament network where ATP-bound ParA filaments depolymerize upon contact with ParB-associated plasmid, causing the cargo to be "pulled" towards the bacterial cell pole [92]–[96]. This model was mainly based on visual observations of fluorescently labeled ParA proteins and their tendency to form linear filaments *in vitro*. But mounting evidence from *in vivo* super resolution microscopy [97], [98], crystallography [81], *in vitro* reconstitution experiments [88], [99], [100] and mathematical modelling [97], [98], [101], [102] have challenged the filament-based theory and provided data that supports the proposed Brownian-ratchet motion as the underlying mechanism for ParAB-driven DNA segregation.

Reconstitution of the F plasmid partition system as a proxy to study the molecular mechanism of ParA-based DNA segregation provided some of the strongest data for the Brownian-ratchet, and against filament-based models. Vecchiarelli and colleagues [91], [99] introduced magnetic beads coated with *sopC* DNA (the "*parS*" of F plasmid), fluorescent SopA (or ParA) and SopB (or ParB), and ATP into a DNA-carpeted flow-cell, which acted as a nucleoid biomimetic. This cell-free setup was then visualized using Total Internal Reflection Fluorescent Microscopy (TIRFM). SopB coated the *sopC*-beads and SopA coated the non-specific DNA carpet; observations that are consistent with SopB forming large foci on F plasmid and SopA coating the nucleoid *in vivo*. Using a magnetic force applied perpendicular to the flow cell, the SopB-bound beads were pulled up and spatially confined to the DNA carpet. Intriguingly, SopA-depleted zones started to form on the DNA carpet in the vicinity of the magnetic beads. Strikingly, many beads were found within the SopA concentration gradient on the perimeter of a SopA depletion zone, and these beads moved in a directed and persistent manner. Importantly, there were no discernible SopA filaments observed. Instead, SopA was distributed homogenously across the DNA carpet.

These observations led the researchers to the possibility that ParA-based plasmid segregation was mediated by self-organizing protein gradients [103]–[106]. This ParA-mediated plasmid segregation mechanism was termed the burnt-bridge Brownian ratchet, due to the inability of SopB-bound beads to retrace its course and move back into SopA depletion zones [107]. Collectively, these experiments demonstrated that the directed and persistent movement of genetic cargo can be mediated by an asymmetric ParA distribution on the nucleoid via a Brownian ratchet mechanism. A deep understanding of the Brownian ratchet-based model for segregation of genetic cargo by ParA family ATPases is pivotal in informing us whether a similar principle can be used

to explain the directed motion and intracellular positioning of large, mesoscale proteinaceous assemblies such as cyanobacterial carboxysomes.

### 1.3.2 McdAB system

In 2010, a pivotal study used fluorescent carboxysomes to show that these protein assemblies are linearly arranged across the long axis of *S. elongatus* cells [52]. This equidistant positioning is believed to ensure an equal complement of carboxysomes is inherited to both daughter cells, which is important because carboxysome number correlates with cyanobacterial fitness under ambient $CO_2$ [10], [23], [52]. Carboxysome distribution and inheritance was found to be dependent upon an oscillating ParA-type ATPase, we later termed McdA, which we have shown to be responsible for spatially positioning both α- and β-carboxysomes (Fig. 1.4A, Movie 1.1) [51], [67]. Similar to ParA ATPases requiring ParB in fulfilling its role in positioning their cognate genetic cargos, we identified a small protein encoded downstream of *mcdA* in its operon called McdB [51], [67]. McdB proteins colocalize with β-carboxysomes in *S. elongatus* (Fig. 1.4B) and α-carboxysomes in *H. neapolitanus* (Fig. 1.4C), and both are essential for proper carboxysome positioning in their respective hosts.

Prior to my work, the McdAB carboxysome positioning system was only studied *in vivo* [51]. Fluorescent McdA in *S. elongatus* was found to display pole-to-pole oscillatory dynamics along the nucleoid, and these dynamics were dependent on McdB and carboxysome copy number [51], [52]. In the absence of either McdA or McdB, β-carboxysomes were found to cluster together, either from their natural tendency to do so in the absence of an "anti-aggregation" system or from incomplete segregation following carboxysome biogenesis and/or budding [51]. When McdA was

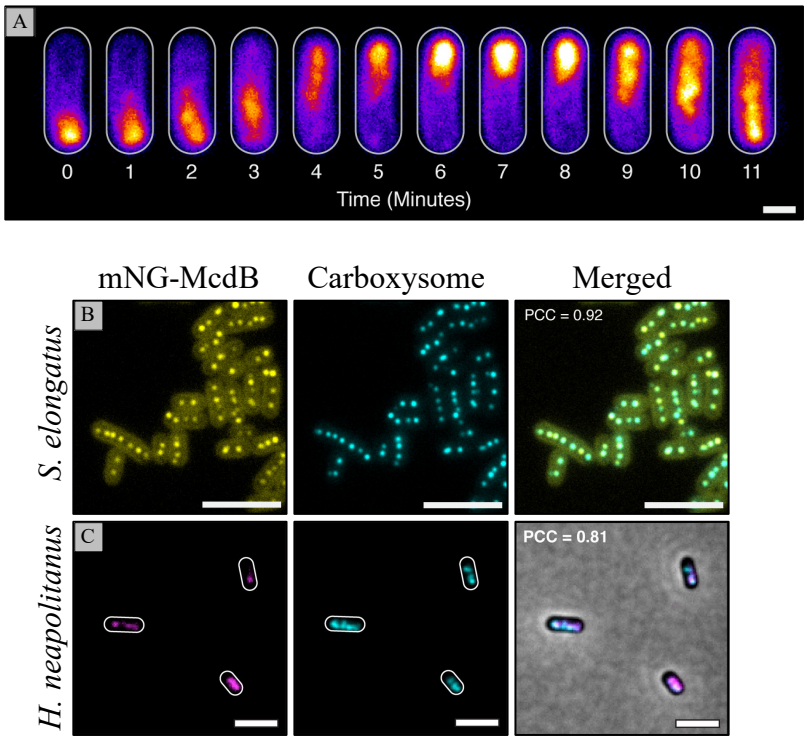


Figure 1.4: **The McdAB system is responsible for positioning carboxysomes in *S. elongatus* and *H. neapolitanus***. A. mNG-McdA waves oscillate predominantly along the central axis of the cell. Scale bar: 1 µm. Fluorescent signal for McdB in *S. elongatus* (B) and *H. neapolitanus* (C) colocalize with a fluorescent carboxysome marker. Scale bar in panel B: 5 µm. Scale bars in panel C: 2 µm. Panel A and B from [31] meanwhile Panel C is from [68]. (for both: https://creativecommons.org/licenses/by/4.0/).

overexpressed, carboxysomes assumed a more rounded phenotype with misshaped edges. When McdB was overexpressed carboxysomes grew larger, and often formed bar-shaped structures that extended up to half of the cell length. This was an unexpected finding for a system that uses a ParA-like ATPase. ParA-based DNA segregation systems only regulate segregation and positioning of its genetic cargo. But for protein-based cargos, the data suggests that ParA-type ATPases involved in bacterial organelle trafficking can potentially function in cargo size and ultrastructure regulation.

α- and β-carboxysome aggregation does not result in a high $CO_2$-requiring phenotype [51], [67], suggesting that McdAB-based distribution of carboxysomes is not essential for cyanobacterial growth under the optimal growth conditions implemented in a lab setting. However, *S. elongatus* cells have recently been shown to display slower growth rates, asymmetric cell division, cell elongation, and increased cellular levels of Rubisco in the absence of the McdAB system [63]. Intriguingly, deletion of McdB resulted in more severe mutant phenotypes compared to that of the Δ*mcdA* strain, which suggests that McdB plays a key role in carbon fixation by carboxysomes, independent of its role in carboxysome positioning with its partner protein McdA.

To date, the McdAB system has only been studied experimentally in *S. elongatus* and *H. neapolitanus* [51], [67]. However, bioinformatic analysis of more than 700 bacterial genomes have found that McdAB systems are widespread among β-cyanobacteria and α-carboxysome-containing proteobacteria [51], [67], [108]. The prevalence of this carboxysome positioning system across the bacterial world highlights the need for a mechanistic understanding of carboxysome trafficking and homeostasis. These findings will also have far-reaching implications in understanding ParA-based organization of other mesoscale assemblies in prokaryotes as well as in utilizing these bacterial organelles for synthetic biology applications.

## 1.4 Dissertation Goals

The study of carboxysome self-assembly and spatial organization in the cell is still in its infancy. Most carboxysome researchers are largely focused on the biogenesis and synthetic application of this protein-based microcompartment. The goal of my dissertation is to elucidate the ATP-driven molecular mechanism governing the spatial organization of carboxysomes in bacterial cells. In Chapter II, I detail the biochemical underpinnings of the McdAB system in

positioning α- and β-carboxysomes. In Chapter III, I dissect the unique interactions between McdA and ATP by mapping out critical events in the ATPase cycle of McdA. In Chapter IV, I report a long-term imaging framework that I have established as a tool for the investigation of carboxysome trafficking and inheritance in growing and dividing cyanobacterial cells. My findings contribute new knowledge that narrows the current gap in utilizing carboxysomes for synthetic biology applications and for understanding BMC inheritance. More generally, my findings expand our understanding of organelle trafficking in bacteria.

## 1.5 References


[1] R. Losick and L. Shapiro, "Changing Views on the Nature of the Bacterial Cell: from Biochemistry to Cytology," *J Bacteriol*, vol. 181, no. 14, pp. 4143–4145, 1999, doi: 10.1128/jb.181.14.4143-4145.1999.

[2] L. Shapiro, H. H. McAdams, and R. Losick, "Why and How Bacteria Localize Proteins," *Science*, vol. 326, no. 5957, pp. 1225–1228, 2009, doi: 10.1126/science.1175685.

[3] Z. Gitai, "The New Bacterial Cell Biology: Moving Parts and Subcellular Architecture," *Cell*, vol. 120, no. 5, pp. 577–586, 2005, doi: 10.1016/j.cell.2005.02.026.

[4] S. D. Axen, O. Erbilgin, and C. A. Kerfeld, "A Taxonomy of Bacterial Microcompartment Loci Constructed by a Novel Scoring Method," *Plos Comput Biol*, vol. 10, no. 10, p. e1003898, 2014, doi: 10.1371/journal.pcbi.1003898.

[5] M. Faulkner *et al.*, "Direct characterization of the native structure and mechanics of cyanobacterial carboxysomes," *Nanoscale*, vol. 9, no. 30, pp. 10662–10673, 2017, doi: 10.1039/c7nr02524f.

[6] C. A. Kerfeld, S. Heinhorst, and G. C. Cannon, "Bacterial Microcompartments," *Microbiology+*, vol. 64, no. 1, pp. 391–408, 2010, doi: 10.1146/annurev.micro.112408.134211.

[7] C. A. Kerfeld, C. Aussignargues, J. Zarzycki, F. Cai, and M. Sutter, "Bacterial microcompartments," *Nat Rev Microbiol*, vol. 16, no. 5, pp. 277–290, 2018, doi: 10.1038/nrmicro.2018.10.

[8] T. O. Yeates, C. A. Kerfeld, S. Heinhorst, G. C. Cannon, and J. M. Shively, "Protein-based organelles in bacteria: carboxysomes and related microcompartments," *Nat Rev Microbiol*, vol. 6, no. 9, pp. 681–691, 2008, doi: 10.1038/nrmicro1913.

[9] J. M. Shively, F. Ball, D. H. Brown, and R. E. Saunders, "Functional Organelles in Prokaryotes: Polyhedral Inclusions (Carboxysomes) of Thiobacillus neapolitanus," *Science*, vol. 182, no. 4112, pp. 584–586, 1973, doi: 10.1126/science.182.4112.584.

[10] B. D. Rae, B. M. Long, M. R. Badger, and G. D. Price, "Functions, Compositions, and Evolution of the Two Types of Carboxysomes: Polyhedral Microcompartments That Facilitate CO2 Fixation in Cyanobacteria and Some Proteobacteria," *Microbiol Mol Biol R*, vol. 77, no. 3, pp. 357–379, 2013, doi: 10.1128/mmbr.00061-12.

[11] C. M. Jakobson and D. Tullman-Ercek, “Dumpster Diving in the Gut: Bacterial Microcompartments as Part of a Host-Associated Lifestyle,” *Plos Pathog*, vol. 12, no. 5, p. e1005558, 2016, doi: 10.1371/journal.ppat.1005558.
[12] E. Kofoid, C. Rappleye, I. Stojiljkovic, and J. Roth, “The 17-Gene Ethanolamine ( eut ) Operon of Salmonella typhimurium Encodes Five Homologues of Carboxysome Shell Proteins,” *J Bacteriol*, vol. 181, no. 17, pp. 5317–5329, 1999, doi: 10.1128/jb.181.17.5317-5329.1999.
[13] T. Bhardwaj and P. Somvanshi, “Pan-genome analysis of Clostridium botulinum reveals unique targets for drug development,” *Gene*, vol. 623, pp. 48–62, 2017, doi: 10.1016/j.gene.2017.04.019.
[14] R. M. Jeter, “Cobalamin-dependent 1,2-propanediol utilization by Salmonella typhimurium,” *Microbiology+*, vol. 136, no. 5, pp. 887–896, 1990, doi: 10.1099/00221287-136-5-887.
[15] T. A. Bobik, G. D. Havemann, R. J. Busch, D. S. Williams, and H. C. Aldrich, “The Propanediol Utilization ( pdu ) Operon of Salmonella enterica Serovar Typhimurium LT2 Includes Genes Necessary for Formation of Polyhedral Organelles Involved in Coenzyme B 12 -Dependent 1,2-Propanediol Degradation,” *J Bacteriol*, vol. 181, no. 19, pp. 5967–5975, 1999, doi: 10.1128/jb.181.19.5967-5975.1999.
[16] H. S. Schindel, J. A. Karty, J. B. McKinlay, and C. E. Bauer, “Characterization of a Glycyl Radical Enzyme Bacterial Microcompartment Pathway in Rhodobacter capsulatus,” *J Bacteriol*, vol. 201, no. 5, 2019, doi: 10.1128/jb.00343-18.
[17] M. Kataoka *et al.*, “A novel NADP+-dependent l-1-amino-2-propanol dehydrogenase from Rhodococcus erythropolis MAK154: a promising enzyme for the production of double chiral aminoalcohols,” *Lett Appl Microbiol*, vol. 43, no. 4, pp. 430–435, 2006, doi: 10.1111/j.1472-765x.2006.01970.x.
[18] E. Mallette and M. S. Kimber, “Structural and kinetic characterization of (S)-1-amino-2-propanol kinase from the aminoacetone utilization microcompartment of Mycobacterium smegmatis,” *J Biol Chem*, vol. 293, no. 51, pp. 19909–19918, 2018, doi: 10.1074/jbc.ra118.005485.
[19] E. Petit *et al.*, “Involvement of a Bacterial Microcompartment in the Metabolism of Fucose and Rhamnose by Clostridium phytofermentans,” *Plos One*, vol. 8, no. 1, p. e54337, 2013, doi: 10.1371/journal.pone.0054337.
[20] O. Erbilgin, K. L. McDonald, and C. A. Kerfeld, “Characterization of a Planctomycetal Organelle: a Novel Bacterial Microcompartment for the Aerobic Degradation of Plant Saccharides,” *Appl Environ Microb*, vol. 80, no. 7, pp. 2193–2205, 2014, doi: 10.1128/aem.03887-13.
[21] E. Jameson *et al.*, “Anaerobic choline metabolism in microcompartments promotes growth and swarming of Proteus mirabilis,” *Environ Microbiol*, vol. 18, no. 9, pp. 2886–2898, 2886, doi: 10.1111/1462-2920.13059.
[22] T. I. Herring, T. N. Harris, C. Chowdhury, S. K. Mohanty, and T. A. Bobik, “A Bacterial Microcompartment Is Used for Choline Fermentation by Escherichia coli 536,” *J Bacteriol*, vol. 200, no. 10, pp. e00764-17, 2018, doi: 10.1128/jb.00764-17.
[23] C. A. Kerfeld and M. R. Melnicki, “Assembly, function and evolution of cyanobacterial carboxysomes,” *Curr Opin Plant Biol*, vol. 31, pp. 66–75, 2016, doi: 10.1016/j.pbi.2016.03.009.
[24] R. J. Ellis, “The most abundant protein in the world,” *Trends Biochem Sci*, vol. 4, no. 11, pp. 241–244, 1979, doi: 10.1016/0968-0004(79)90212-3.

[25] M. R. Badger and G. D. Price, “CO2 concentrating mechanisms in cyanobacteria: molecular components, their diversity and evolution,” *J Exp Bot*, vol. 54, no. 383, pp. 609–622, 2003, doi: 10.1093/jxb/erg076.
[26] C. B. Field, M. J. Behrenfeld, J. T. Randerson, and P. Falkowski, “Primary Production of the Biosphere: Integrating Terrestrial and Oceanic Components,” *Science*, vol. 281, no. 5374, pp. 237–240, 1998, doi: 10.1126/science.281.5374.237.
[27] L. C. M. Mackinder *et al.*, “A repeat protein links Rubisco to form the eukaryotic carbon-concentrating organelle,” *Proc National Acad Sci*, vol. 113, no. 21, pp. 5958–5963, 2016, doi: 10.1073/pnas.1522866113.
[28] F. R. Tabita, “Microbial ribulose 1,5-bisphosphate carboxylase/oxygenase: A different perspective,” *Photosynth Res*, vol. 60, no. 1, pp. 1–28, 1999, doi: 10.1023/a:1006211417981.
[29] M. Sommer, F. Cai, M. Melnicki, and C. A. Kerfeld, “β-Carboxysome bioinformatics: identification and evolution of new bacterial microcompartment protein gene classes and core locus constraints,” *J Exp Bot*, vol. 68, no. 14, pp. 3841–3855, 2017, doi: 10.1093/jxb/erx115.
[30] B. M. Long, L. Tucker, M. R. Badger, and G. D. Price, “Functional Cyanobacterial β-Carboxysomes Have an Absolute Requirement for Both Long and Short Forms of the CcmM Protein,” *Plant Physiol*, vol. 153, no. 1, pp. 285–293, 2010, doi: 10.1104/pp.110.154948.
[31] J. C. Cameron, S. C. Wilson, S. L. Bernstein, and C. A. Kerfeld, “Biogenesis of a Bacterial Organelle: The Carboxysome Assembly Pathway,” *Cell*, vol. 155, no. 5, pp. 1131–1140, 2013, doi: 10.1016/j.cell.2013.10.044.
[32] B. D. Rae, B. M. Long, M. R. Badger, and G. D. Price, “Structural Determinants of the Outer Shell of β-Carboxysomes in Synechococcus elongatus PCC 7942: Roles for CcmK2, K3-K4, CcmO, and CcmL,” *Plos One*, vol. 7, no. 8, p. e43871, 2012, doi: 10.1371/journal.pone.0043871.
[33] C. A. Kerfeld *et al.*, “Protein Structures Forming the Shell of Primitive Bacterial Organelles,” *Science*, vol. 309, no. 5736, pp. 936–938, 2005, doi: 10.1126/science.1113397.
[34] M. Sommer *et al.*, “Heterohexamers Formed by CcmK3 and CcmK4 Increase the Complexity of Beta Carboxysome Shells,” *Plant Physiol*, vol. 179, no. 1, p. pp.01190.2018, 2018, doi: 10.1104/pp.18.01190.
[35] F. Cai, M. Sutter, J. C. Cameron, D. N. Stanley, J. N. Kinney, and C. A. Kerfeld, “The Structure of CcmP, a Tandem Bacterial Microcompartment Domain Protein from the β-Carboxysome, Forms a Subcompartment Within a Microcompartment,” *J Biol Chem*, vol. 288, no. 22, pp. 16055–16063, 2013, doi: 10.1074/jbc.m113.456897.
[36] A. M. Larsson, D. Hasse, K. Valegård, and I. Andersson, “Crystal structures of β-carboxysome shell protein CcmP: ligand binding correlates with the closed or open central pore,” *J Exp Bot*, vol. 68, no. 14, pp. erx070-, 2017, doi: 10.1093/jxb/erx070.
[37] M. Sutter, S. C. Wilson, S. Deutsch, and C. A. Kerfeld, “Two new high-resolution crystal structures of carboxysome pentamer proteins reveal high structural conservation of CcmL orthologs among distantly related cyanobacterial species,” *Photosynth Res*, vol. 118, no. 1–2, pp. 9–16, 2013, doi: 10.1007/s11120-013-9909-z.
[38] T. J. Keeling, B. Samborska, R. W. Demers, and M. S. Kimber, “Interactions and structural variability of β-carboxysomal shell protein CcmL,” *Photosynth Res*, vol. 121, no. 2–3, pp. 125–133, 2014, doi: 10.1007/s11120-014-9973-z.
[39] A. H. Chen, A. Robinson-Mosher, D. F. Savage, P. A. Silver, and J. K. Polka, “The Bacterial Carbon-Fixing Organelle Is Formed by Shell Envelopment of Preassembled Cargo,” *Plos One*, vol. 8, no. 9, p. e76127, 2013, doi: 10.1371/journal.pone.0076127.

[40] C. V. Iancu, D. M. Morris, Z. Dou, S. Heinhorst, G. C. Cannon, and G. J. Jensen, "Organization, Structure, and Assembly of α-Carboxysomes Determined by Electron Cryotomography of Intact Cells," *J Mol Biol*, vol. 396, no. 1, pp. 105–117, 2010, doi: 10.1016/j.jmb.2009.11.019.
[41] G. C. Cannon *et al.*, "Organization of Carboxysome Genes in the Thiobacilli," *Curr Microbiol*, vol. 46, no. 2, pp. 0115–0119, 2003, doi: 10.1007/s00284-002-3825-3.
[42] F. Cai *et al.*, "Advances in Understanding Carboxysome Assembly in Prochlorococcus and Synechococcus Implicate CsoS2 as a Critical Component," *Life*, vol. 5, no. 2, pp. 1141–1171, 2015, doi: 10.3390/life5021141.
[43] Y. Liu *et al.*, "Deciphering molecular details in the assembly of alpha-type carboxysome," *Sci Rep-uk*, vol. 8, no. 1, p. 15062, 2018, doi: 10.1038/s41598-018-33074-x.
[44] L. M. Oltrogge, T. Chaijarasphong, A. W. Chen, E. R. Bolin, S. Marqusee, and D. F. Savage, "Multivalent interactions between CsoS2 and Rubisco mediate α-carboxysome formation.," *Nat Struct Mol Biol*, pp. 1–7, 2020, doi: 10.1038/s41594-020-0387-7.
[45] E. W. Roberts, F. Cai, C. A. Kerfeld, G. C. Cannon, and S. Heinhorst, "Isolation and Characterization of the Prochlorococcus Carboxysome Reveal the Presence of the Novel Shell Protein CsoS1D," *J Bacteriol*, vol. 194, no. 4, pp. 787–795, 2012, doi: 10.1128/jb.06444-11.
[46] A. Bekker *et al.*, "Dating the rise of atmospheric oxygen," *Nature*, vol. 427, no. 6970, pp. 117–120, 2004, doi: 10.1038/nature02260.
[47] P. G. Falkowski, T. Fenchel, and E. F. Delong, "The Microbial Engines That Drive Earth's Biogeochemical Cycles," *Science*, vol. 320, no. 5879, pp. 1034–1039, 2008, doi: 10.1126/science.1153213.
[48] J. W. Schopf, "The paleobiological record of photosynthesis," *Photosynth Res*, vol. 107, no. 1, pp. 87–101, 2011, doi: 10.1007/s11120-010-9577-1.
[49] L. A. Lewis, "Hold the salt: Freshwater origin of primary plastids," *Proc National Acad Sci*, vol. 114, no. 37, pp. 9759–9760, 2017, doi: 10.1073/pnas.1712956114.
[50] P. Flombaum *et al.*, "Present and future global distributions of the marine Cyanobacteria Prochlorococcus and Synechococcus," *Proc National Acad Sci*, vol. 110, no. 24, pp. 9824–9829, 2013, doi: 10.1073/pnas.1307701110.
[51] J. S. MacCready *et al.*, "Protein gradients on the nucleoid position the carbon-fixing organelles of cyanobacteria," *Elife*, vol. 7, p. e39723, 2018, doi: 10.7554/elife.39723.
[52] D. F. Savage, B. Afonso, A. H. Chen, and P. A. Silver, "Spatially Ordered Dynamics of the Bacterial Carbon Fixation Machinery," *Science*, vol. 327, no. 5970, pp. 1258–1261, 2010, doi: 10.1126/science.1186090.
[53] R. Yokoo, R. D. Hood, and D. F. Savage, "Live-cell imaging of cyanobacteria," *Photosynth Res*, vol. 126, no. 1, pp. 33–46, 2015, doi: 10.1007/s11120-014-0049-x.
[54] S. V. Shestakov and N. T. Khyen, "Evidence for genetic transformation in blue-green alga Anacystis nidulans," *Mol Gen Genetics Mgg*, vol. 107, no. 4, pp. 372–375, 1970, doi: 10.1007/bf00441199.
[55] A. I. Flamholz *et al.*, "Functional reconstitution of a bacterial CO2 concentrating mechanism in E. coli," *Elife*, vol. 9, p. e59882, 2020, doi: 10.7554/elife.59882.
[56] M. Baumgart, I. Huber, I. Abdollahzadeh, T. Gensch, and J. Frunzke, "Heterologous expression of the Halothiobacillus neapolitanus carboxysomal gene cluster in Corynebacterium glutamicum," *J Biotechnol*, vol. 258, pp. 126–135, 2017, doi: 10.1016/j.jbiotec.2017.03.019.
[57] B. M. Long *et al.*, "Carboxysome encapsulation of the CO2-fixing enzyme Rubisco in tobacco chloroplasts," *Nat Commun*, vol. 9, no. 1, p. 3570, 2018, doi: 10.1038/s41467-018-06044-0.

[58] M. T. Lin, A. Occhialini, P. J. Andralojc, M. A. J. Parry, and M. R. Hanson, "A faster Rubisco with potential to increase photosynthesis in crops," *Nature*, vol. 513, no. 7519, pp. 547–550, 2014, doi: 10.1038/nature13776.
[59] A. Occhialini, M. T. Lin, P. J. Andralojc, M. R. Hanson, and M. A. J. Parry, "Transgenic tobacco plants with improved cyanobacterial Rubisco expression but no extra assembly factors grow at near wild-type rates if provided with elevated CO2," *Plant J*, vol. 85, no. 1, pp. 148–160, 2016, doi: 10.1111/tpj.13098.
[60] Y. Fang *et al.*, "Engineering and Modulating Functional Cyanobacterial CO2-Fixing Organelles," *Front Plant Sci*, vol. 9, p. 739, 2018, doi: 10.3389/fpls.2018.00739.
[61] Y. Sun *et al.*, "Light Modulates the Biosynthesis and Organization of Cyanobacterial Carbon Fixation Machinery through Photosynthetic Electron Flow," *Plant Physiol*, vol. 171, no. 1, pp. 530–541, 2016, doi: 10.1104/pp.16.00107.
[62] Y. Sun, A. Wollman, F. Huang, M. Leake, and L. Liu, "Single-organelle quantification reveals the stoichiometric and structural variability of carboxysomes dependent on the environment," *Plant Cell*, vol. 31, no. 7, p. tpc.00787.2018, 2019, doi: 10.1105/tpc.18.00787.
[63] R. Rillema, Y. Hoang, J. S. MacCready, and A. G. Vecchiarelli, "Carboxysome Mispositioning Alters Growth, Morphology, and Rubisco Level of the Cyanobacterium Synechococcus elongatus PCC 7942," *Mbio*, vol. 12, no. 4, pp. e02696-20, 2021, doi: 10.1128/mbio.02696-20.
[64] G. C. Cannon and J. M. Shively, "Characterization of a homogenous preparation of carboxysomes from Thiobacillus neapolitanus," *Arch Microbiol*, vol. 134, no. 1, pp. 52–59, 1983, doi: 10.1007/bf00429407.
[65] M. F. Schmid *et al.*, "Structure of Halothiobacillus neapolitanus Carboxysomes by Cryo-electron Tomography," *J Mol Biol*, vol. 364, no. 3, pp. 526–535, 2006, doi: 10.1016/j.jmb.2006.09.024.
[66] G. C. Cannon, C. E. Bradburne, H. C. Aldrich, S. H. Baker, S. Heinhorst, and J. M. Shively, "Microcompartments in Prokaryotes: Carboxysomes and Related Polyhedra," *Appl Environ Microb*, vol. 67, no. 12, pp. 5351–5361, 2001, doi: 10.1128/aem.67.12.5351-5361.2001.
[67] J. S. MacCready, L. Tran, J. L. Basalla, P. Hakim, and A. G. Vecchiarelli, "The McdAB system positions α-carboxysomes in proteobacteria," *Mol Microbiol*, 2021, doi: 10.1111/mmi.14708.
[68] S. Heinhorst, E. B. Williams, F. Cai, C. D. Murin, J. M. Shively, and G. C. Cannon, "Characterization of the Carboxysomal Carbonic Anhydrase CsoSCA from Halothiobacillus neapolitanus ▿ ," *J Bacteriol*, vol. 188, no. 23, pp. 8087–8094, 2006, doi: 10.1128/jb.00990-06.
[69] T. D. Dunham, W. Xu, B. E. Funnell, and M. A. Schumacher, "Structural basis for ADP-mediated transcriptional regulation by P1 and P7 ParA," *Embo J*, vol. 28, no. 12, pp. 1792–1802, 2009, doi: 10.1038/emboj.2009.120.
[70] J. C. Baxter and B. E. Funnell, "Plasmid Partition Mechanisms," *Microbiol Spectr*, vol. 2, no. 6, 2014, doi: 10.1128/microbiolspec.plas-0023-2014.
[71] A. Badrinarayanan, T. B. K. Le, and M. T. Laub, "Bacterial Chromosome Organization and Segregation," *Annu Rev Cell Dev Bi*, vol. 31, no. 1, pp. 171–199, 2015, doi: 10.1146/annurev-cellbio-100814-125211.
[72] J. Lutkenhaus and M. Sundaramoorthy, "MinD and role of the deviant Walker A motif, dimerization and membrane binding in oscillation," *Mol Microbiol*, vol. 48, no. 2, pp. 295–303, 2003, doi: 10.1046/j.1365-2958.2003.03427.x.

[73] D. Kiekebusch, K. A. Michie, L.-O. Essen, J. Löwe, and M. Thanbichler, "Localized Dimerization and Nucleoid Binding Drive Gradient Formation by the Bacterial Cell Division Inhibitor MipZ," *Mol Cell*, vol. 46, no. 3, pp. 245–259, 2012, doi: 10.1016/j.molcel.2012.03.004.
[74] D. Schumacher *et al.*, "The PomXYZ Proteins Self-Organize on the Bacterial Nucleoid to Stimulate Cell Division," *Dev Cell*, vol. 41, no. 3, pp. 299-314.e13, 2017, doi: 10.1016/j.devcel.2017.04.011.
[75] H. Ono, A. Takashima, H. Hirata, M. Homma, and S. Kojima, "The MinD homolog FlhG regulates the synthesis of the single polar flagellum of Vibrio alginolyticus," *Mol Microbiol*, vol. 98, no. 1, pp. 130–141, 2015, doi: 10.1111/mmi.13109.
[76] J. S. Schuhmacher *et al.*, "MinD-like ATPase FlhG effects location and number of bacterial flagella during C-ring assembly," *Proc National Acad Sci*, vol. 112, no. 10, pp. 3092–3097, 2015, doi: 10.1073/pnas.1419388112.
[77] M. A. J. Roberts, G. H. Wadhams, K. A. Hadfield, S. Tickner, and J. P. Armitage, "ParA-like protein uses nonspecific chromosomal DNA binding to partition protein complexes," *Proc National Acad Sci*, vol. 109, no. 17, pp. 6698–6703, 2012, doi: 10.1073/pnas.1114000109.
[78] S. Ringgaard, M. Zepeda-Rivera, X. Wu, K. Schirner, B. M. Davis, and M. K. Waldor, "ParP prevents dissociation of CheA from chemotactic signaling arrays and tethers them to a polar anchor," *Proc National Acad Sci*, vol. 111, no. 2, pp. E255–E264, 2014, doi: 10.1073/pnas.1315722111.
[79] A. S. B. Jalal and T. B. K. Le, "Bacterial chromosome segregation by the ParABS system," *Open Biology*, vol. 10, no. 6, 2020, doi: 10.1098/rsob.200097.
[80] M. J. Davey and B. E. Funnell, "Modulation of the P1 Plasmid Partition Protein ParA by ATP, ADP, and P1 ParB," *J Biol Chem*, vol. 272, no. 24, pp. 15286–15292, 1997, doi: 10.1074/jbc.272.24.15286.
[81] H. Zhang and M. A. Schumacher, "Structures of partition protein ParA with nonspecific DNA and ParB effector reveal molecular insights into principles governing Walker-box DNA segregation.," *Gene Dev*, vol. 31, no. 5, pp. 481–492, 2017, doi: 10.1101/gad.296319.117.
[82] C. M. Hester and J. Lutkenhaus, "Soj (ParA) DNA binding is mediated by conserved arginines and is essential for plasmid segregation," *Proc National Acad Sci*, vol. 104, no. 51, pp. 20326–20331, 2007, doi: 10.1073/pnas.0705196105.
[83] J. Castaing, J. Bouet, and D. Lane, "F plasmid partition depends on interaction of SopA with non-specific DNA," *Mol Microbiol*, vol. 70, no. 4, pp. 1000–1011, 2008, doi: 10.1111/j.1365-2958.2008.06465.x.
[84] A. G. Vecchiarelli *et al.*, "ATP control of dynamic P1 ParA–DNA interactions: a key role for the nucleoid in plasmid partition," *Mol Microbiol*, vol. 78, no. 1, pp. 78–91, 2010, doi: 10.1111/j.1365-2958.2010.07314.x.
[85] F. Pratto, A. Cicek, W. A. Weihofen, R. Lurz, W. Saenger, and J. C. Alonso, "Streptococcus pyogenes pSM19035 requires dynamic assembly of ATP-bound ParA and ParB on parS DNA during plasmid segregation," *Nucleic Acids Res*, vol. 36, no. 11, pp. 3676–3689, 2008, doi: 10.1093/nar/gkn170.
[86] A. Sanchez *et al.*, "Stochastic Self-Assembly of ParB Proteins Builds the Bacterial DNA Segregation Apparatus," *Cell Syst*, vol. 1, no. 2, pp. 163–173, 2015, doi: 10.1016/j.cels.2015.07.013.
[87] B. E. Funnell, "ParB Partition Proteins: Complex Formation and Spreading at Bacterial and Plasmid Centromeres," *Frontiers Mol Biosci*, vol. 3, p. 44, 2016, doi: 10.3389/fmolb.2016.00044.

[88] L. C. Hwang *et al.*, "ParA-mediated plasmid partition driven by protein pattern self-organization," *Embo J*, vol. 32, no. 9, pp. 1238–1249, 2013, doi: 10.1038/emboj.2013.34.
[89] A. G. Vecchiarelli, J. C. Havey, L. L. Ing, E. O. Y. Wong, W. G. Waples, and B. E. Funnell, "Dissection of the ATPase Active Site of P1 ParA Reveals Multiple Active Forms Essential for Plasmid Partition," *J Biol Chem*, vol. 288, no. 24, pp. 17823–17831, 2013, doi: 10.1074/jbc.m113.469981.
[90] A. Volante and J. C. Alonso, "Molecular Anatomy of ParA-ParA and ParA-ParB Interactions during Plasmid Partitioning*," *J Biol Chem*, vol. 290, no. 30, pp. 18782–18795, 2015, doi: 10.1074/jbc.m115.649632.
[91] A. G. Vecchiarelli, K. C. Neuman, and K. Mizuuchi, "A propagating ATPase gradient drives transport of surface-confined cellular cargo," *Proc National Acad Sci*, vol. 111, no. 13, pp. 4880–4885, 2014, doi: 10.1073/pnas.1401025111.
[92] G. Ebersbach and K. Gerdes, "Bacterial mitosis: partitioning protein ParA oscillates in spiral-shaped structures and positions plasmids at mid-cell," *Mol Microbiol*, vol. 52, no. 2, pp. 385–398, 2004, doi: 10.1111/j.1365-2958.2004.04002.x.
[93] G. Ebersbach, S. Ringgaard, J. Møller-Jensen, Q. Wang, D. J. Sherratt, and K. Gerdes, "Regular cellular distribution of plasmids by oscillating and filament-forming ParA ATPase of plasmid pB171," *Mol Microbiol*, vol. 61, no. 6, pp. 1428–1442, 2006, doi: 10.1111/j.1365-2958.2006.05322.x.
[94] M. A. Fogel and M. K. Waldor, "Distinct segregation dynamics of the two Vibrio cholerae chromosomes," *Mol Microbiol*, vol. 55, no. 1, pp. 125–136, 2005, doi: 10.1111/j.1365-2958.2004.04379.x.
[95] T. Hatano, Y. Yamaichi, and H. Niki, "Oscillating focus of SopA associated with filamentous structure guides partitioning of F plasmid," *Mol Microbiol*, vol. 64, no. 5, pp. 1198–1213, 2007, doi: 10.1111/j.1365-2958.2007.05728.x.
[96] S. Ringgaard, J. van Zon, M. Howard, and K. Gerdes, "Movement and equipositioning of plasmids by ParA filament disassembly," *Proc National Acad Sci*, vol. 106, no. 46, pp. 19369–19374, 2009, doi: 10.1073/pnas.0908347106.
[97] H. C. Lim, I. V. Surovtsev, B. G. Beltran, F. Huang, J. Bewersdorf, and C. Jacobs-Wagner, "Evidence for a DNA-relay mechanism in ParABS-mediated chromosome segregation," *Elife*, vol. 3, p. e02758, 2014, doi: 10.7554/elife.02758.
[98] A. L. Gall *et al.*, "Bacterial partition complexes segregate within the volume of the nucleoid," *Nat Commun*, vol. 7, no. 1, p. 12107, 2016, doi: 10.1038/ncomms12107.
[99] A. G. Vecchiarelli, L. C. Hwang, and K. Mizuuchi, "Cell-free study of F plasmid partition provides evidence for cargo transport by a diffusion-ratchet mechanism," *Proc National Acad Sci*, vol. 110, no. 15, pp. E1390–E1397, 2013, doi: 10.1073/pnas.1302745110.
[100] A. G. Vecchiarelli, Y. Seol, K. C. Neuman, and K. Mizuuchi, "A moving ParA gradient on the nucleoid directs subcellular cargo transport via a chemophoresis force.," *Bioarchitecture*, vol. 4, no. 4–5, pp. 154–9, 2014, doi: 10.4161/19490992.2014.987581.
[101] L. Hu, A. G. Vecchiarelli, K. Mizuuchi, K. C. Neuman, and J. Liu, "Directed and persistent movement arises from mechanochemistry of the ParA/ParB system," *Proc National Acad Sci*, vol. 112, no. 51, pp. E7055–E7064, 2015, doi: 10.1073/pnas.1505147112.
[102] L. Hu, A. G. Vecchiarelli, K. Mizuuchi, K. C. Neuman, and J. Liu, "Brownian Ratchet Mechanism for Faithful Segregation of Low-Copy-Number Plasmids," *Biophys J*, vol. 112, no. 7, pp. 1489–1502, 2017, doi: 10.1016/j.bpj.2017.02.039.

[103] J. Lutkenhaus, “Assembly Dynamics of the Bacterial MinCDE System and Spatial Regulation of the Z Ring,” *Biochemistry-us*, vol. 76, no. 1, pp. 539–562, 2007, doi: 10.1146/annurev.biochem.75.103004.142652.
[104] A. G. Vecchiarelli, M. Li, M. Mizuuchi, and K. Mizuuchi, “Differential affinities of MinD and MinE to anionic phospholipid influence Min patterning dynamics in vitro,” *Mol Microbiol*, vol. 93, no. 3, pp. 453–463, 2014, doi: 10.1111/mmi.12669.
[105] K. Mizuuchi and A. G. Vecchiarelli, “Mechanistic insights of the Min oscillator via cell-free reconstitution and imaging,” *Phys Biol*, vol. 15, no. 3, p. 031001, 2018, doi: 10.1088/1478-3975/aa9e5e.
[106] A. G. Vecchiarelli *et al.*, “Membrane-bound MinDE complex acts as a toggle switch that drives Min oscillation coupled to cytoplasmic depletion of MinD,” *Proc National Acad Sci*, vol. 113, no. 11, pp. E1479–E1488, 2016, doi: 10.1073/pnas.1600644113.
[107] L. Hu, A. G. Vecchiarelli, K. Mizuuchi, K. C. Neuman, and J. Liu, “Brownian ratchet mechanisms of ParA-mediated partitioning,” *Plasmid*, vol. 92, pp. 12–16, 2017, doi: 10.1016/j.plasmid.2017.05.002.
[108] J. S. MacCready, J. L. Basalla, and A. G. Vecchiarelli, “Origin and Evolution of Carboxysome Positioning Systems in Cyanobacteria,” *Mol Biol Evol*, 2020, doi: 10.1093/molbev/msz308.

# CHAPTER II

## McdAB is an Essential Two-component System for Proper Carboxysome Positioning

This chapter is based in part on the previously published articles listed below. J.L. Basalla performed the experiment and analysis in Fig 2.5B. I performed all other experiments and data analyses detailed in the Results subsection in this chapter. J.S. MacCready and A.G. Vecchiarelli performed the experiments and related analyses highlighted in the Introduction subsection.

J.S. MacCready, P. Hakim, E.J. Young, L. Hu, J. Liu, K.W. Osteryoung, A.G. Vecchiarelli and D.C. Ducat, "Protein gradients on the nucleoid position the carbon-fixing organelles of cyanobacteria". *eLife*, 7:e39723, 2018, doi: 10.7554/eLife.39723.

J.S. MacCready, L. Tran, J.L. Basalla, P. Hakim and A.G. Vecchiarelli. "The McdAB system positions α-carboxysomes in proteobacteria". *Mol Micro*, vol. 116, no.1, pp. 277-297, 2021, doi: 10.1111/mmi.14708.

### 2.1 Abstract

Carboxysomes are essential proteinaceous bacterial organelles encapsulating critical enzymes of the Calvin-Benson-Bassham cycle. In the model β-cyanobacterium *Synechococcus elongatus* PCC 7942, previous work has implicated a ParA-like protein (we have since termed McdA) as a key component responsible for spatially organizing β-carboxysomes along the long axis of the cell. It

was also previously found that McdA formed dynamic oscillations in the cell, which were interpreted as a dynamic cytoskeletal scaffold for carboxysome positioning. How self-organization of McdA emerges and contributes to carboxysome positioning is unknown. Here, I found that McdA does not form a cytoskeletal polymer to position carboxysomes, as subscribed by previous models. Instead, I show that McdA has ATP-dependent non-specific DNA binding activity *in vitro*, which translates to nucleoid binding *in vivo*. I also show that McdA has ATPase activity that is significantly higher than other classical ParA/MinD family ATPases. Finally, we identify the partner protein to McdA, we term McdB, a previously uncharacterized partner protein to McdA in carboxysome positioning. I find that McdB directly interacts with McdA, stimulating its ATPase activity and release from DNA. McdB also displays strong self-association activity and directly associates with several carboxysome shell components. Together, the data allows us to propose a diffusion-ratchet mechanism for carboxysome positioning, whereby McdB-bound carboxysomes generate dynamic gradients of McdA on the nucleoid. We recently found that the McdAB system is also present in α-carboxysome containing proteobacteria. In the model chemoautotrophic proteobacterium *Halothiobacillus neapolitanus* bearing α-carboxysomes, I find that α-McdB directly associates with α-McdA. Together, my findings provide the biochemical underpinnings of a positioning mechanism for structurally and phyletically distinct α- and β-carboxysomes.

## 2.2 Introduction

In the DNA partition process, ParA-type ATPases successively bind ATP, dimerize, and bind non-specifically to DNA [83]–[85], [110]. *In vivo*, this mechanism establishes the nucleoid as the biological surface upon which directed DNA cargo motion occurs [84], [99], [111], [112]. In the model rod-shaped cyanobacterium *S. elongatus*, the ParA-like protein we call McdA

(Synpcc7942_1833; Maintenance of carboxysome distribution protein A) is required for positioning carboxysomes and has been shown to undergo remarkable pole-to-pole oscillations via an unknown mechanism [53]. The ParA/MinD family of ATPases have MinD-type members that form dynamic oscillations on the membrane to position the divisome at midcell and ParA-type members that oscillate on the bacterial chromosome to position plasmids and chromosomes. McdA, on the other hand, has been broadly hypothesized to form cytoskeletal filaments that position carboxysomes via an unknown mechanism. Therefore, it remained unclear if McdA uses a biological surface to self-organize in the cell or if it indeed formed a free-standing cytoskeletal network as previously proposed [53].

It has been largely speculated that McdA oscillations represent dynamic motions of cytoskeletal polymers that generate forces for distributing carboxysomes down the cell length. By directly visualizing the interaction between fluorescent McdA and a DNA-coated flowcell surface, we found that McdA uniformly binds a DNA carpet in an ATP-dependent manner with no evidence of polymer formation [31]. It is also worthwhile to note that no free-standing McdA filaments have been observed under any *in vitro* condition, nor in electron micrographs of *S. elongatus* strains overexpressing McdA. When imaged in DAPI-stained *S. elongatus* cells, the cell-traversing mNG-McdA signal closely resembled that of the stained nucleoid, suggesting that the nucleoid is the surface upon which McdA dynamics are occurring (Fig. 2.1). But given that S. elongatus is polyploid and can harbor as many as a dozen copies of its chromosome, it remains difficult to spatially resolve the nucleoid and cytoplasmic regions of the cell. Therefore, it remains to be determined if McdA oscillations are indeed occurring on the nucleoid *in vivo*.

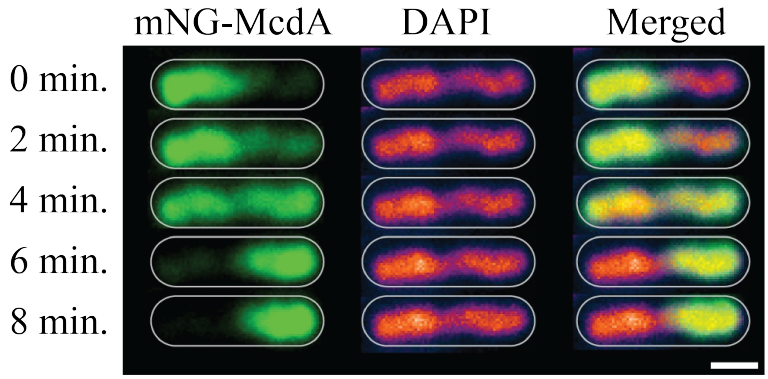


Figure 2.1**: Oscillating mNG-McdA signal colocalized with DAPI-stained nucleoid.** Oscillation of mNG-McdA colocalizes with DAPI staining of nucleoid DNA, which is also centrally localized and is excluded from peripheral thylakoid membranes. Scale bar: 1 μm. Figure from [31] (https://creativecommons.org/licenses/by/4.0/).

ParA/MinD family ATPases that have been shown to undergo dynamic oscillations *in vivo* require a partner protein to stimulate their ATPase activity and promote oscillatory dynamics. Using gene neighborhood analysis and deletion studies, we identified a gene downstream of *mcdA* that we termed maintenance of carboxysome distribution B (*mcdB*). We found that McdB protein is responsible for emergent McdA subcellular dynamics [9] and fluorescent McdB has been shown to colocalize with a fluorescent carboxysome reporter *in vivo*. But how McdB associates with the carboxysome remains unknown.

The ParA/MinD family of ATPases are defined by the presence of two lysine residues within their deviant Walker-A motif (KGGXXGKT) required for dimerization, ATP-binding, and ATP hydrolysis [113], [114]. Interestingly, *S. elongatus* McdA lacks the defining amino terminal lysine residue of this protein family termed the "signature lysine" [113], suggesting that McdA might have an activity uncharacteristic of previously studied ParA/MinD ATPases. While other studies [53], [115] have shown that McdA is involved in proper positioning and inheritance of carboxysomes, the characterization of its ATPase activity remains unreported.

The McdAB carboxysome positioning system is not restricted to *S. elongatus*. We recently discovered that there are two distinct types of McdAB systems (Type 1 and Type 2) responsible for positioning β-carboxysomes in β-cyanobacteria [109]. Intriguingly, we also found that α-carboxysome-containing α-cyanobacteria completely lack the McdAB system. This lack of McdAB systems in α-cyanobacteria suggested that α-carboxysome containing proteobacteria may also lack McdAB-based positioning [9] because α-carboxysomes are thought to have initially emerged in proteobacteria and subsequently horizontally transferred into what we now call α-cyanobacteria. Surprisingly however, we have found that a distinct McdAB system functions to position α-carboxysomes in proteobacteria, using the model chemoautotroph *Halothiobacillus neapolitanus c2* [68].

Here I explored the association between McdA, McdB and nsDNA *in vitro* for the first time. Specifically, I found that purified McdA has non-specific DNA binding activity only in the presence of ATP. I also found that McdA possess ATPase activity that is uncharacteristically high for ParA family members studied thus far. Additionally, I showed that McdB can directly interact with McdA to stimulate its ATPase activity and release it from DNA *in vitro*, which promotes McdA pole-to-pole oscillation *in vivo* [31]. I also discovered that α-McdA and α-McdB in *H. neapolitanus* interact, similar to their counterparts in the β-cyanobacterium *S. elongatus*. Taken together, the data in this chapter provide a biochemical basis for the mechanism responsible for distributing α- and β-carboxysomes in the cell.

## 2.3 Results

### 2.3.1 nsDNA binding activity of McdA is ATP-dependent and inhibited by McdB

*In vivo* mNG-McdA oscillations seemed to colocalize with the DAPI-stained nucleoid (Fig 2.1) [31]. However, given the polyploidy of *S. elongatus* [116] and the lack of cytoplasmic space, it is difficult to determine with certainty that McdA oscillations are occurring on the nucleoid. And if this is indeed the case, it is not known if this oscillatory patterning occurs via direct interactions with the bacterial chromosome or protein components of the nucleoid. To directly answer these questions, I purified McdA to assay its ability to interact with non-specific DNA. While I found that wild-type McdA and His-mNG-McdA were insoluble and prone to degradation, an N-terminal fusion of McdA to Maltose Binding Protein (MBP) (His-MBP-McdA) was highly soluble. I purified this McdA fusion and examined its capacity to bind DNA via an Electrophoretic Mobility Shift Assays (EMSA). I observed that His-MBP-McdA significantly shifted non-specific DNA (nsDNA) only in the presence of ATP, and showed no appreciable DNA shifts when ADP or the non-hydrolyzable ATP-analog ATP-γ-S were added, or in the absence of any nucleotide (Fig. 2.2A). This result is consistent with our visualization of McdA-GFP-His uniformly binding the DNA carpet when infused into a flowcell with ATP [31].

Partner proteins to ParA-type ATPases are known to localize to the positioned cargo and locally stimulate the ATPase and displace it from the nucleoid [117]–[119]. I therefore assayed if McdB influenced McdA binding to a DNA substrate in the EMSA. As shown previously (Fig. 2.2A), with ATP present, non-specific DNA fragments exhibit slowed mobility in the presence of increasing concentrations of purified His-MBP-McdA (Fig. 2.2B). Strikingly, when the experiment was conducted with a constant concentration of His-MBP-McdA (2.5 mM), the shift

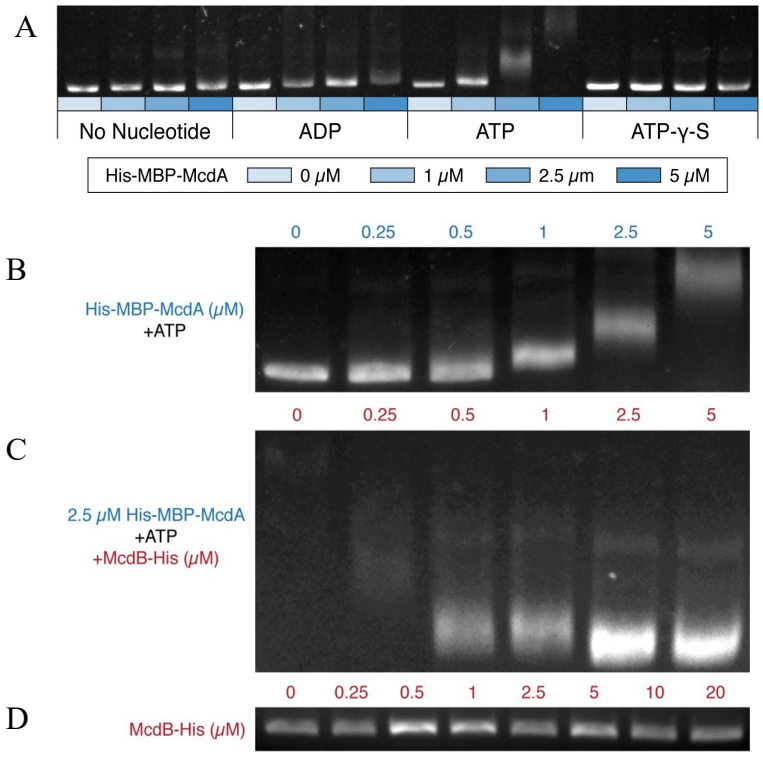


Figure 2.2: **McdA binds nsDNA when ATP is present.** A and B. Purified His-MBP-McdA slows the migration of DNA in an ATP-dependent manner in an EMSA. C. Increasing concentrations of McdB-His resolves the gel shift provided by 2.5 μM of His-MBP-McdA and ATP. D. Titration of McdB-His alone (no McdA present) shows McdB does not directly bind nsDNA.

in DNA mobility was reversed by addition of increasing amounts of McdB-His (Fig. 2.2C). The data suggest that McdB stimulates the release of McdA from DNA. McdB-His alone did not exhibit any DNA binding activity in the gel shift assay, which shows the inhibition of McdA binding to DNA is not the result of competition for binding the DNA substrate (Fig. 2.2D). Taken together, my results show that McdA has ATP-dependent non-specific DNA binding activity, and McdA interaction with McdB inhibits this activity.

### 2.3.2 McdA interacts with McdB and McdB associates with carboxysome via its shell-proteins

Given the functional association between McdA and McdB in the EMSAs, I sought to determine if McdA and McdB directly interact by performing a bacterial two-hybrid assay (B2H) between N- and C-terminally tagged McdA and McdB (Fig. 2.3A). McdA and McdB were able to self-associate in the B2H analysis. Self-association of C-terminally tagged McdA proteins was faint but confirmed on X-gal plates (Fig. 2.3B). I also observed a reciprocal interaction between N-terminally tagged McdA and N-terminally tagged McdB (Fig. 2.3A). However, C-terminally tagged McdB failed to show an interaction with McdA, while C-terminally tagged McdA association with McdB was dependent upon expression conditions. These results suggest that N-

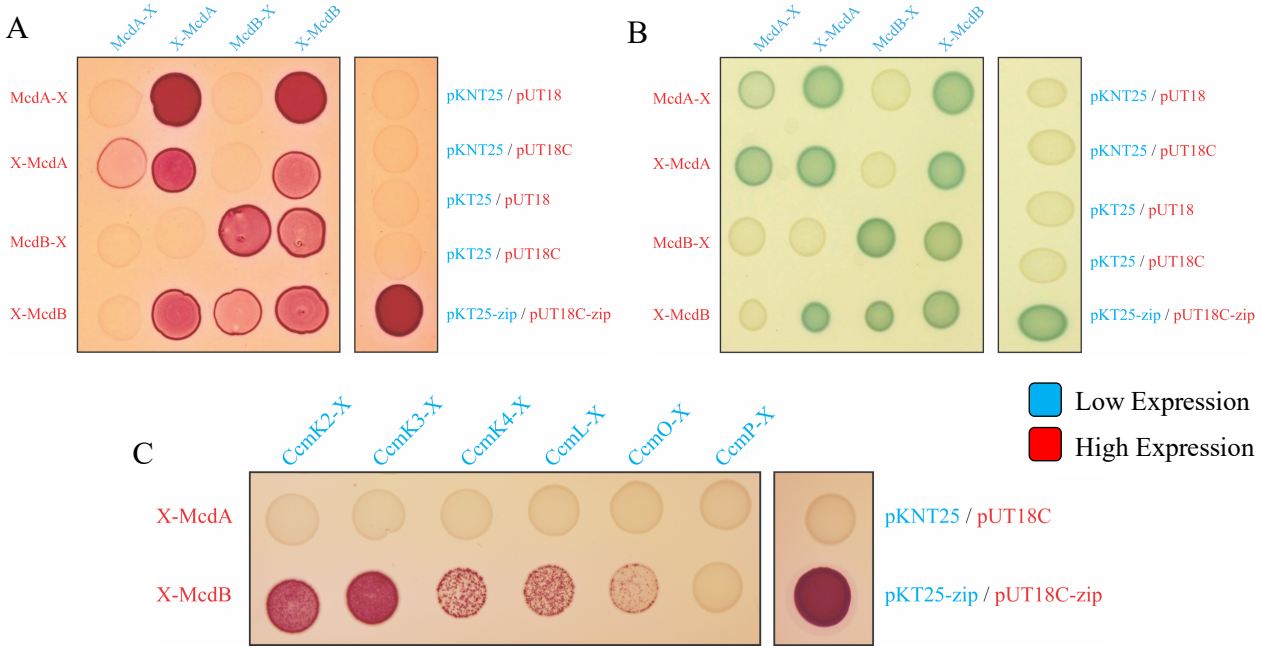


Figure 2.3: **McdA interacts with McdB, but only McdB can interact with carboxysome shell proteins**. A and B. Bacterial two-hybrid interactions between McdA and McdB tagged at their N-termini (X-McdA, X-McdB) or C-termini (McdA-X, McdB-X) on a MacConkey agar plate (A) and X-gal supplemented LB plate (B). (C) Bacterial two-hybrid of McdA and McdB against carboxysome shell proteins. All images are representative of 3 independent trials.

terminally tagged McdA only interacts with N-terminally tagged McdB, while C-terminal fusions of either protein partially disrupts function. These B2H findings are consistent with our *in vivo* observations where mNG-McdA is fully functional in distributing carboxysomes, whereas McdA-mNG is not.

mNG-McdB colocalizes with carboxysomes *in vivo*, but how McdB associates is unknown. I therefore investigated if McdB interaction with the carboxysome is direct, and if so, what carboxysome components bind McdB. Carboxysome biogenesis occurs from the inside-out. Carboxysomes first form a core structure containing Rubisco and carbonic anhydrase, which are coordinated into an ordered array through interactions with CcmM [32], [33], [120], [121]. This core is thought to recruit outer shell proteins through the adaptor protein CcmN, thereby forming the carboxysome coat [122], [123] (Fig. 1.2B). CcmK2 is the dominant shell protein that composes the facets of the shell, and has been shown to directly interact with CcmN [122]. Along with CcmK2, proteins CcmO, CcmL, CcmK3, CcmK4, and CcmP are also recruited to complete compartmentalization (Fig. 1.2B) [34], [37], [124], [125], although the relative arrangement of these structural components of the shell remains uncertain. I explored if the outer shell proteins of the carboxysome could be involved in recruiting McdB through a bacterial two-hybrid screen. Using N-terminally tagged McdA or McdB as bait, the assay suggested N-terminally tagged McdB interacts with the shell proteins CcmK2, CcmK3, CcmK4, CcmL, and CcmO, but not CcmP (Fig. 2.3C). In contrast, I did not find evidence for direct interaction between McdA and any carboxysome component (Fig. 2.3C, top row). Taken together, my findings further support a direct interaction between McdA and McdB, while McdB association with the carboxysome is mediated by multiple shell protein interactions.

### 2.3.3 McdA has ATPase activity that is stimulated by McdB and nsDNA

The ParA/MinD family of ATPases are defined by the presence of two lysine residues within their deviant Walker-A motif (KGGXXGKT) required for dimerization, ATP-binding, and ATP hydrolysis [114]. Interestingly, *S. elongatus* McdA lacks the signature amino terminal lysine residue (Fig. 2.4A, top panel), suggesting that McdA might have an ATPase activity uncharacteristic of members from this family. Therefore, I first set out to determine if McdA had ATPase activity. His-MBP-McdA displayed strong ATPase activity alone, significantly higher (>200 fold) than that of traditional ParA family ATPases, such as SopA of F plasmid and ParA of P1 plasmid (Fig. 2.4A). Because the ATPase activity was uncharacteristically high, I confirmed that the measured ATPase activity co-eluted with His-MBP-McdA from a size exclusion chromatography column and could not be attributed to a contaminating ATPase (Fig. 2.4B). Relative to the constant specific activity of F SopA-His and P1 ParA with increasing protein concentrations (Fig. 2.4C), the specific ATPase activity of His-MBP-McdA declined at higher protein concentrations (Fig. 2.4D). This decrease in ATPase activity was not due to substrate limitation during the course of the *in vitro* assay, as ATP was provided in excess, but could be indicative of a regulatory mechanism or product inhibition that is not characteristic of traditional ParA family members.

ParB partners stimulate the ATPase activity of their cognate ParA synergistically with nsDNA [117]–[119]. ParB stimulation is suggested to be coupled to ParA release from the nucleoid in the vicinity of ParB-bound cargo, as ADP does not support ParA binding to nsDNA [83]–[85], [110]. I tested whether McdB-His could stimulate McdA ATPase activity, analogously to traditional ParB members. When adding only nsDNA or McdB-His to the reactions, I observed very mild stimulation of His-MBP-McdA ATPase activity (Fig. 2.4E). When both nsDNA and

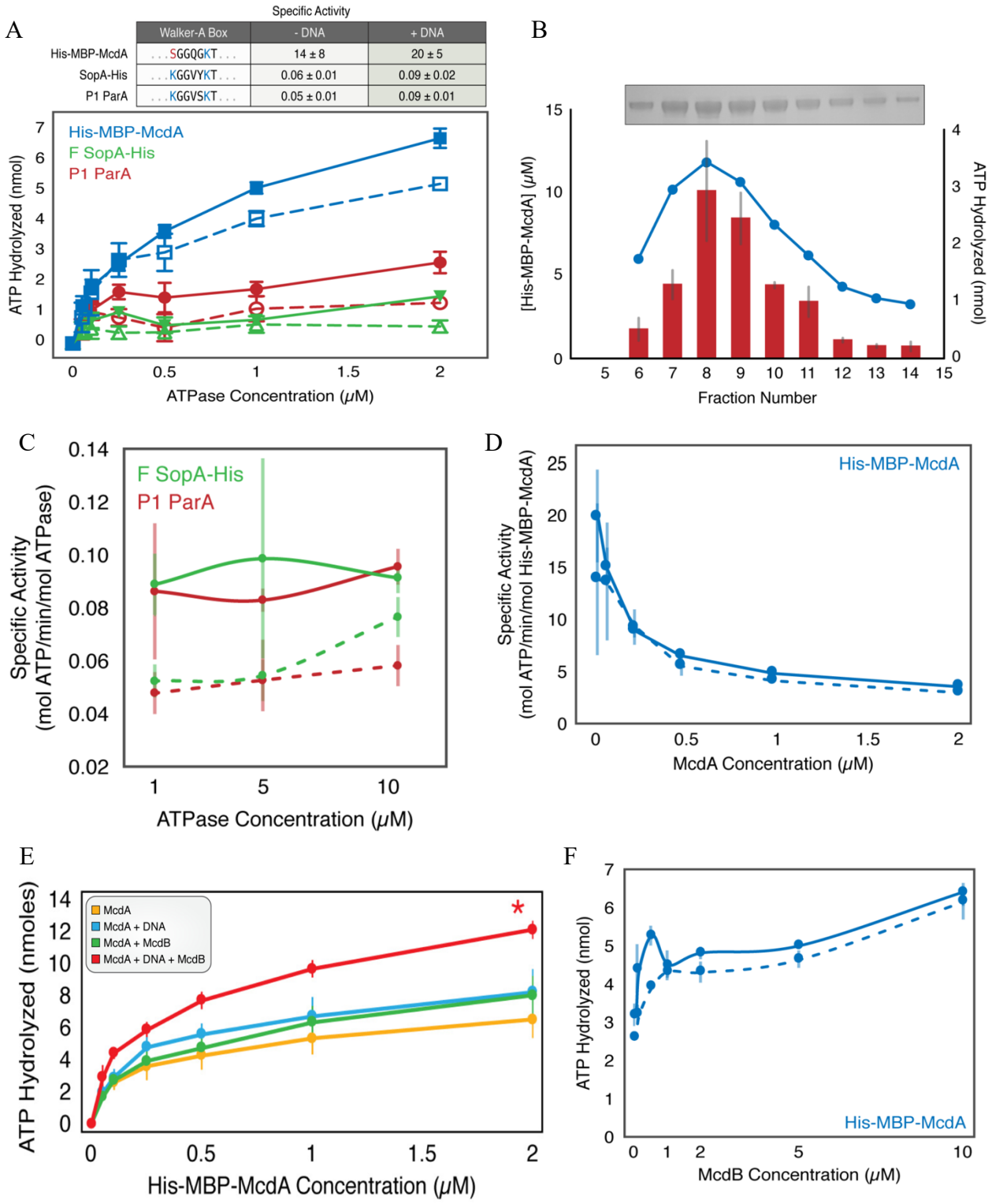


Figure 2.4: **McdA has an uncharacteristically high ATPase activity that is stimulated by nsDNA and McdB.** A. (Top) The deviant Walker A-box motif and specific activities of McdA, F SopA-His and P1 ParA with and without DNA. (Bottom) Comparison of the ATPase activities of His-MBP-McdA, F SopA-His, and P1 ParA in the presence (solid line, filled symbols) and absence

(dashed line, open symbols) of nsDNA. B. Coelution of ATPase activity with His-MBP-McdA concentration. Purified His-MBP-McdA was further purified over a Superdex 200 column. Protein concentration (bar) and ATPase activity (line) were measured for each fraction indicated. Inset shows an SDS-PAGE gel of the purified fractions. C. Comparison of ATPase-specific activity of P1 ParA and F SopA-His in the presence (solid line) and absence (dashed line) of nsDNA. D. Concentration dependency on the specific activity of His-MBP-McdA in the presence (solid line) and absence (dashed line) of nsDNA. E. ATPase activity assays of His-MBP-McdA reveals stimulatory roles of DNA and McdB-His. F. Comparison of the ATPase activity of His-MBP-McdA in the presence of increasing McdB concentration with (solid line) or without (dashed line) nsDNA present. Error bars represent SD from at least three independent experiments.

McdB-His were added simultaneously, the ATPase activity of His-MBP-McdA was further stimulated (Fig. 2.4E). Intriguingly, in comparison to classic examples within the ParA/ParB family, McdB stimulation of McdA ATPase activity is relatively mild (2–3 fold; Fig. 2.4F).

Overall, the unusually high ATPase activity of McdA compared to more canonical ParA family members could be indicative of biochemical adaptations that are important in the trafficking of high-copy protein-based cargos, such as the carboxysome, as opposed to low-copy genetic cargos, such as a plasmid or chromosome.

### 2.3.4 α-McdA self-associates and interacts with monomeric α-McdB

Carboxysomes are categorized into two major groups; β-carboxysomes that are prevalent in cyanobacteria like *S. elongatus* and α-carboxysomes that are present in some chemoautotrophs such as *H. neapolitanus* [10]. MacCready *et al*. suggested that many anoxygenic photosynthetic proteobacteria as well as chemoautotrophic bacteria also possess α-carboxysomes and potentially encode for McdA and McdB within their carboxysome operon [109]. We have recently identified a novel α-McdAB system responsible for positioning α-carboxysomes in *H. neapolitanus* which display some shared characteristics with the β-McdAB system in *S. elongatus* [68]. Similar to what I have done in *S. elongatus*, I sought to determine if α-McdA and α-McdB of *H. neapolitanus* self-

associate and directly interact with each other via B2H assays in *E. coli*. Consistent with ParA family members forming dimers [126], α-McdA was positive for self-association (Fig. 2.5). Also, like the β-McdAB system of *S. elongatus*, α-McdA directly interacts with α-McdB. Surprisingly, however, I found that *H. neapolitanus* α-McdB did not self-associate, whereas *S. elongatus* β-

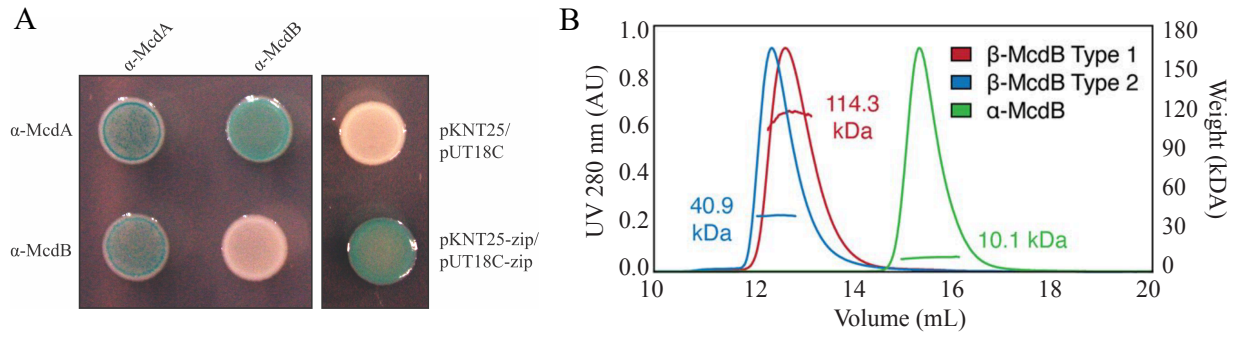


Figure 2.5: **α-McdB interacts with α-McdA.** A. Bacterial-Two Hybrid (B2H) analysis of α-McdA and α-McdB. α-McdA was positive for self-association. α-McdA directly interacts with α-McdB. α-McdB did not self-associate. B2H image is representative of three independent trials. B. SEC-MALS plot for a representative β- McdB Type 1 (*S. elongatus* McdB; monomer MW = 17 kDa), β- McdB Type 2 (*Synechococcus sp. PCC 7002* McdB; monomer MW = 21 kDa), and α- McdB (*H. neapolitanus* McdB; monomer MW = 10 kDa).

McdB strongly self-associates (Fig. 2.3A, B). It is difficult to draw firm conclusions on the lack of McdB self-interaction because the T18/T25 domains may sterically hinder the interaction, or influence protein stability. Therefore, we subsequently performed Size Exclusion Chromatography—Multiple Angle Laser Light Scattering (SEC-MALS) and found that purified *H. neapolitanus* α-McdB, indeed, remains a monomer in solution while β- McdB proteins can form higher-order oligomers (Fig. 2.5B). This difference in α- and β-McdB self-association has implications for understanding how McdB proteins are recruited to structurally distinct α- and β-carboxysomes as well as how McdBs interact with their cognate McdA ATPase on the nucleoid.

## 2.4 Discussion

Carboxysomes are essential components of the photosynthetic metabolism of cyanobacteria, yet the mechanisms underlying their positioning within the cell has remained an outstanding question. Prior work in *S. elongatus* showed that a ParA-like protein (McdA) was required for maintaining carboxysome positioning [53]. Our model of self-organized carboxysome positioning is both informed by the ParA-based mechanisms used to segregate low-copy number plasmids, but also provides a novel platform to study the dynamics of self-organized protein segregation systems. Low-copy plasmids often contain DNA regions (e.g. *parS*) that are bound by ParB. The resulting nucleoprotein complex drives the directed and persistent movement of the plasmid or chromosome cargo by chasing increased concentrations of ParA on the nucleoid [85], [99]. In this way, it is proposed that ParA can provide a positional cue allowing genetic cargo to 'surf' along the larger bacterial chromosome without the use of a separate cytoskeletal system [127].

Here, I observe activities for McdA that are consistent with other ParA family members, including ATP-dependent DNA binding (Fig. 2.2A-B), self-association (Fig. 2.3A-B), and ATPase activity stimulated by DNA and its partner protein (Fig. 2.4E). Taken together, these results suggest that McdA attaches to the nucleoid body at the center of the cell, using it as a scaffolding surface to support an ATP-driven oscillating wave from one end of the cell to the other [31]. In this chapter, I also provide evidence that carboxysomes are dynamically tethered to the nucleoid through interactions between carboxysome-associated McdB and nucleoid-bound McdA. These results provide our first insights into the molecular mechanism of carboxysome positioning by the McdAB system, and provide the first biochemical characterization in the literature of this unusual ParA-family member.

### 2.4.1 McdA is a ParA-like ATPase that utilizes the nucleoid to position McdB-bound carboxysomes

While conceptual similarities exist between ParAB-based plasmid partitioning and McdAB-based carboxysome positioning, a number of key distinctions separate the proposed mechanisms of action. *S. elongatus* McdA lacks the signature lysine residue in the Walker A box that defines the ParA family of ATPases (KGGXXGT; Fig. 2.4A). The serine substitution in McdA at a position universally conserved in ParA members may underlie the unusually high ATPase activity of McdA (Fig. 2.4A), which displays a maximum specific activity that is roughly two orders of magnitude greater than that of other well-studied ParA systems [85], [128]. McdB is an even more divergent protein, bearing no identifiable sequence similarity to any known ParB proteins; indeed, no homologous proteins have been characterized in other species [109]. This novel protein also recognizes and binds a large protein-based cargo (carboxysomes; Fig. 2.3C), further distinguishing it from all characterized ParB-like proteins that recognize genetic cargo [109]. Even though McdB and ParB share no similarity, I find that McdB: (i) interacts with McdA (Fig. 2.3A), (ii) stimulates McdA ATPase activity (Fig. 2.3E-F) and (iii) removes McdA from DNA (Fig. 2.2C); analogous roles played by ParB in well-characterized plasmid partitioning systems. In addition, we observed in our previous work that a pool of McdB enriched at the carboxysome is necessary to locally deplete McdA, suggesting that prolonged McdB activity may stimulate the local release of McdA from the nucleoid. We propose that McdB is therefore acting to interface carboxysomes with nucleoid-bound McdA, processively pulling this protein cargo towards the highest local McdA concentration, and thereupon stimulating McdA ATPase activity and release. The parallels between features of the McdAB system and Brownian-ratchet ParAB models make it tempting to speculate that McdB has a distinct evolutionary origin from ParB-family members, but that these

independent protein families convergently evolved to use dynamic gradients of ParA-like proteins on the nucleoid to segregate entirely different classes of macromolecular structures [109].

### 2.4.2 McdB as the localized adaptor protein that mediates McdA's interaction with α- and β-carboxysomes

The colocalization between mNG-McdB and carboxysomes (RbcS-mTQ) (Fig. 1.4B), coupled with the carboxysome requirement for providing site-specificity to mNG-McdB *in vivo*, provide strong evidence that McdB is associating with carboxysomes and that this interaction is needed for emergent dynamics of McdA (Fig. 1.4A, Movie 1.1). It is curious that McdB is able to associate with a number of different shell proteins as shown my B2H assay (Fig. 2.3C). The most parsimonious hypothesis is that McdB-carboxysome shell interactions are mediated by structural and/or charge features common to many distinct shell proteins. Indeed, evolutionarily distant hexameric shell proteins of the bacterial microcompartment (BMC-H) family share a number of similarities in structural features and key residues at hexamer interfaces that are largely conserved [29], [129], [130]. This suggests some of these common structural features could be important in mediating interactions with McdB, which might explain why McdB displays an interaction with different shell protein paralogs. My B2H analysis also indicates that McdB may have a higher affinity to some shell proteins (CcmK2 and CcmK3) than others (CcmK4, CcmL and CcmO) (Fig. 2.3C). This may be related to the observation of clustered carboxysomes in Δ*ccmK3-4* mutants [34], as this may reduce the amount of McdB recruited to the carboxysome surface. We note however, that given McdB's poor sequence conservation [109] and without further knowledge of the structure and interaction domains of McdB, we cannot rule out that McdB is a 'sticky' protein by the B2H assay (Fig. 2.3C) and is instead recruited through an alternative adaptor protein to the

vicinity of carboxysomes. Moreover, deleting individual shell components, such as CcmK2, CcmL or CcmO, prevents mature carboxysomes formation and subsequent biogenesis [33], preventing *in vivo* testing of McdB/carboxysomes interaction. Additional experiments will be required to identify the domain(s) that mediate McdB-carboxysome shell interaction, and without a more detailed analysis, it remains possible that McdB can directly integrate within the shell of mature carboxysomes. Some indirect evidence would argue against the possibility that McdB is an integral shell protein, including both our observation that Δ*mcdB* strains did not possess a high $CO_2$-requiring phenotype and McdB has not been identified in previously published carboxysome purification studies [5].

Protein sequence analysis of α-McdB proteins suggested that they are almost completely disordered meanwhile β-McdB proteins are predicted to possess coiled-coil regions, suggesting that these proteins form oligomers [68]. Purified *S. elongatus* Type 1 β-McdB has been shown to form a hexamer complex [68] meanwhile *H. neapolitanus* α-McdB remained a monomer (Fig. 2.5B). These findings are consistent with my B2H data, where β-McdB of *S. elongatus* strongly self-associates (Fig. 2.3A-B), whereas *H. neapolitanus* α- McdB showed no self-association (Fig. 2.5A). We conclude that the predicted coiled-coil domains exclusive to β-McdB proteins are likely required for oligomerization and are important for β-carboxysome positioning and function, whereas α-McdB proteins function as monomers.

Collectively, my results in this chapter have important implications for understanding the biochemical characteristics of diverse McdA and McdB proteins as it relates to structurally and phyletically distinct α- and β-carboxysomes, and also have much broader implications for understanding the equidistant positioning of diverse catabolic BMCs across the bacterial domain.

## 2.5 Materials and Methods

### 2.5.1 Bacterial Two-Hybrid Analysis

N- and C-terminal T18 and T25 fusions of McdA, McdB and shell proteins CcmK2, CcmK3, CcmK4, CcmL, CcmO and CcmP were constructed using plasmid pKT25, pKNT25, pUT18C and pUT18, sequence-verified and co-transformed into *E. coli* BTH101 in all pairwise combinations [131]. Several colonies of T18/T25 cotransformants were isolated and grown in LB medium with 100mg/ml ampicillin, 50mg/ml kanamycin and 0.5 mM IPTG overnight at 30°C with 225rpm shaking. Due to the self-assembling nature of carboxysome shell proteins, overnight IPTG induction for cotransformants bearing T18/T25 shell protein fusions was carried out at 0.1 mM IPTG. Overnight cultures were spotted on indicator MacConkey plates supplemented with 100mg/ml ampicillin, 50mg/ml kanamycin and 0.5 mM IPTG. Plates were incubated at 30°C up to 48 hr before imaging.

### 2.5.2 6xHis-MBP-McdA expression and purification

Due to insolubility issues encountered when expressing McdA fusions, a construct was designed where a 6xHis-MBP-tag was encoded upstream of a Tobacco Etch Virus (TEV) cleavage site and fused to the N-terminus of the *mcdA* gene in a pET15b expression backbone to create pAH2 plasmid. pAH2 was transformed into ArcticExpress (DE3) competent cells (Agilent) and protein expression was carried out by growing transformants at 37°C and 225 rpm until an OD600 of 0.6–0.8 was reached. Following an ice bath plunge to lower the culture temperature to 15°C, protein expression was induced with the addition of 0.5 mM IPTG. Induction was allowed to continue overnight at 15°C. The cells were pelleted, flash frozen with liquid nitrogen, and stored at -80℃. Cells were then lysed in Buffer A (50 mM HEPES pH 7.6, 50 mM KCl, 10% glycerol, 20 mM

imidazole pH 7.4, 5 mM BME, 50 mg/ml lysozyme, 1.25 kU benzonase, 2 protease inhibitor cocktail tablets) using a probe sonicator with 15 s on, 15 s off pulsation for 8 min. Cell debris was removed by centrifugation at 14,000 rpm for 40 min in a FiberliteTM F15-8 x 50 cy Fixed Angle Rotor (ThermoFisher Scientific) and the resulting lysate was filtered through a 0.45 mm syringe filter prior to being loaded onto a HiTrap$^{TM}$Q HP 5 ml cassette (GE) connected in tandem to a 5 ml HiTrap$^{TM}$ TALON Crude cassette (GE). The protein was eluted from the Q cassette with a 50 mM – 1 M KCl gradient in an anion exchange chromatography step. The His-tagged protein was then eluted from the TALON column with a 20 mM –1M imidazole gradient. Peak fractions were pooled, concentrated and further separated by gel filtration on a Superdex200 10/300 GL column (GE) pre-equilibrated with 50 mM HEPES pH 7.6, 50 mMKCl, 10% glycerol, 5 mM DTT. Individual peak fractions were concentrated to no higher than 20mM and frozen aliquots were kept at -80°C.

### 2.5.3 ATPase Assay

ATPase assays were performed in a buffer containing 50 mM HEPES (pH 7.6), 10 mM $MgCl_2$, 100mM KCl, 0.1 mg/ml BSA, 2 mM DTT, and 0.1 mg/ml sonicated salmon sperm DNA (when present). Unlabeled ATP was spiked with [g-32P]-ATP and purified from contaminating $^{32}P_i$ prior to use with a 1 ml gel filtration (P-2 fine resin, Bio-Rad) column. The radiolabeled ATP mix was added to reactions at 1 mM. Reactions were assembled on ice at the protein concentrations indicated, with His-MBP-McdA, McdA-GFP-His, F SopA-His or P1 ParA being added last. The 20 µl reactions were incubated for 1 hr at 30℃ and immediately quenched by adding 10 ml of a 1% SDS, 20 mM EDTA solution. Two microliters of the quenched reactions were spotted and analyzed by thin-layer chromatography as previously described [132]. Due to the feeble ATPase

activities of SopA-His and P1 ParA, specific activities were determined from experiments carried out as shown above, but the 30°C incubation period was carried out for 3 hr.

### 2.5.4 DNA binding assay

Electrophoretic mobility shift assays (EMSAs) were performed in a final reaction volume of 10 µl in a buffer containing 50 mM HEPES (pH 7.6), 5 mM $MgCl_2$, and 100 mM KCl with 10 nM pUC19 plamsid (2.8 kb) as the DNA substrate. At the concentrations indicated, His-MBP-McdA was incubated for 30 min at 23°C with ADP, ATP or ATPgS (1 mM). When used, McdB-His was added at the concentrations specified. Reactions were then mixed with 1 µl 80% glycerol, run on 1% agarose gel in 1X TAE at 110V for 45 min and stained with ethidium bromide for imaging. The peak fractions representing the dimer form of His-MBP-McdA from Superdex200 size exclusion chromatography were used.

### 2.5.5 Size-exclusion chromatography with multi- angle light scattering (SEC–MALS)

Five hundred µl of the α-McdB at 1.5 mg/ml was passed over an SEC column (Superdex 200 Increase 10/300 GL; GE Healthcare Life Sciences) at a flow rate of 0.15 ml/min in buffer (50 mM Tris-HCl pH 8.5, 150 mM KCl, 5 mM BME) at 4°C. Following SEC, the sample were analyzed using an A280 UV detector (AKTA pure; GE Healthcare Life Sciences), the DAWN HELEOS-II MALS detector (Wyatt Technology), and the Optilab rEX refractive index detector (Wyatt Technology). The data were analyzed to calculate mass using ASTRA software (Wyatt Technology). Bovine serum albumin was used as the standard for calibration.

## 2.6 Acknowledgements

We would like to thank the labs of Dr. Matthew Chapman and Dr. Kiyoshi Mizuuchi labs for use of equipment and reagents, as well as Dr. Cheryl Kerfeld and Dr. Beronda Montgomery for helpful conversations and suggestions. The pET15b expression vector used for His-MBP fusion to McdA was a kind gift from Dr. Maria Schumacher. We would also like to thank Dr. JK Nandakumar for assistance in the SEC- MALS experiments. Purified P1 ParA and F SopA-His were kind gifts from the Funnell and Mizuuchi labs respectively. This work was supported by the National Science Foundation (Award Numbers 1517241; to KWO and DCD and 1817478 and 1941966; to AGV), NSF GRFP Award to L.T. (DGE 1841052), Rackham Graduate Student Research Grant to L.T, the Michigan Life Sciences Fellows Program to J.S.M. and by research initiation funds to AGV provided by the MCDB Department, University of Michigan. Additional institutional and equipment support was provided by Office of Basic Energy Sciences, Office of Science, US Department of Energy (DE–FG02–91ER20021; to DCD).

## 2.7 References

[1] T. A. Leonard, P. J. Butler, and J. Lowe, "Bacterial chromosome segregation: structure and DNA binding of the Soj dimer - a conserved biological switch," *Embo J*, vol. 24, no. 2, pp. 270–282, 2005, doi: 10.1038/sj.emboj.7600530.
[2] C. M. Hester and J. Lutkenhaus, "Soj (ParA) DNA binding is mediated by conserved arginines and is essential for plasmid segregation," *Proc National Acad Sci*, vol. 104, no. 51, pp. 20326–20331, 2007, doi: 10.1073/pnas.0705196105.
[3] J. Castaing, J. Bouet, and D. Lane, "F plasmid partition depends on interaction of SopA with non-specific DNA," *Mol Microbiol*, vol. 70, no. 4, pp. 1000–1011, 2008, doi: 10.1111/j.1365-2958.2008.06465.x.
[4] A. G. Vecchiarelli *et al.*, "ATP control of dynamic P1 ParA–DNA interactions: a key role for the nucleoid in plasmid partition," *Mol Microbiol*, vol. 78, no. 1, pp. 78–91, 2010, doi: 10.1111/j.1365-2958.2010.07314.x.
[5] T. Hatano and H. Niki, "Partitioning of P1 plasmids by gradual distribution of the ATPase ParA," *Mol Microbiol*, vol. 78, no. 5, pp. 1182–1198, 2010, doi: 10.1111/j.1365-2958.2010.07398.x.

[6] M. Sengupta, H. J. Nielsen, B. Youngren, and S. Austin, “P1 Plasmid Segregation: Accurate Redistribution by Dynamic Plasmid Pairing and Separation ▿ †,” *J Bacteriol*, vol. 192, no. 5, pp. 1175–1183, 2010, doi: 10.1128/jb.01245-09.
[7] A. L. Gall *et al.*, “Bacterial partition complexes segregate within the volume of the nucleoid,” *Nat Commun*, vol. 7, no. 1, p. 12107, 2016, doi: 10.1038/ncomms12107.
[8] D. F. Savage, B. Afonso, A. H. Chen, and P. A. Silver, “Spatially Ordered Dynamics of the Bacterial Carbon Fixation Machinery,” *Science*, vol. 327, no. 5970, pp. 1258–1261, 2010, doi: 10.1126/science.1186090.
[9] J. S. MacCready *et al.*, “Protein gradients on the nucleoid position the carbon-fixing organelles of cyanobacteria,” *Elife*, vol. 7, p. e39723, 2018, doi: 10.7554/elife.39723.
[10] E. V. Koonin, “A Superfamily of ATPases with Diverse Functions Containing Either Classical or Deviant ATP-binding Motif,” *J Mol Biol*, vol. 229, no. 4, pp. 1165–1174, 1993, doi: 10.1006/jmbi.1993.1115.
[11] J. Lutkenhaus, “The ParA/MinD family puts things in their place,” *Trends Microbiol*, vol. 20, no. 9, pp. 411–418, 2012, doi: 10.1016/j.tim.2012.05.002.
[12] I. H. Jain, V. Vijayan, and E. K. O’Shea, “Spatial ordering of chromosomes enhances the fidelity of chromosome partitioning in cyanobacteria,” *P Natl Acad Sci Usa*, vol. 109, no. 34, pp. 13638–43, 2012, doi: 10.1073/pnas.1211144109.
[13] J. S. MacCready, J. L. Basalla, and A. G. Vecchiarelli, “Origin and Evolution of Carboxysome Positioning Systems in Cyanobacteria,” *Mol Biol Evol*, 2020, doi: 10.1093/molbev/msz308.
[14] J. S. MacCready, L. Tran, J. L. Basalla, P. Hakim, and A. G. Vecchiarelli, “The McdAB system positions α-carboxysomes in proteobacteria,” *Mol Microbiol*, 2021, doi: 10.1111/mmi.14708.
[15] M. Griese, C. Lange, and J. Soppa, “Ploidy in cyanobacteria,” *Fems Microbiol Lett*, vol. 323, no. 2, pp. 124–131, 2011, doi: 10.1111/j.1574-6968.2011.02368.x.
[16] M. A. Davis, K. A. Martin, and S. J. Austin, “Biochemical activities of the ParA partition protein of the P1 plasmid,” *Mol Microbiol*, vol. 6, no. 9, pp. 1141–1147, 1992, doi: 10.1111/j.1365-2958.1992.tb01552.x.
[17] J. Bouet and B. E. Funnell, “P1 ParA interacts with the P1 partition complex at parS and an ATP–ADP switch controls ParA activities,” *Embo J*, vol. 18, no. 5, pp. 1415–1424, 1999, doi: 10.1093/emboj/18.5.1415.
[18] J.-Y. Bouet, J. A. Surtees, and B. E. Funnell, “Stoichiometry of P1 Plasmid Partition Complexes*,” *J Biol Chem*, vol. 275, no. 11, pp. 8213–8219, 2000, doi: 10.1074/jbc.275.11.8213.
[19] B. M. Long, M. R. Badger, S. M. Whitney, and G. D. Price, “Analysis of Carboxysomes from Synechococcus PCC7942 Reveals Multiple Rubisco Complexes with Carboxysomal Proteins CcmM and CcaA*,” *J Biol Chem*, vol. 282, no. 40, pp. 29323–29335, 2007, doi: 10.1074/jbc.m703896200.
[20] S. S.-W. Cot, A. K.-C. So, and G. S. Espie, “A Multiprotein Bicarbonate Dehydration Complex Essential to Carboxysome Function in Cyanobacteria ▿ †,” *J Bacteriol*, vol. 190, no. 3, pp. 936–945, 2008, doi: 10.1128/jb.01283-07.
[21] B. M. Long, L. Tucker, M. R. Badger, and G. D. Price, “Functional Cyanobacterial β-Carboxysomes Have an Absolute Requirement for Both Long and Short Forms of the CcmM Protein,” *Plant Physiol*, vol. 153, no. 1, pp. 285–293, 2010, doi: 10.1104/pp.110.154948.
[22] J. C. Cameron, S. C. Wilson, S. L. Bernstein, and C. A. Kerfeld, “Biogenesis of a Bacterial Organelle: The Carboxysome Assembly Pathway,” *Cell*, vol. 155, no. 5, pp. 1131–1140, 2013, doi: 10.1016/j.cell.2013.10.044.

[23] J. N. Kinney, A. Salmeen, F. Cai, and C. A. Kerfeld, "Elucidating Essential Role of Conserved Carboxysomal Protein CcmN Reveals Common Feature of Bacterial Microcompartment Assembly*," *J Biol Chem*, vol. 287, no. 21, pp. 17729–17736, 2012, doi: 10.1074/jbc.m112.355305.
[24] C. Fan, S. Cheng, S. Sinha, and T. A. Bobik, "Interactions between the termini of lumen enzymes and shell proteins mediate enzyme encapsulation into bacterial microcompartments," *Proc National Acad Sci*, vol. 109, no. 37, pp. 14995–15000, 2012, doi: 10.1073/pnas.1207516109.
[25] S. Tanaka *et al.*, "Atomic-Level Models of the Bacterial Carboxysome Shell," *Science*, vol. 319, no. 5866, pp. 1083–1086, 2008, doi: 10.1126/science.1151458.
[26] S. Tanaka, M. R. Sawaya, M. Phillips, and T. O. Yeates, "Insights from multiple structures of the shell proteins from the β-carboxysome," *Protein Sci*, vol. 18, no. 1, pp. 108–120, 2009, doi: 10.1002/pro.14.
[27] B. D. Rae, B. M. Long, M. R. Badger, and G. D. Price, "Structural Determinants of the Outer Shell of β-Carboxysomes in Synechococcus elongatus PCC 7942: Roles for CcmK2, K3-K4, CcmO, and CcmL," *Plos One*, vol. 7, no. 8, p. e43871, 2012, doi: 10.1371/journal.pone.0043871.
[28] F. Cai, M. Sutter, J. C. Cameron, D. N. Stanley, J. N. Kinney, and C. A. Kerfeld, "The Structure of CcmP, a Tandem Bacterial Microcompartment Domain Protein from the β-Carboxysome, Forms a Subcompartment Within a Microcompartment," *J Biol Chem*, vol. 288, no. 22, pp. 16055–16063, 2013, doi: 10.1074/jbc.m113.456897.
[29] B. D. Rae, B. M. Long, M. R. Badger, and G. D. Price, "Functions, Compositions, and Evolution of the Two Types of Carboxysomes: Polyhedral Microcompartments That Facilitate CO2 Fixation in Cyanobacteria and Some Proteobacteria," *Microbiol Mol Biol R*, vol. 77, no. 3, pp. 357–379, 2013, doi: 10.1128/mmbr.00061-12.
[30] M. A. Schumacher, "Structural biology of plasmid segregation proteins," *Curr Opin Struc Biol*, vol. 17, no. 1, pp. 103–109, 2007, doi: 10.1016/j.sbi.2006.11.005.
[31] M. A. Schumacher, M. Henderson, and H. Zhang, "Structures of maintenance of carboxysome distribution Walker-box McdA and McdB adaptor homologs.," *Nucleic Acids Res*, vol. 47, no. 11, pp. 5950–5962, 2019, doi: 10.1093/nar/gkz314.
[32] A. G. Vecchiarelli, K. Mizuuchi, and B. E. Funnell, "Surfing biological surfaces: exploiting the nucleoid for partition and transport in bacteria," *Mol Microbiol*, vol. 86, no. 3, pp. 513–523, 2012, doi: 10.1111/mmi.12017.
[33] Y. Ah-Seng, F. Lopez, F. Pasta, D. Lane, and J.-Y. Bouet, "Dual Role of DNA in Regulating ATP Hydrolysis by the SopA Partition Protein*," *J Biol Chem*, vol. 284, no. 44, pp. 30067–30075, 2009, doi: 10.1074/jbc.m109.044800.
[34] F. Cai, M. Sutter, S. L. Bernstein, J. N. Kinney, and C. A. Kerfeld, "Engineering Bacterial Microcompartment Shells: Chimeric Shell Proteins and Chimeric Carboxysome Shells," *Acs Synth Biol*, vol. 4, no. 4, pp. 444–453, 2015, doi: 10.1021/sb500226j.
[35] M. Sommer, F. Cai, M. Melnicki, and C. A. Kerfeld, "β-Carboxysome bioinformatics: identification and evolution of new bacterial microcompartment protein gene classes and core locus constraints," *J Exp Bot*, vol. 68, no. 14, pp. 3841–3855, 2017, doi: 10.1093/jxb/erx115.
[36] E. J. Young *et al.*, "Engineering the Bacterial Microcompartment Domain for Molecular Scaffolding Applications," *Front Microbiol*, vol. 8, p. 1441, 2017, doi: 10.3389/fmicb.2017.01441.
[37] M. Faulkner *et al.*, "Direct characterization of the native structure and mechanics of cyanobacterial carboxysomes," *Nanoscale*, vol. 9, no. 30, pp. 10662–10673, 2017, doi: 10.1039/c7nr02524f.

[38] G. Karimova, J. Pidoux, A. Ullmann, and D. Ladant, “A bacterial two-hybrid system based on a reconstituted signal transduction pathway,” *Proc National Acad Sci*, vol. 95, no. 10, pp. 5752–5756, 1998, doi: 10.1073/pnas.95.10.5752.
[39] E. Fung, J. Bouet, and B. E. Funnell, “Probing the ATP-binding site of P1 ParA: partition and repression have different requirements for ATP binding and hydrolysis,” *Embo J*, vol. 20, no. 17, pp. 4901–4911, 2001, doi: 10.1093/emboj/20.17.4901.

# CHAPTER III

## Dissection of the ATPase Active Site of McdA Reveals the Sequential Steps Essential for Carboxysome Distribution

This chapter is based in full on the previously published article listed below. Y Hoang conducted the experiment and data analysis to generate Figures 3.3A and portions of Figure 3.5C. I performed all other experiments and data analysis shown in this chapter.

P. Hakim, Y. Hoang and A.G. Vecchiarelli, "Dissection of the ATPase active site of McdA reveals the sequential steps essential for carboxysome distribution". *Mol Biol Cell,* vol. 32, no. 20, pp. 1–14, 2021, doi:10.1091/mbc.E21-03-015.

### 3.1 Abstract

Carboxysomes, the most prevalent and well-studied anabolic bacterial microcompartment, play a central role in efficient carbon fixation by cyanobacteria and proteobacteria. In previous studies (see Chapter 2), we identified the two-component system called McdAB that spatially distributes carboxysomes across the bacterial nucleoid. McdA, partition protein A (ParA)-like ATPase, forms a dynamic oscillating gradient on the nucleoid in response to the carboxysome-localized McdB. As McdB stimulates McdA ATPase activity, McdA is removed from the nucleoid in the vicinity of carboxysomes, propelling these proteinaceous cargos toward regions of highest McdA

concentration via a Brownian-ratchet mechanism. How the ATPase cycle of McdA governs its *in vivo* dynamics and carboxysome positioning remains unresolved. Here, by strategically introducing amino acid substitutions in the ATP-binding region of McdA, I sequentially trap McdA at specific steps in its ATP cycle. I map out critical events in the ATPase cycle of McdA that allows the protein to bind ATP, dimerize, change its conformation into a DNA-binding state, interact with McdB-bound carboxysomes, hydrolyze ATP, and release from the nucleoid. I also find that McdA is a member of a previously unstudied subset of ParA family ATPases, harboring unique interactions with ATP and the nucleoid for trafficking their cognate intracellular cargos.

## 3.2 Introduction

ParA family members are defined by the presence of a deviant Walker A motif, along with Walker A' and Walker B motifs [4]. Aside from these motifs that make up the ATP-binding pocket, few similarities exist at the sequence level. But structurally, all ParA family members solved to date form very similar nucleotide-sandwich dimers [5], [6], [7]. ATP binding stabilizes dimerization because of an invariant "signature" lysine residue that defines the deviant Walker A box, which makes cross-contacts with the γ-phosphate of the opposing monomer making up the sandwich dimer [8].

A growing list of protein-based cargos have been shown to also require a ParA-type ATPase for their subcellular organization, including carboxysomes [1], [2]. In 2010, Savage and colleagues showed that a ParA-like ATPase, now termed Maintenance of carboxysome distribution protein A (McdA), was required for the equidistant positioning of carboxysomes down the length of the rod-shaped cyanobacterium *Synechococcus elongatus* PCC 7942 (henceforth *S. elongatus*) [26]. More recently, I found that McdA functions with a partner protein, called McdB,

which I found associates with the carboxysome cargo and is required for the dynamic oscillatory behavior of McdA *in vivo* [27] (see Chapter 2). ATP-bound McdA has nonspecific DNA-binding activity and McdB stimulates McdA ATPase activity as well as its release from a nsDNA substrate *in vitro*. From these biochemical findings, I proposed that McdB-bound carboxysomes locally stimulate the release of McdA from the nucleoid, and the resulting McdA gradients are then used to drive the movement and equidistant positioning of carboxysomes across the nucleoid region of the cell; akin to DNA partitioning by ParABS systems. However, it remains to be determined how the ATP cycle of McdA governs the molecular events required for its dynamic oscillatory patterning and the positioning of McdB-bound carboxysomes across the nucleoid.

There are notable differences that set *S. elongatus* McdA apart from classical ParA family ATPases. For example, the signature lysine residue that defines the ParA family is absent in the deviant Walker A box of McdA. Also intriguing was my finding that McdA possesses a substantially higher ATPase activity compared with ParA ATPases involved in DNA partitioning [15], [27], [28] (See Chapter 2). These differences drove us to dissect the molecular events of carboxysome positioning by McdA and identify how these steps are coupled to its ATP cycle.

Despite these differences, it was recently shown that an McdA homolog shares the adenine-nucleotide sandwich dimer structure solved for several other ParA family ATPases [6] (Fig. 3.1A). Additionally, many of the invariant amino acids critical for ATP-dependent functions are also conserved in McdA, with the exception of the signature lysine residue in the Walker A box (Fig. 3.1A-B). To dissect how ATP binding and hydrolysis mediates McdA function in carboxysome positioning, I introduced strategic amino acid substitutions in the ATP-binding pocket of McdA. The mutations are synonymous with “trap” mutants made in several well-studied ParA family members involved in the positioning of plasmids [15], [20], [29]–[31], chromosomes [32], the

divisome [33]–[35], flagella [36], [37], and chemotaxis clusters [38], [39] (Fig. 3.1C). The data presented in this chapter connect key steps in the ATP cycle of McdA to the stepwise events required for distributing McdB-bound carboxysomes across the cyanobacterial nucleoid.

## 3.3 Results

### 3.3.1 Strategy for trapping and imaging McdA at specific steps of its ATPase cycle

I performed *in vivo* fluorescence microscopy to determine how McdA dynamics and carboxysome organization were altered for McdA mutants predicted to be trapped at specific steps of its ATP cycle based on synonymous mutants of biochemically characterized ParAs (Fig 3.1C). To visualize carboxysomes, as also shown in Chapter 2, the fluorescent protein monomeric Turquoise2 (mTQ) was fused to the C-terminus of the small subunit of the Rubisco enzyme (RbcS) yielding RbcS-mTQ. RbcS-mTQ was expressed using a second copy of its native promoter, inserted at neutral site 1 (NS1) in addition to wild-type *rbcS* at its native locus. NS1 is a well-characterized integration site on the *S. elongatus* chromosome where insertions have been shown to have no significant effects on cellular physiology [40]. To simultaneously image the McdA trap mutants in our carboxysome reporter strain, the amino acid substitutions were made in the ATP-binding pocket of our McdA variant that was N-terminally fused to the fluorescent protein monomeric NeonGreen (mNG) [41]. As shown in Chapter 2, mNG-McdA is fully functional for carboxysome positioning when expressed as the only copy of McdA at its native locus [27]. Finally, I also performed phase-contrast imaging to monitor for changes in cell morphology, as we have recently shown that carboxysome mispositioning in *mcdA* or *mcdB* deletion strains triggers cell elongation, which we proposed is a response to carbon limitation in this obligate photoautotroph [42].

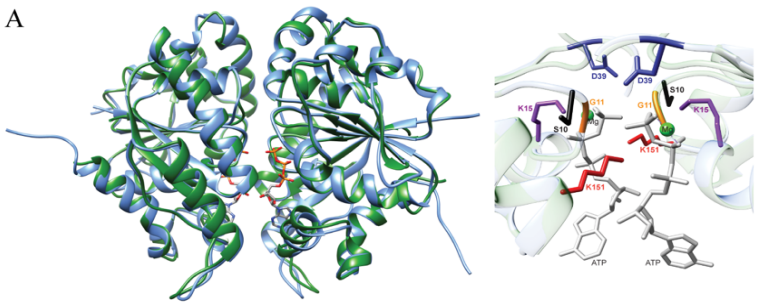


B

| Cargo | | | Walker A | Walker A' | Walker B |
|---|---|---|---|---|---|
| Plasmid | *E. coli* | P1 ParA | KGGVSKT | ILVIDLD-PQ | DFILVD |
| Plasmid | *E. coli* | F SopA | KGGVYKT | VLLVEGNDPQ | DVIVID |
| Chromosome | *B. subtilis* | Soj | KGGVGKT | VLLVDID-PQ | DYIIID |
| Chromosome | *C. crescentus* | ParA | KGGVGKT | VLLIDAD-PQ | TYVLID |
| Divisome | *E. coli* | MinD | KGGVGKT | TVVIDFDIGL | EFIVCD |
| Divisome | *C. crescentus* | MipZ | KGGAGKS | VAVIDLDLRQ | DFILID |
| Divisome | *M. xanthus* | PomZ | KGGTGKT | VLLIDLD-SQ | DVVVFD |
| Flagella | *V. alginolyticus* | FlhG | KGGVGKS | VMVLDADLGL | DVLLID |
| Chemotaxis cluster | *R. sphaeroides* | PpfA | KGGVGKT | VLLVDLD-PQ | DWVLID |
| Chemotaxis cluster | *V. cholerae* | ParC | KGGVGKT | VLMVDTD-PH | DYVLID |
| **Carboxysome** | ***S. elongatus*** | **McdA** | SGGQGKT | VLMIDAD-PQ | DFCVID |

Signature Lysine
Invariant Glycine
Catalytic Lysine
Catalytic Aspartate

C

| Residue | Mutations | ParA ATPase | Phenotype | References |
|---|---|---|---|---|
| Signature Lysine | K to A | MipZ | ATP-binding deficient; Unable to interact with FtsZ; minicell formation | Corrales-Guerrero *et al.* 2020 |
| | | MinD | ATP and lipid-binding deficient, Unable to activate MinC | Zhou *et al.* 2005 |
| | | FlhG | ATP-hydrolysis deficient; Decreased cellular motility | Ono *et al.* 2015 |
| | | *Mx*ParA | Dimerization deficient; Unable to bind DNA | Lin *et al.* 2017 |
| Invariant Glycine | G to V | Soj | ATP-binding proficient; Dimerization-deficient | Leonard *et al.* 2005 |
| | | MipZ | ATP-binding proficient; Dimerization-deficient; Minicell formation | Kiekebusch *et al.* 2012 |
| | | PomZ | ATP-binding proficient; Dimerization-deficient; Cells defective in division | Schumacher *et al.* 2017 |
| | | ParC | ATP-binding proficient; Impaired interaction with ParP and CheA | Ringgaard *et al.* 2011 |
| | | *Cc*ParA | ATP-binding proficient; dimerization deficient | Ptacin *et al.* 2010; 2014 |
| | | *Mx*ParA | Dimerization deficient; Unable to bind DNA | Lin *et al.* 2017 |
| | | PpfA | Impaired binding to TlpT and DNA | Roberts *et al.* 2012 |
| Catalytic Lysine | K to A | Soj | ATP-binding deficient | Leonard *et al.* 2005 |
| | | PpfA | Impaired binding to TlpT and DNA | Roberts *et al.* 2012 |
| | K to Q | P1 ParA | ATP-binding proficient; ATP-dependent confirmation change deficient | Fung *et al.* 2001; Vecchiarelli *et al.* 2010; 2013 |
| | | MipZ | ATP-binding deficient; Minicell formation | Kiekebusch *et al.* 2012 |
| | | PomZ | ATP-binding deficient; Cells defective in division | Schumacher *et al.* 2017 |
| | | ParC | ATP-binding deficient; Impaired interaction with ParP and CheA | Ringgaard *et al.* 2014 |
| | | *Cc*ParA | ATP-binding deficient | Ptacin *et al.* 2010; 2014 |
| | | SopA | Does not oscillate *in vivo*; No SopB-stimulated increase of ATPase activity | Hatano *et al.* 2007; Libante *et al.* 2001 |
| | K to R | P1 ParA | ATP-binding and dimerization proficient; Trapped in ParB-ATP-DNA complex | Fung *et al.* 2001; Hwang & Vecchiarelli *et al.* 2013; Vecchiarelli *et al.* 2013 |
| | | *Mx*ParA | ATP-binding and dimerization proficient; Trapped in ATP-DNA complex | Lin *et al.* 2017 |
| | | SopA | Does not oscillate *in vivo*; Reduced ATPase activity | Hatano *et al.* 2007; Libante *et al.* 2001 |
| | | *Cc*ParA | Incomplete chromosome segregated; Minicells formation | Toro *et al.* 2008 |
| Catalytic Aspartate | D to A | Soj | ATP-binding, dimerization and DNA-binding proficient; ATP-hydrolysis deficient | Leonard *et al.* 2005 |
| | | MipZ | ATP-binding, dimerization and DNA-binding proficient; ATP-hydrolysis deficient; filamentous cells | Thanbichler & Shapiro 2006; Kiekebusch *et al.* 2012; Corrales-Guerrero *et al.* 2020 |
| | | MinD | ATP-binding, dimerization and DNA-binding proficient; ATP-hydrolysis deficient | Park *et al.* 2012 |
| | | PomZ | ATP-binding, dimerization and DNA-binding proficient; ATP-hydrolysis deficient | Treuner-Lange *et al.* 2013; Schumacher *et al.* 2017 |
| | | FlhG | ATP-binding proficient; ATP-hydrolysis deficient | Ono *et al.* 2015; Schuhmacher et al. 2015 |
| | | *Cc*ParA | ATP-binding, dimerization and DNA-binding proficient; ATP-hydrolysis deficient | Ptacin *et al.* 2010; 2014 |
| | | *Mx*ParA | ATP-binding, dimerization and DNA-binding proficient; ATP-hydrolysis deficient | Lin *et al.* 2017 |
| | | PpfA | Trapped in ATP-TlpT-DNA complex | Roberts *et al.* 2012 |

Figure 3.1: **McdA shares structure and sequence conservation with ParA-type ATPases.** A. The crystal structure of *Cyanothece* McdA[D38A] (blue; PDB entry 6nop) was superimposed on to the modeled structure of S. elongatus McdA (green) with ATP molecules (sticks) in the sandwich dimer interface (left). The ATP-binding pocket of McdA showing amino acid residues mutated in this study (right). B. Amino acid sequence alignment of the Walker A, A', and B motifs conserved among ParA family ATPases. Invariant residues are shaded gray. The signature lysine (green), invariant glycine (orange) and catalytic lysine (purple) in the Walker A motif and the catalytic aspartate (blue) in the Walker A' motif were mutated in this study. C. Summary of strategic mutations studied in ParA family members and their associated phenotypes; Cc: *Caulobacter crescentus*, Mx: *Myxococcus xanthus*.

### 3.3.2 Predicted ATP binding and dimerization mutants of McdA are diffuse in the cytoplasm and carboxysomes are mispositioned

I first set out to determine the *in vivo* localization pattern of McdA mutants predicted to be unbound from ATP, and its impact on carboxysome positioning. I substituted the invariant catalytic lysine to an alanine (K15A) or glutamine (K15Q) in the deviant Walker A box of McdA (Fig. 3.1B). Synonymous mutations in several other ParA-type ATPases have been shown to prevent ATP binding (Fig 3.1C). In wild-type *S. elongatus* cells, as shown previously, mNG-McdA oscillates on the nucleoid to equidistantly position RbcS-mTQ-labeled carboxysomes down the long axis of the cell (Fig. 3.2A, Movie 1.1 and 3.1). Both predicted ATP-binding mutants of McdA no longer oscillated on the nucleoid, but rather were found to be diffuse in the cytoplasm and carboxysomes were mispositioned (Fig. 3.2B-C, Movie 3.1). I then substituted the invariant glycine to a valine (G11V) in the deviant Walker A box of McdA (see Fig. 3.1B-C), which allows for ATP binding, but the bulky side-chain of valine sterically prevents dimerization [1]. As with the predicted ATP-binding mutants, the predicted dimerization mutant of McdA was also diffuse in the cytoplasm, and carboxysomes were no longer uniformly distributed in the cell (Fig 3.2D). Immunoblot analysis against McdA showed that these mutants were expressed at levels slightly lower or similar to that of wild type (Fig 3.3A). Therefore, the diffuse localization observed for these variants was not due to cleavage of the fusion proteins. When I compared the nearest-neighbor spacing of carboxysome foci as a function of cell length, wild-type showed the same uniform spacing (0.6 ± 0.2 μm) regardless of cell length (Fig. 3.E-F). All three mutants, on the other hand, displayed increased spacing, and variability in spacing, as cell length increased. The average cell lengths of the predicted ATP-binding and dimerization mutants were significantly longer compared with the

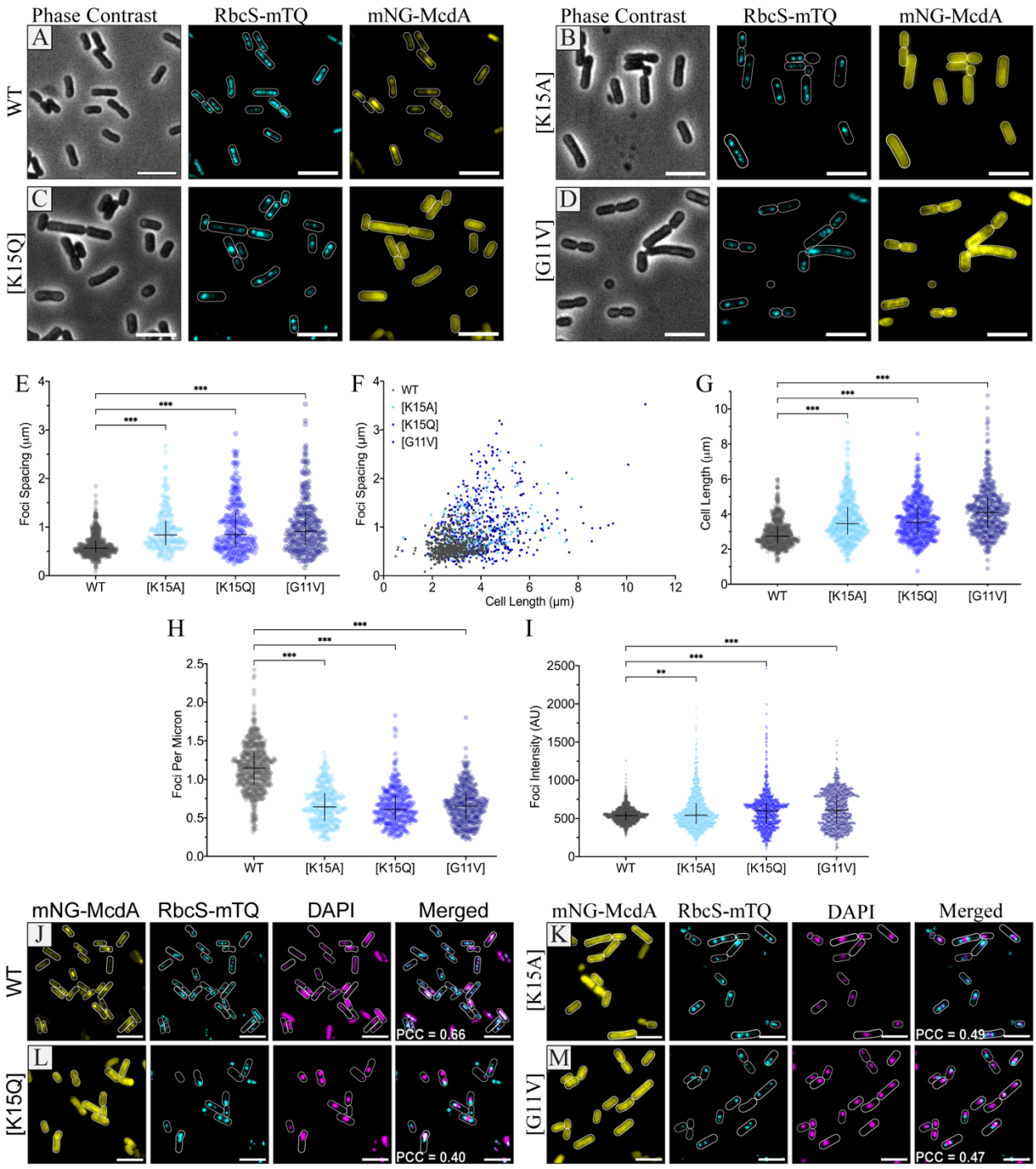


Figure 3.2: **McdA mutants predicted to be deficient in ATP binding and dimerization are unable to interact with the nucleoid and position carboxysomes.** A. mNG-McdA dynamically oscillates and positions carboxysomes labeled with RbcS-mTQ (cyan). B-D. Predicted ATP-binding (K15A and K15Q) and dimerization (G11V) mutants of mNG-McdA no longer oscillate and carboxysomes aggregate. Cell outlines in fluorescent channels are based on the phase-contrast image. E. Spacing between carboxysome foci in the same cell. F. Distribution of spacing between carboxysome foci as a function of cell length. For E and F: WT n = 558 cells; $n$ > 200 cells per

mutant strain. G. Cell lengths of specified strains. WT n = 561 cells; *n* > 400 cells per mutant strain. H. Number of carboxysome foci per unit cell length for each strain. WT n = 578 cells; *n* > 200 cells per mutant strain. I. Carboxysome foci intensity for each cell strain (arbitrary units = AU). WT n = 1925 foci; *n* > 1000 foci per mutant strain. Data represent median with interquartile range. ***p < 0.001, **p < 0.005 by Kruskal–Wallis test. J-M. Microscopy images of cells with ciprofloxacin-compacted nucleoids. mNG-McdA and the specified variants (yellow), carboxysome foci (cyan), and DAPI-stained nucleoids (magenta). Carboxysome and DAPI channels are merged. All PCC values were calculated from the merged RbcS-mTQ and DAPI channels from at least 300 cells per cell population. Scale bars: 5 μm.

wild-type strain (Fig. 3.2G); spacing resulted in fewer carboxysome foci per unit cell length (Fig. 3.2H). Comparing the fluorescence intensity of carboxysome foci suggested that the increased spacing in all three mutant populations was the result of carboxysome aggregation (Fig. 3.2I). Overall, McdA mutant strains predicted to be defective for ATP binding and dimerization displayed a cell elongation phenotype, and possessed few and irregularly spaced carboxysome aggregates. These phenotypes match what I have previously observed in the *mcdA* deletion strain [42], which suggests a complete loss of function in carboxysome positioning when McdA cannot bind ATP and dimerize.

### 3.3.3 ATP binding and dimerization are predicted to be required for McdA to position carboxysomes on the nucleoid

Plasmids deleted for their ParA-type partitioning system are no longer distributed along the nucleoid. Rather, the plasmids become nucleoid "excluded" [2], [43], [44]. I have shown that nucleoid exclusion also occurs for carboxysomes in *S. elongatus* strains deleted for *mcdA* [27]. I set out to determine if carboxysomes are nucleoid excluded in the predicted ATP-binding and dimerization mutants of McdA. Due to the polyploid nature of *S. elongatus*, DAPI staining does not easily resolve the nucleoid region from the cytoplasm (Fig. 3.3C). I therefore used the gyrase

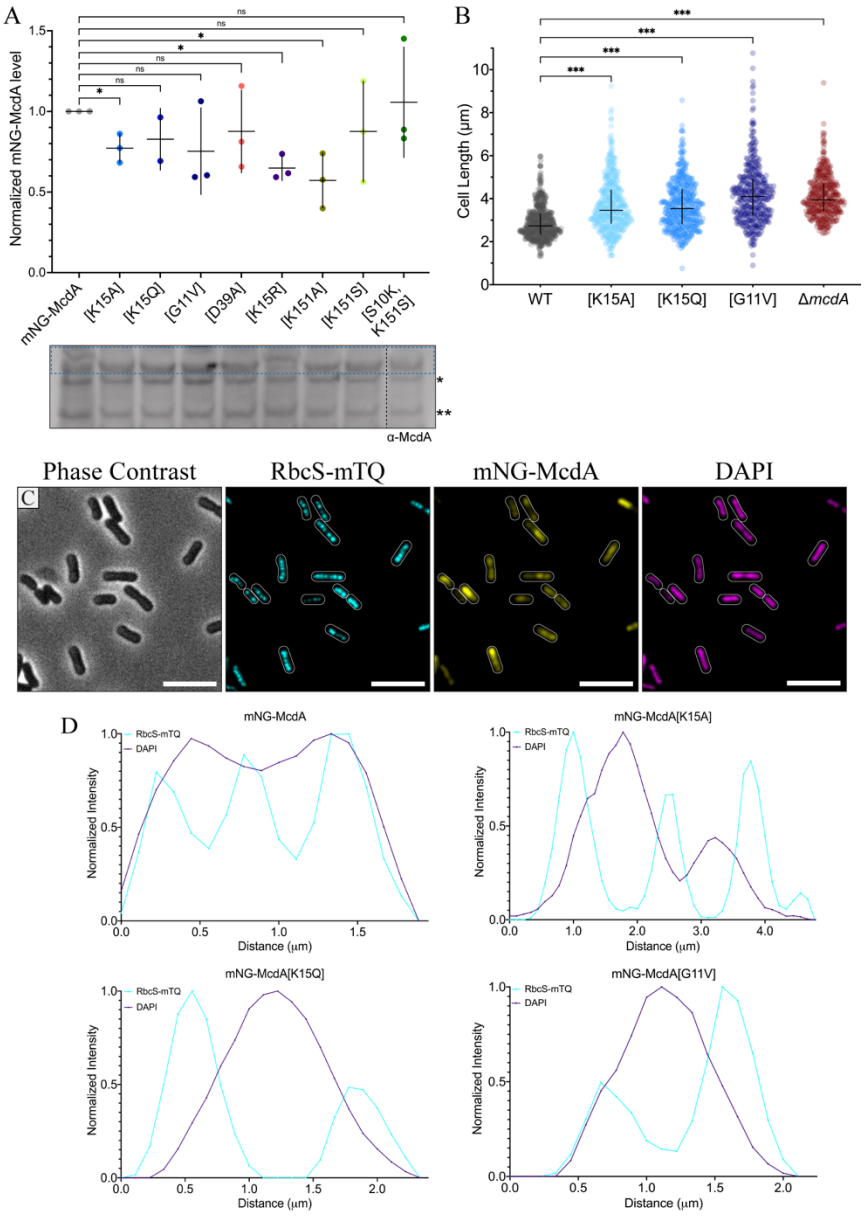


Figure 3.3: **Fluorescent McdA fusion proteins are intact and expressed at similar level with wildtype.** A. Immunoblot quantification of mNG-McdA variants in *S. elongatus* cells probed against McdA polyclonal antibody. Bands in the dashed blue box represent mNG-McdA, which is absent in our *ΔmcdA* strain [42]. Bands marked with * and ** are non-specific proteins also present in immunoblots of the *ΔmcdA* strain. Non-specific band ** was used to mNG-McdA band intensities across samples loaded in the same gel. Immunoblot analysis was performed in triplicate. Data represent the mean and SD. * $p < 0.05$, ns = not significant by Welch's t test. Black dashed line denotes that the [S10K, K151S] lane was run on a different gel. B. Comparison of cell lengths among WT and the specified McdA mutants. WT $n = 558$ cells; $n > 380$ cells per mutant strain. *** $p < 0.001$ by Kruskal-Wallis test. C. Microscopy images of cells expressing mNG-McdA (as in Fig. 3.2A), but with DAPI-stained nucleoids (magenta). Scale bars: 5 μm. D. Line scans of carboxysome and nucleoid signals of specified strains. Each line scan graph is from a representative cell from each strain.

inhibitor ciprofloxacin to induce nucleoid compaction [45], which increased the cytoplasmic space observable by epifluorescence microscopy. Conveniently, when wild-type *S. elongatus* cells were treated with ciprofloxacin, mNG-McdA still oscillated on the compacted nucleoid (Movie 3.2), and carboxysomes were still distributed over the nucleoid region of the cell and not in the cytoplasmic spaces. The Pearson correlation coefficient (PCC) was used to indicate the degree of colocalization [46] between the DAPI-stained nucleoid and RbcS-mTQ-labeled carboxysomes (PCC = 0.66, n = 324 cells) (Fig. 3.2J; Table 3.1). The predicted ATP-binding and dimerization mutants of mNG-McdA, on the other hand, remained diffuse in the cytoplasm and carboxysomes were nucleoid excluded, but in a surprising manner (Fig. 3.2K-M). Rather than having carboxysomes randomly distributed in the cytoplasmic region of the cell, the carboxysome aggregates butted up against the ends of the compacted nucleoid (Fig. 3.3D). As a result, the PCC values calculated for carboxysomes and the nucleoid signal were significantly lower for all three mutant strains (PCC mNG-McdA[K15A] = 0.49, n = 338 cells; mNG-McdA[K15Q] = 0.40, n = 305 cells; mNG-McdA[G11V] = 0.47, n = 365 cells) compared with the wild-type strain (PCC = 0.66, n = 324 cells). (Fig. 3.2J-M, merged panels, and Table 3.1). A similar observation was recently found for plasmids lacking their partition system [44], suggesting this is a widespread mesoscale phenomenon for both genetic and proteinaceous complexes in a bacterial cell.

I am currently unable to purify the McdA variants used in this study due to solubility issues. The McdA mutations made here were modeled after the biochemically characterized mutants of other ParA family proteins (Fig. 3.1C). Many of these ParA family ATPases have been shown to be monomeric in their apo forms and dimerize on ATP binding, which then licenses nsDNA binding *in vitro* or nucleoid binding *in vivo* [1], [3]. Taken together, our data suggest that ATP

binding and dimerization are prerequisite steps needed for McdA to bind the nucleoid and distribute carboxysomes within the nucleoid region of the cell.

### 3.3.4 The predicted ATP-Trap mutant McdA[D39A] does not associate with the nucleoid or McdB *in vivo*

To solve the sandwich-dimer structure of an McdA homolog from the cyanobacterium *Cyanothece* sp. PCC 7424, the Schumacher group made an ATP-trap mutant by substituting the catalytic aspartate residue to an alanine in the Walker A' box (see Fig. 3.1A-B) [6]. Synonymous ParA family mutants have been shown to form ATP-bound dimers competent for DNA-binding and interaction with their cognate ParB, but are deficient in ATP-hydrolysis (see Fig. 3.1C). I made the corresponding mutation in McdA (D39A) to determine the *in vivo* localization pattern of an McdA mutant presumably trapped as an ATP-bound dimer, and its effect on carboxysome positioning. Unexpectedly, mNG-McdA[D39A] was diffuse in the cytoplasm and carboxysomes were mispositioned in a manner that was identical to our predicted ATP-binding and dimerization mutants of McdA (Fig. 3.4A). Immunoblot analysis verified that the diffuse localization was not due to cleavage of the fusion protein (Fig. 3.3A). The data suggest McdA[D39A] cannot bind the nucleoid due to a loss in non-specific DNA binding activity. The Schumacher group showed that ATP-bound McdA[D38A] from *Cyanothece* can dimerize and bind a non-specific DNA substrate *in vitro* [6], however the affinities for dimerization and interaction with DNA were not compared to wild-type McdA. Since *S. elongatus* McdA is highly insoluble, I purified the McdA homolog from *Cyanothece* (*Ct*McdA) and its ATP-trap variant *Ct*McdA[D38A] (used to solve the McdA structure), and found via electrophoretic mobility shift assays (EMSAs) that *Ct*McdA[D38A] has significantly reduced DNA-binding activity compared to wild-type **(**Fig. 3.4B**)**. This finding is

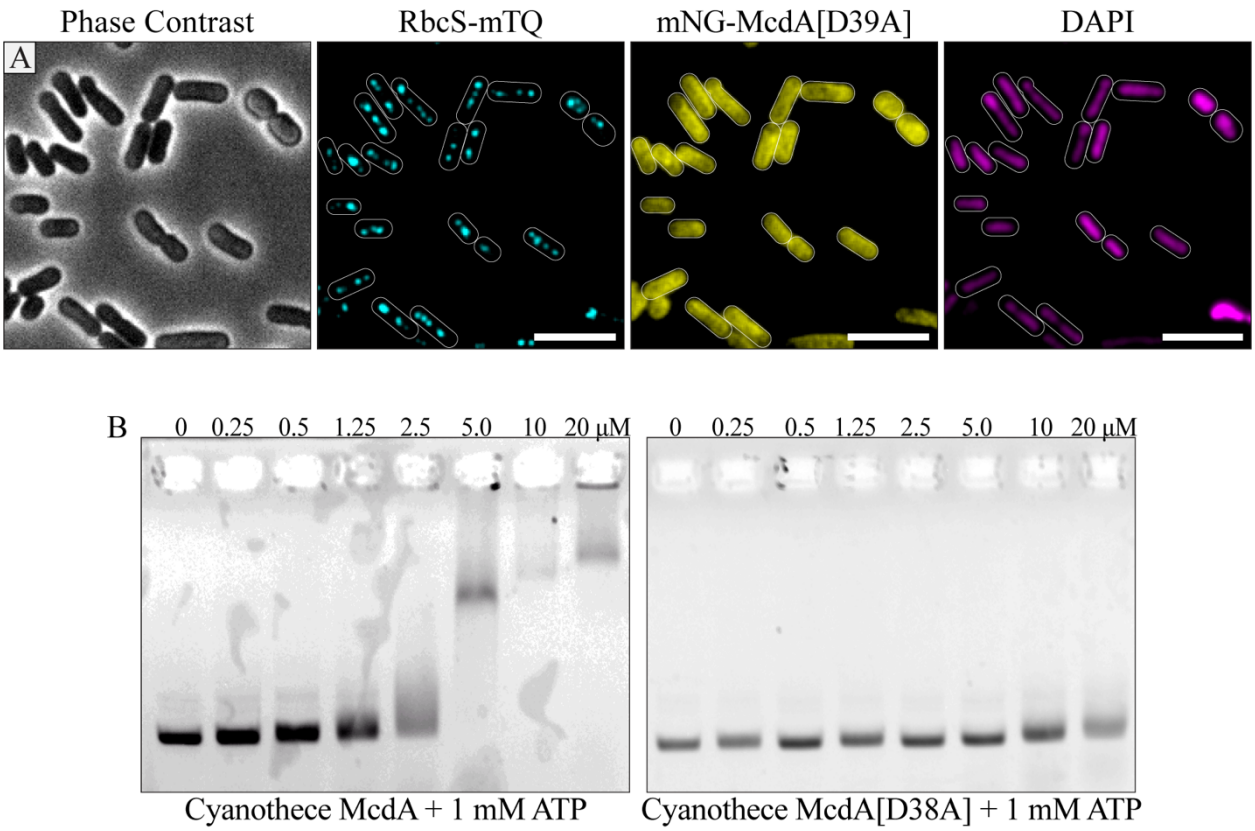


Figure 3.4: **The predicted ATP-trap mutant McdA[D39A] does not associate with DNA *in vivo* and *in vitro*.** A. Microscopy images of the mNG-McdA[D39A] strain of *S. elongatus*. Scale bars: 5 µm. B. Electrophoretic Mobility Shift Assay (EMSA) showing that wildtype *Ct*McdA binds and slows the migration of a non-specific plasmid DNA substrate in the presence of 1 mM ATP, while *Ct*McdA[D38A] does not.

consistent with our *in vivo* observations of the corresponding mutant in *S. elongatus* (Fig. 3.4A). I propose McdA[D39A] is either impaired in its dimerization activity or does not go through the conformational change that licenses nucleoid binding, which our data suggest are prerequisites for McdB interaction and distributing carboxysomes over the nucleoid.

### 3.3.5 The predicted ATP-Trap mutant McdA[K15R] locks onto McdB-bound carboxysomes

I set out to construct another ATP-trap mutant of McdA that can adopt the nucleoid-binding state and interact with McdB. One of the best-studied ATP-trap mutants from the ParA family of ATPases comes from the P1 plasmid partitioning system [29]. Mutating the catalytic lysine to an arginine in the deviant Walker A box of P1 ParA (K122R) has shown robust *in vitro* and *in vivo* phenotypes (see Fig. 3.1B-C). *In vitro*, ParA[K122R] can bind ATP, dimerize, and bind nsDNA with an affinity comparable to wild type, but irreversibly associates with ParB because ParB cannot stimulate the ATPase activity required for releasing this association [20], [29]. *In vivo*, ParA[K122R] results in a worse-than-null and dominant-negative phenotype called ParPD for "propagation-defective," whereby plasmids are less stable than when they have no partition system at all [47]. Given the severity of the mutation, the mechanism for the $Par^{PD}$ phenotype has not been directly identified *in vivo*. However, the inability to disassemble the DNA-ParA[K122R]-ParB-plasmid complex *in vitro* suggests a likely mechanism [19], [20]. Strikingly, the corresponding mutation, mNG-McdA[K15R], resulted in nearly complete colocalization with carboxysomes (PCC = 0.83, n = 558 cells) (Fig. 3.5A; Table 3.1). When *mcdB* was deleted from this strain, mNG-McdA[K15R] no longer associated with carboxysomes (PCC = 0.60, n = 391 cells), instead, coating the nucleoid, thus showing its ability to still bind nsDNA (Fig. 3.5B). The data suggest that the predicted ATP-trap mutant, McdA[K15R], locks carboxysomes onto the nucleoid via a more stable association with McdB. Consistently, bacterial two-hybrid (B2H) analysis also suggested that McdA[K15R] more stably associates with McdB compared with wild-type McdA (Fig. 3.5C). However, immunoblot analysis showed that this increased signal may be due to McdA[K15R] being produced at higher levels than wild-type McdA. All other McdA mutants

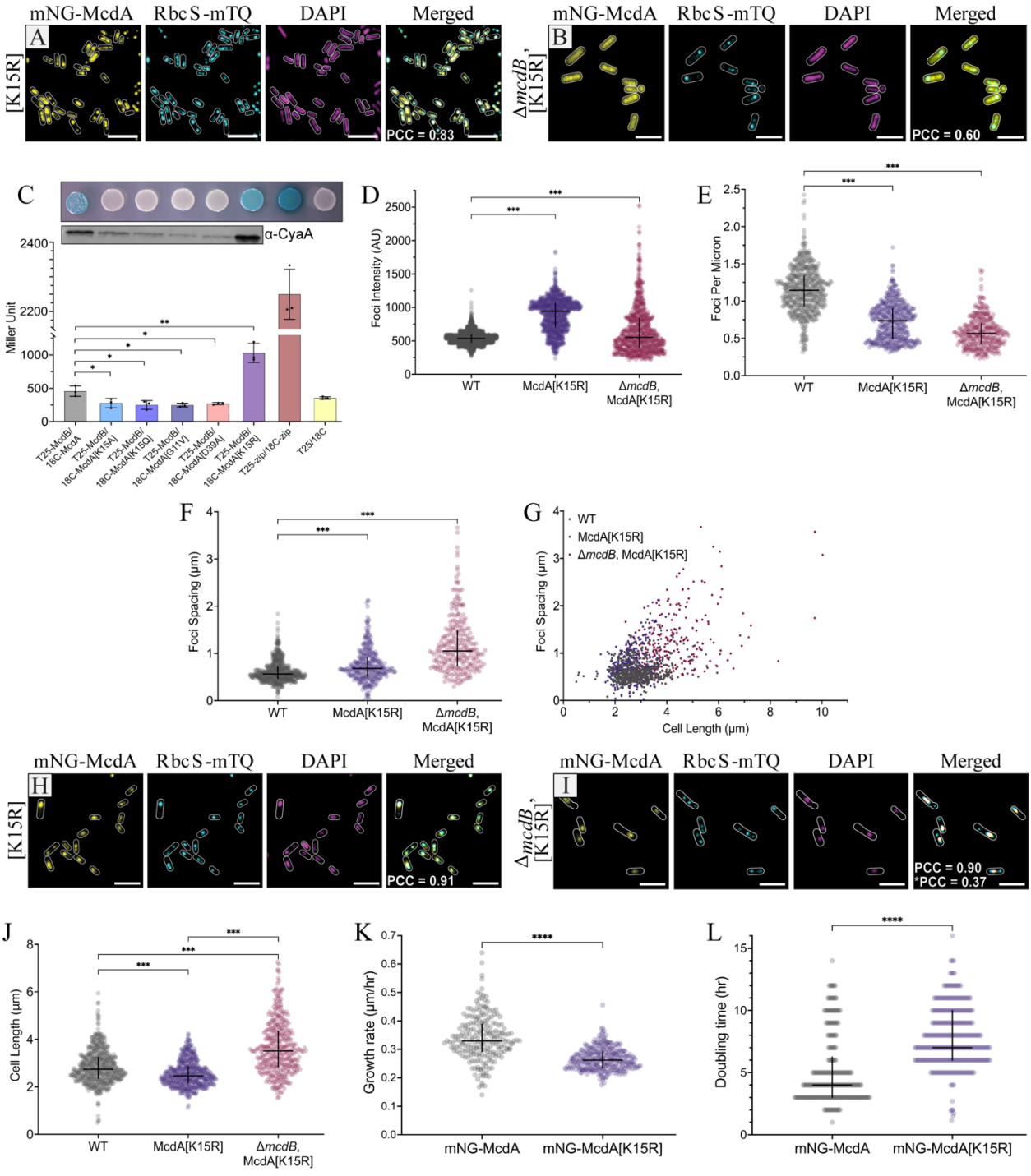


Figure 3.5: **The predicted ATP-trap mutant McdA[K15R] locks McdB-bound carboxysomes onto the nucleoid.** A. Microscopy images of mNG-McdA[K15R] (yellow), RbcS-mTQ-labeled carboxysomes (cyan), and DAPI-stained nucleoid (magenta). Merged image overlays mNG-McdA[K15R] and RbcS-mTQ labeled carboxysomes with a PCC value calculated from these two signals. B. Microscopy images of mNG-McdA[K15R] in a Δ*mcdB* background strain. Merged image shows mNG-McdA[K15R] and RbcS-mTQ-labeled carboxysomes with a PCC value

calculated from these two signals. C. (Top) B2H interaction assay between the indicated protein pairs. The image is representative of three independent experiments. (Middle) Western blot detection of T18 domain in 18C-McdA and its mutant fusions using CyaA antibody. (Bottom) Quantitative analysis of the B2H interactions. Data represent the mean and SD from three independent biological replicates. *p < 0.05 **p < 0.001 by Welch's t test. D. Carboxysome foci intensity for specified cell strains. (arbitrary units = AU). WT n = 1925 foci, *n* > 820 foci per mutant strain. E. Carboxysome foci number as a function of cell length. WT n = 578 cells; *n* > 370 cells per mutant strain. F. Spacing of carboxysome foci. WT n = 558 cells; *n* > 260 cells per mutant strain. G. Distribution of spacing between carboxysome foci as a function of cell length. WT n = 558 cells; *n* > 380 cells per mutant strain. H. Microscopy images of mNG-McdA[K15R] (yellow), carboxysome foci (cyan), and DAPI-stained nucleoid (magenta) with ciprofloxacin treatment. Merged image shows mNG-McdA[K15R] and carboxysome signals and the PCC value calculated from these two signals. I. Microscopy images of mNG-McdA[K15R] (yellow), carboxysome foci (cyan), and DAPI-stained nucleoid (magenta) in the Δ*mcdB* background strain treated with ciprofloxacin. Merged image overlays all three channels. PCC value (top) is for colocalization between mNG-McdA[K15R] and DAPI signals. *PCC value (bottom) is for colocalization between DAPI and carboxysome signals. All PCC values were calculated from at least 300 cells per population. J. Cell lengths of specified strains. WT n = 558 cells; *n* > 260 cells per mutant strain. Scale bars: 5 μm. (K) Growth rate of mNG-McdA and mNG-McdA[K15R] strains. For both strains n = 300 cells. (L) Doubling time of mNG-McdA and mNG-McdA[K15R] strains. WT n = 222 cells; mNG-McdA[K15R] n = 296 cells. Data represent median with interquartile range. ****p < 0.0001 by Welch's t test.

studied thus far showed no interaction with McdB via B2H analysis. But in this case, immunoblot analysis revealed that all McdA mutants predicted to be defective for dimerization (K15A, K15Q, G11V, and D39A) had significantly lower cellular levels compared with wild type and the K15R variant when expressed in *Escherichia coli*. Taken together, it is possible that the increased B2H signal for McdA[K15R] is due to this predicted ATP-trap mutant being a more stable dimer compared with wild-type McdA or the predicted dimerization-deficient mutants of McdA. Compared to wild type, the McdA[K15R] mutant displayed significantly higher carboxysome foci intensities, a phenotype that was dependent on the presence of McdB (Fig. 3.5D). Consistent with carboxysome aggregation, the McdA[K15R] mutant displayed fewer carboxysome foci per unit cell length (Fig. 3.5E). The data suggest that McdB-stimulated ATP hydrolysis by McdA is required to disaggregate and distribute carboxysomes in the cell. mNG-McdA[K15R] remained

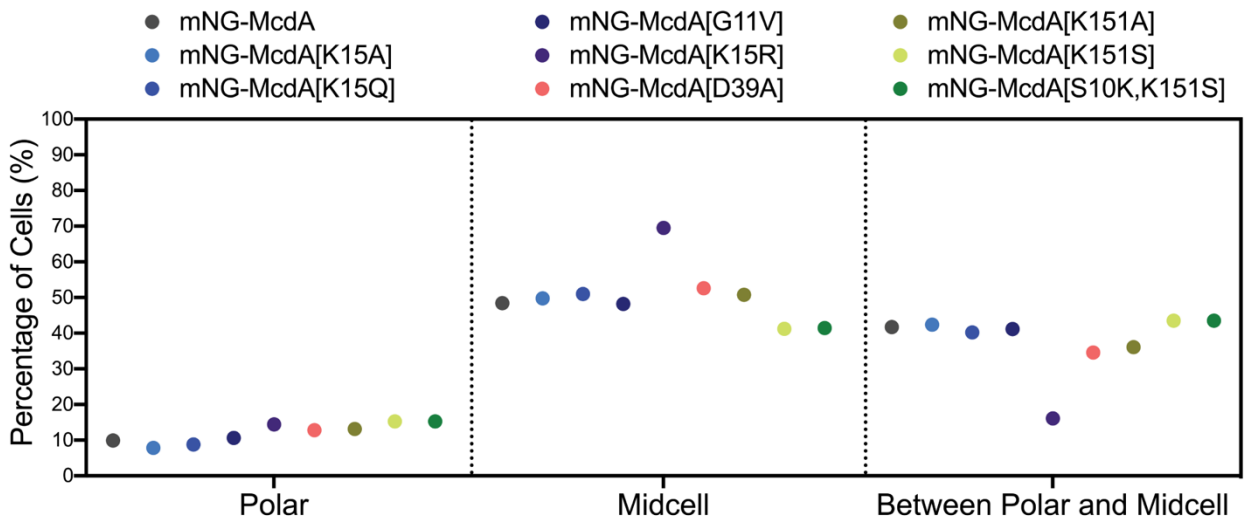


Figure 3.6: **The McdA[K15R] cell population significantly deviates from all other McdA variants in regards to carboxysome foci positioning in the cell.** Binned subcellular localization of carboxysomes in the specified cell strains. Quantification was performed in MicrobeJ where carboxysome signals located within the region extending from the tip of the cell pole to a position on the medial axis located half the width away from the cell pole tip, are considered as "polar" localized. Carboxysome signals located within the region extending from the cell center to a position on the medial axis located half the width away from the cell center, are considered as "midcell" localized. Carboxysomes located between these two defined regions were grouped as "between polar and midcell". WT $n$ = 1000 foci; $n$ > 800 foci per mutant strain.

associated with the compacted nucleoid (PCC 0.90, n = 346), once again showing this mutant retains nonspecific DNA-binding activity, while carboxysomes became nucleoid excluded (PCC = 0.37, n = 346) (Fig. 3.5I). Together, the data show that the predicted ATP-trap mutant McdA[K15R] locks carboxysome aggregates onto the nucleoid via a more stable association with McdB.

Finally, I asked if locking carboxysome aggregates onto the nucleoid in the McdA[K15R] strain resulted in the same cell elongation phenotype found for all other McdA mutants described thus far. Surprisingly, the McdA[K15R] strain did not elongate (Fig. 3.5J). In fact, the McdA[K15R] cells were slightly smaller than wild type. I performed multigenerational time-lapse microscopy (Movie 3.3) and found that McdA[K15R] cells are smaller than wild type because the mutant cells have a reduced growth rate (Fig. 3.5K) as well as a longer doubling time (Fig. 3.5L).

When *mcdB* was deleted in the McdA[K15R] strain, the cell elongation phenotype returned (Fig. 3.5J). The findings suggest that the pseudopositioning of carboxysome aggregates locked onto the nucleoid is sufficient to prevent cell elongation induced by the mispositioning of nucleoid-excluded carboxysome aggregates. But, locking carboxysome aggregates onto the nucleoid still compromises cell growth.

### 3.3.6 McdA represents an unstudied subclass of ParA family ATPases

Despite the McdA structure adopting an ATP-sandwich dimer as shown for other ParA ATPases [6], McdA lacks the classical "signature lysine" residue in the deviant Walker A box that defines this family (see Fig. 3.1B). Instead, the McdA structure identified a lysine residue, not only outside of the deviant Walker A box but in the C-terminal half of the protein at position 151, which is employed as the signature lysine (Fig. 3.7A) [6]. As with the classical signature lysine, Lys151 interacts with the ATP molecule bound in the adjacent McdA monomer, making the same cross-contacts to the oxygen atom connecting the β- and γ-phosphates. Sequence alignments of McdA homologues that lack the classical signature lysine in the deviant Walker A box invariably encode for a lysine that corresponds to Lys151 in *S. elongatus* McdA (Fig. 3.7A). Given the McdA structure, sequence conservation, and biochemical data suggesting Lys151 is important for ATP binding and dimerization [6], I next observed the effect of mutating Lys151 to an alanine *in vivo*. The majority of mNG-McdA[K151A] remained diffuse in the cytoplasm, while a minor fraction colocalized with few and irregularly spaced carboxysome aggregates (PCC = 0.76, n = 365 cells) (Fig. 3.7B; Table 3.1). Carboxysome foci intensity, spacing, and average cell length were identical to those found for the other predicted ATP-binding and dimerization mutants of McdA tested in this study (Fig. 3.8A-D). Also, ciprofloxacin treatment showed carboxysome aggregates were nucleoid excluded (PCC = 0.55, n = 301 cells) and once again butted up against the nucleoid poles

(Fig. 3.7C). The findings highlight the importance of Lys151 as the "signature lysine" for an unstudied ParA subclass in forming the ATP-bound McdA dimer competent for nucleoid binding and positioning carboxysomes.

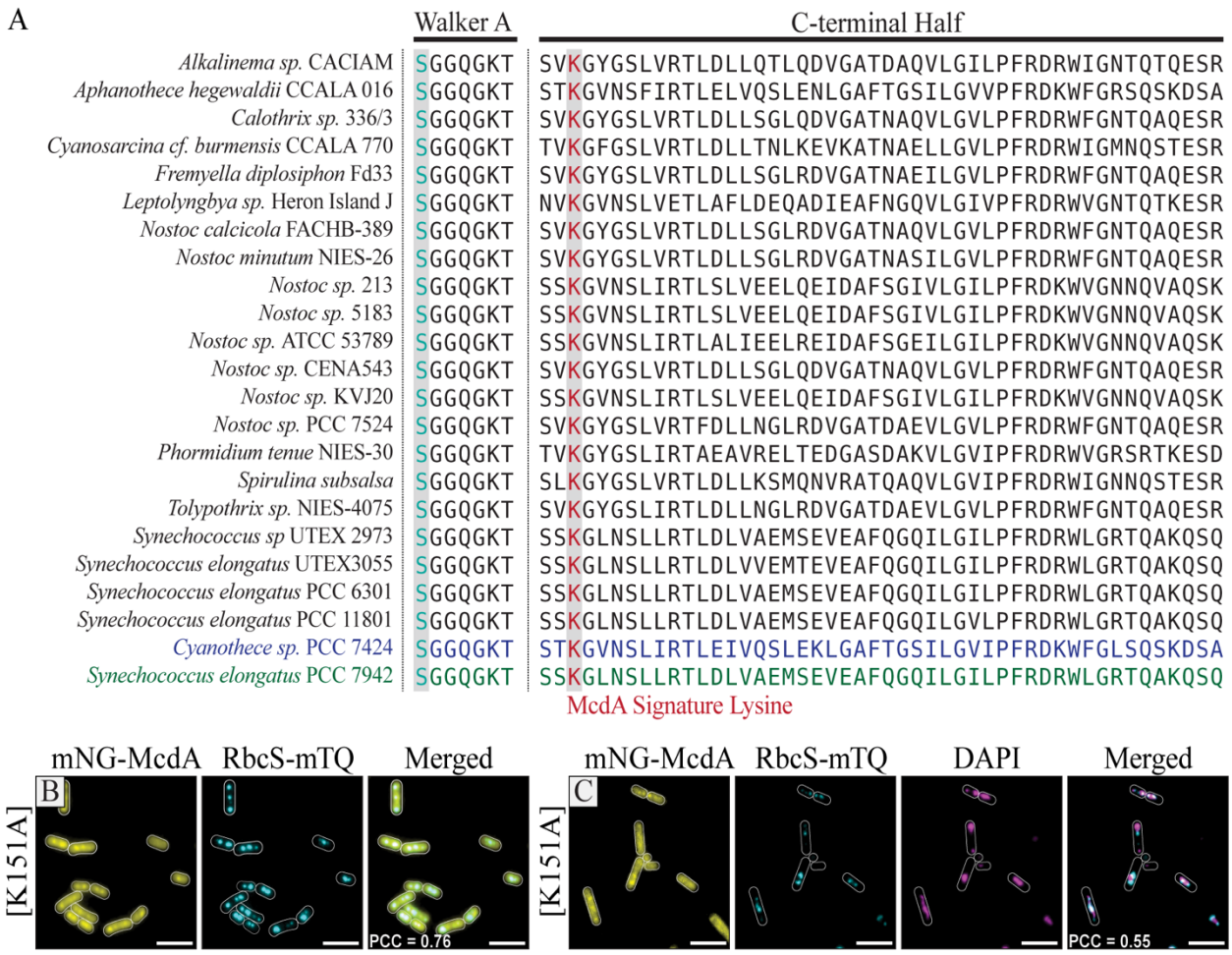


Figure 3.7: **McdA is a member of an unstudied subclass of ParA-type ATPase characterized by a different signature lysine position.** A. Sequence alignment of McdA homologues possessing a serine residue in place of the signature lysine the Walker A box that co-occurs with an invariant lysine residue in the C-terminal half of protein - the McdA signature lysine. B. Microscopy images of mNG-McdA[K151A] and RbcS-mTQ-labeled carboxysomes (cyan). Merged image shows mNG-McdA[K151A] and carboxysome signals and the PCC value calculated from these two signals. C. Microscopy images of mNG-McdA[K151A] (yellow), carboxysome foci (cyan), and DAPI-stained nucleoid (magenta) with ciprofloxacin treatment. Merged image shows carboxysome and DAPI signals and the PCC value calculated from these two signals. PCC values were calculated from at least 300 cells per cell population. Scale bars: 5 μm.

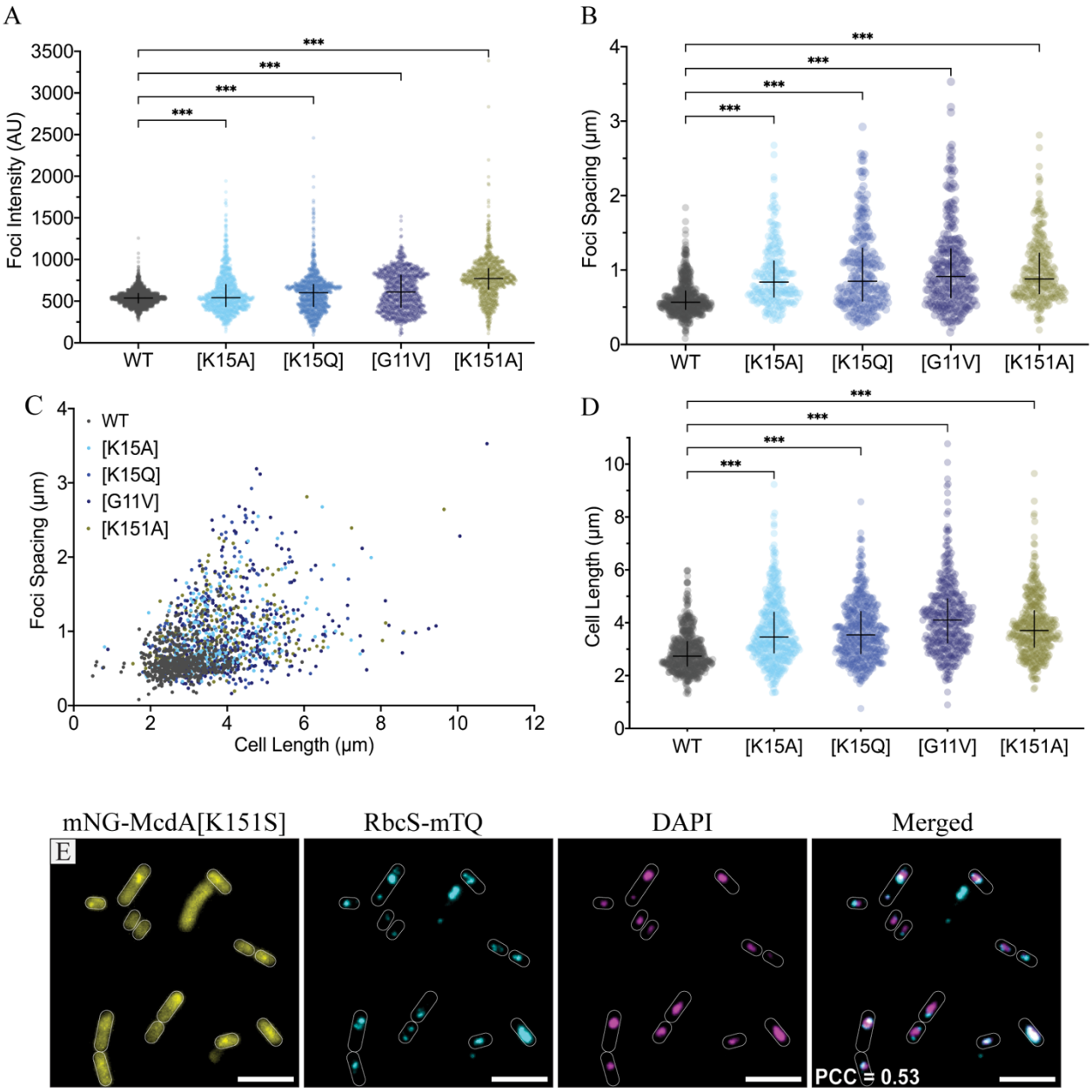


Figure 3.8: **Signature lysine 151 is essential for proper McdA function in carboxysome positioning.** A. Comparison of carboxysome foci intensity for specified strains (Arbitrary Units = AU). WT *n* = 1925 foci; n > 960 foci per mutant strain. B. Comparison of carboxysome foci spacing of specified cell strains. C. Distribution of carboxysome spacing as a function of cell length in the specified strains. For B and C: WT *n* = 558 cells; n > 220 cells per mutant strain. **(D)** Comparison between the cell length of specified mNG-McdA mutants cell strains. WT *n* = 561 cells; n > 360 cells per mutant strain. (**E**) Microscopy images of mNG-McdA[K151S] (yellow), carboxysome foci (cyan) and DAPI-stained nucleoid (magenta) when treated with ciprofloxacin. Merged image shows carboxysome and DAPI signals. PCC value calculated from the merged RbcS-mTQ and DAPI channels from at least 300 cells. Scale bars: 5 µm.

### 3.3.7 Moving the signature lysine of McdA into the Walker A box reconstitutes carboxysome pseudopositioning

Remarkably, Lys151 of the McdA structure overlays exceptionally well onto the signature lysine position in the deviant Walker A box of classical ParA family members [6]. This finding suggested that it may be possible to maintain carboxysome positioning with an McdA mutant that has its signature lysine at position 151 reintroduced into the classical position in the deviant Walker A box at position 10 (see Fig. 3.7A). To make the signature lysine mutant, McdA[S10K, K151S], I swapped the serine at position 10 in the deviant Walker A box with the lysine at position 151. The mNG-McdA[K151S] phenotype mirrored that of McdA[K151A]—largely diffuse in the cytoplasm with nucleoid-excluded carboxysome aggregates (PCC = 0.53, n = 325 cells) (Fig. 3.8E; Table 3.1). Immunoblot analysis verified that the diffuse localization of mNG-McdA[K151S] was not due to cleavage of the fusion protein (Fig. 3.3A). The mNG-McdA[S10K, K151S], on the other hand, largely colocalized with carboxysome foci (PCC = 0.84, n = 320 cells) (Fig. 3.9A; Table 3.1). Also, carboxysome spacing (Fig. 3.9B) and intensity (Fig. 3.9C) both trended back toward wild-type values, and ciprofloxacin treatment showed that carboxysomes strongly colocalized with mNG-McdA[S10K, K151S] (PCC = 0.85, n = 309 cells) and were now positioned within the nucleoid region of the cell (PCC = 0.78, n = 309 cells) (Fig. 3.9D). Together, the data suggest a pseudorestoration of carboxysome positioning on the nucleoid. Consistently, the McdA[S10K, K151S] cell population had cell lengths revert back to wild type (Fig. 3.9E), suggesting this pseudopositioning of carboxysomes is sufficient to alleviate the cell elongation mutant phenotype.

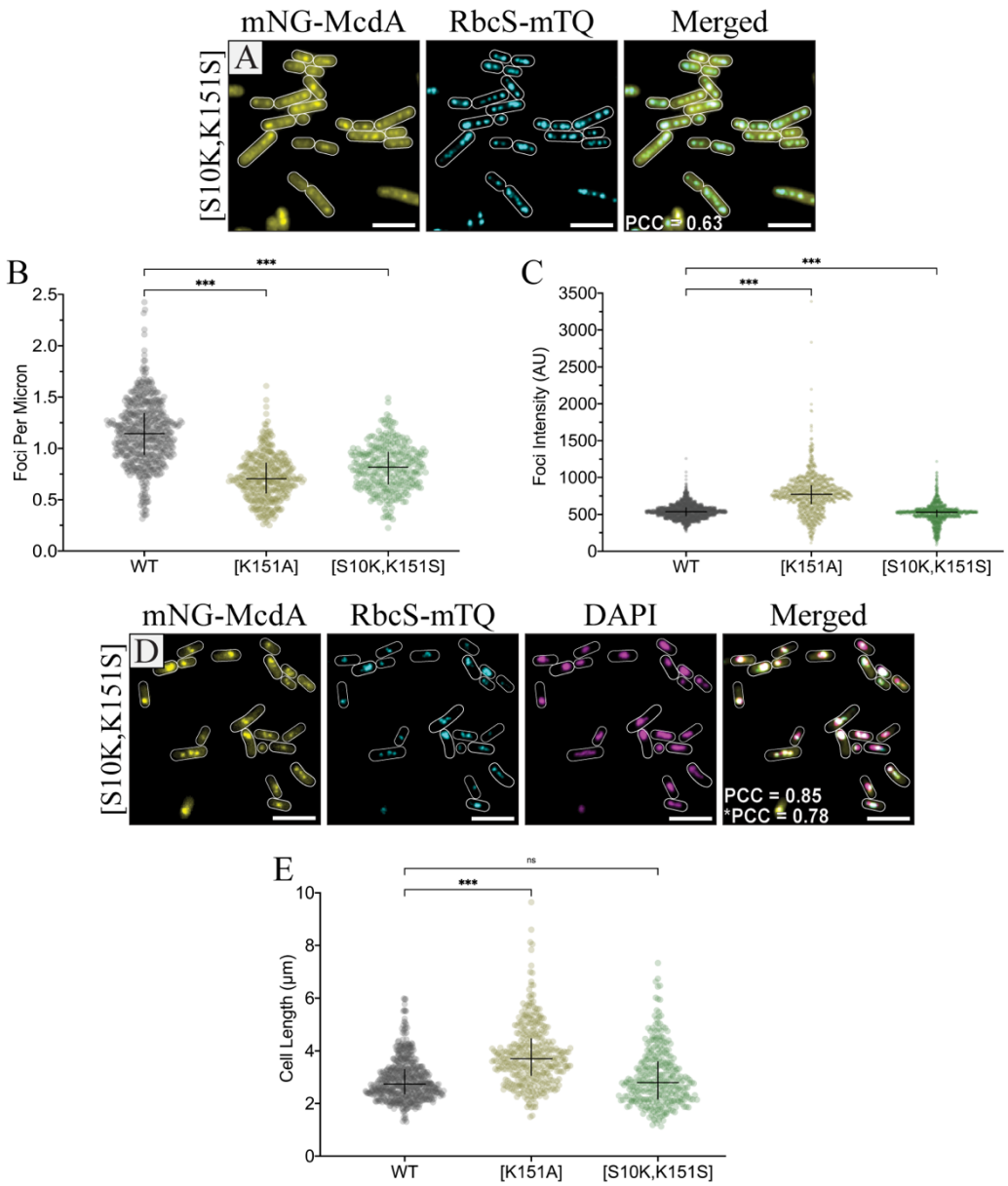


Figure 3.9: **Carboxysomes are pseudopositioned when the McdA signature lysine is moved into the classical Walker A box position.** A. Microscopy images of mNG-McdA[S10K, K151S] and RbcS-mTQ-labeled carboxysomes (cyan). Merged image shows the overlay and calculated PCC values of these two signals. B. Number of carboxysome foci per unit cell length. WT n = 578 cells; n > 315 cells per mutant strain. C. Carboxysome foci intensity. (arbitrary units = AU). WT n = 1925 foci; n > 950 foci per mutant strain. D. Microscopy images of mNG-McdA[S10K, K151S] (yellow), carboxysome foci (cyan), and DAPI-stained nucleoid (magenta) with ciprofloxacin treatment. Merged image overlays carboxysome, mNG-McdA[S10K, K151S] and DAPI signals. PCC value (top) is for colocalization between mNG-McdA[S10K, K151S] and carboxysome signals. *PCC value (bottom) is for colocalization between DAPI and carboxysome signals. All PCC values were calculated from at least 300 cells per population. E. Cell lengths of specified strains. ***$p < 0.001$, ns = not significant by Kruskal–Wallis test. WT n = 561 cells; n > 315 cells per mutant strain. Scale bars: 5 µm.

| Merged Figure Panel | *S. elongatus* Strain | Signal #1 | Signal #2 | Pearson Correlation Coefficient (PCC) | Cipro Treatment ? |
|---|---|---|---|---|---|
| 3.2J | mNG-McdA (wildtype) | RbcS-mTQ | DAPI | 0.66 | Yes |
| 3.2K | mNG-McdA[K15A] | RbcS-mTQ | DAPI | 0.49 | Yes |
| 3.2L | mNG-McdA[K15Q] | RbcS-mTQ | DAPI | 0.40 | Yes |
| 3.2M | mNG-McdA[G11V] | RbcS-mTQ | DAPI | 0.47 | Yes |
| 3.5A | mNG-McdA[K15R] | mNG-McdA[K15R] | RbcS-mTQ | 0.83 | |
| 3.5B | mNG-McdA[K15R], Δ*mcdB* | mNG-McdA[K15R] | RbcS-mTQ | 0.60 | |
| 3.5H | mNG-McdA[K15R] | mNG-McdA[K15R] | RbcS-mTQ | 0.91 | Yes |
| 3.5I | mNG-McdA[K15R], Δ*mcdB* | mNG-McdA[K15R] | DAPI | 0.90 | Yes |
| 3.5I | mNG-McdA[K15R], Δ*mcdB* | RbcS-mTQ | DAPI | 0.37 | Yes |
| 3.7B | mNG-McdA[K151A] | mNG-McdA[K151A] | RbcS-mTQ | 0.76 | |
| 3.7C | mNG-McdA[K151A] | RbcS-mTQ | DAPI | 0.55 | Yes |
| 3.8E | mNG-McdA[K151S] | RbcS-mTQ | DAPI | 0.53 | Yes |
| 3.9A | mNG-McdA[S10K,K151S] | mNG-McdA[S10K,K151S] | RbcS-mTQ | 0.84 | |
| 3.9D | mNG-McdA[S10K,K151S] | mNG-McdA[S10K,K151S] | RbcS-mTQ | 0.85 | Yes |
| 3.9D | mNG-McdA[S10K,K151S] | RbcS-mTQ | DAPI | 0.78 | Yes |

Table 3.1: **Summary of Pearson Correlation Coefficients (PCCs) for colocalization of indicated signals.**

## 3.4 Discussion

Members of the ParA family of ATPases position a wide variety of genetic and proteinaceous cargos involved in diverse biological processes [1]–[3]. ATP cycling by the ParA ATPase is critical for its dynamic patterning behavior in the cell as well as its positioning activity on the cognate cargo. We recently found that the McdAB system is widespread across cyanobacteria and carboxysome-containing proteobacteria [48], [49], yet it remains unknown how the ATPase cycle of McdA controls its oscillatory dynamics and its function in distributing carboxysomes across the

nucleoid length. Several well-researched amino acid substitutions in the conserved ATP-binding site of ParA family ATPases have been used to trap the ATP cycle at specific steps. These trap mutants have served as useful probes for dissecting the molecular steps involved in ParA-based positioning reactions (Fig. 3.1C). To dissect how ATP mediates McdA function in positioning fluorescently labeled carboxysomes, I introduced synonymous amino acid substitutions in the ATP-binding pocket of fluorescently labeled McdA to trap it at specific steps of the ATP cycle. While I am currently unable to purify and biochemically characterize the McdA variants used in this study, the phenotypes of these trap mutants have allowed us to correlate the known biochemistry of well studied ParA family ATPases with specific steps in McdA action I observed here *in vivo*.

Overall, my findings suggest that ATP binding, dimerization, and an ATP-specific conformational change in McdA are all prerequisite steps for McdA to associate with the nucleoid via nonspecific DNA-binding activity (Fig. 3.10A). The findings also suggest that McdB-bound carboxysomes can only interact with McdA in this DNA-binding state. Nucleoid-associated McdA tethers McdB-bound carboxysomes to the nucleoid. But ultimately, McdB stimulates ATP hydrolysis by McdA, which reverts McdA back into its monomeric form that can no longer bind the nucleoid in the vicinity of the carboxysome. Through this Brownian-ratchet mechanism [27], McdB-bound carboxysomes are uniformly distributed as they locally generate McdA depletion zones on the nucleoid and then move up the resulting McdA gradient toward higher concentrations (Fig. 3.10B).

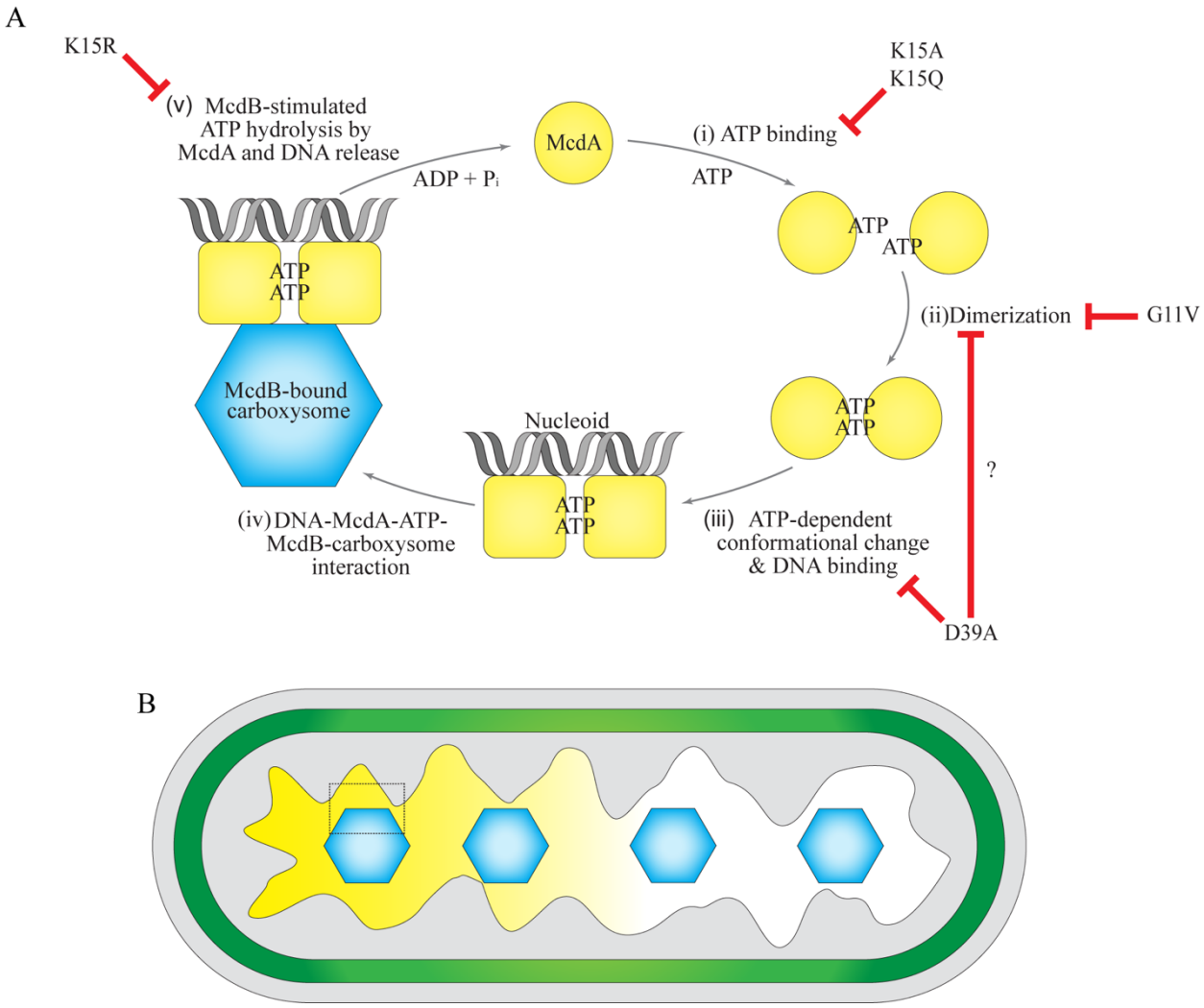


Figure 3.10: **Model for ATP-cycling by McdA and associated functions in carboxysome positioning.** A. The ATPase cycle of McdA. Trap mutants of McdA predicted in this study are indicated. (i) When unbound from ATP, McdA monomers are diffuse in the cytoplasm. (ii) On ATP binding, McdA is competent for dimerization. (iii) ATPbound McdA dimers must go through an ATP-dependent conformational change that licenses nsDNA binding to the nucleoid. (iv) McdB-bound carboxysomes are tethered via interactions with McdA-ATP dimers on the nucleoid. (v) McdB stimulates McdA ATPase activity and its release from the nucleoid in the vicinity of a carboxysome. B. McdB-bound carboxysomes are uniformly distributed as they continually move toward higher concentrations of McdA on the nucleoid. The dashed box indicates the cellular region where step (iv) occurs in A.

McdA mutants predicted to be unable to bind ATP, dimerize, or undergo the ATP-specific conformational change required for nucleoid binding were diffuse in the cytoplasm, and carboxysomes were observed as nucleoid-excluded aggregates. These mutant strains also

displayed cell elongation. We have recently shown that *mcdA* and *mcdB* deletion strains also elongate [42]. Heterotrophic bacteria have been shown to undergo cell elongation as a carbon-limitation response [50]. We also recently proposed that carboxysome aggregation results in decreased carbon-fixation efficiency, and that cell elongation is a response triggered by the resulting carbon limitation in this photoautotroph [42]. Since the phenotype of these predicted McdA trap mutants mirrors the *mcdA* deletion strain, our findings suggest a complete loss of function in carboxysome positioning when McdA cannot bind ATP, dimerize, and adopt its nucleoid-binding conformation.

### 3.4.1 Nucleoid-excluded carboxysomes are trapped at the cytoplasm–nucleoid interface

We previously showed that in Δ*mcdA* or Δ*mcdB* strains of *S. elongatus*, carboxysomes still fully assemble, but coalesce into nucleoid-excluded aggregates [27]. Given the polyploid nature of *S. elongatus*, there is insufficient cytoplasmic space to resolve whether carboxysomes aggregated due to physical interactions with each other or if they simply coalesced because of nucleoid exclusion. We used the gyrase-inhibitor ciprofloxacin to compact the nucleoid and increase the cytoplasmic space of *S. elongatus* cells. Surprisingly, in the absence of a functional McdAB system, carboxysome aggregates did not diffuse into the increased cytoplasmic space of ciprofloxacin-treated cells. Instead, the aggregates were maintained at the cytoplasm–nucleoid interface. It was recently shown that large plasmids lacking their ParA-based partition system, or large DNA circles excised from the chromosome, also localize to this interface [44]. This phenomenon was plasmid-size dependent; only plasmids larger than 100 kb preferentially localized to the nucleoid edge and did not diffuse into the nucleoid-free cytoplasmic space of the cell. My findings here show that this preferential localization to the nucleoid edge is not specific to plasmids but rather is a

widespread phenomenon in bacteria for both genetic and proteinaceous complexes on the mesoscale. Given the size dependence of nucleoid-evicted complexes being unable to penetrate the cytoplasm, we believe the most parsimonious explanation is that carboxysomes, and other mesoscale complexes, perceive the cytoplasmic environment as glassy [51] and thus exhibit caging and subdiffusive behaviors at the nucleoid–cytoplasm interface. Remarkably, wild-type cells treated with ciprofloxacin still displayed mNG-McdA oscillations and carboxysomes were still distributed over the highly compacted nucleoid (Movie 3.2). The data suggest that the McdAB system can distribute carboxysomes regardless of whether the nucleoid is expanded or in an extremely compacted state. This finding has implications for identifying the forces responsible for carboxysome movement and positioning within the nucleoid region of the cell. The predicted ATP-trap mutant McdA[K15R] locks carboxysomes onto the nucleoid I identified the predicted ATP-trap mutant, McdA[K15R], that locks the nucleoid-McdA-McdB-carboxysome ternary complex. In the absence of McdB, mNG-McdA[K15R] still coated the nucleoid showing that it retains nonspecific DNA-binding activity, but carboxysomes were nucleoid excluded. In the presence of McdB, mNG-McdA[K15R] completely colocalized with massive carboxysome aggregates over the nucleoid. Together the findings show that McdA on the nucleoid transiently interacts with McdB on carboxysomes. McdB then stimulates McdA ATP hydrolysis and release from the nucleoid in the vicinity of carboxysomes, which allows for continued movement up the resulting McdA gradient. When McdB cannot stimulate the ATPase activity of McdA[K15R], the stable association tethers carboxysomes to the nucleoid. Since the ATP cycle cannot rest, McdB-bound carboxysomes act as a sink for all McdA[K15R] in the cell, which explains the lack of mNG-McdA[K15R] redistribution across the nucleoid. All McdA mutants that resulted in nucleoid-excluded carboxysome aggregation also showed a cell elongation phenotype. The McdA[K15R]

strain, on the other hand, displayed carboxysome aggregates on the nucleoid and no cell elongation phenotype. In contrast, the cells were slightly shorter than wild type due to reduced growth rate. We have two hypotheses that could explain this phenotype. First, tethering carboxysomes to the nucleoid could allow for pseudopositioning of carboxysomes. This "pilot-fish" mode of carboxysome positioning and inheritance could sufficiently improve carbon-fixation efficiency, thereby preventing carbon limitation and the cell elongation response. Even though elongation was prevented, tethering carboxysomes to the nucleoid still resulted in smaller cells and a slower growth rate. It is plausible that carboxysomes locked on the nucleoid have detrimental effects to a variety of DNA transactions such as DNA replication, transcription, nucleoid organization and compaction, and faithful chromosome segregation.

### 3.4.2 Swapping the signature lysine position in McdA resulted in carboxysome pseudopositioning on the nucleoid

McdA represents a previously unstudied subclass of the ParA family, where the signature lysine residue that defines this ATPase family is located in the C-terminal half of the protein, rather than in the Walker A box (Fig. 3.7A). I find here that Lysine151 is indeed necessary for McdA to bind the nucleoid and position carboxysomes. Strikingly, I also found that repositioning this lysine into the classical signature lysine position in the Walker A box reconstituted carboxysome pseudopositioning—carboxysome spacing and focal intensity trended back to wild-type values. This mutant also reverted back to wild-type cell lengths. However, the oscillatory dynamics observed with wild-type McdA were not reconstituted. Instead, mNG-McdA[S10K, K151S] colocalized with carboxysomes over the nucleoid. This mode of carboxysome positioning is similar to that observed for the P1 plasmid partition system. P1 ParB forms punctate foci by

loading onto and around a DNA-binding site called *parS* on the plasmid to be partitioned [52], [53]. The ParA ATPase uniformly distributes over the nucleoid but also forms foci that colocalize with relatively immobile ParB-bound plasmids [54]. During plasmid partitioning and movement, the colocalized ParA foci disappear and only reappear once the sister plasmids have reached the ¼ and ¾ positions of the cell where they once again become relatively immobile. McdA has an ATPase activity two orders of magnitude greater than ParA ATPases with a classical signature lysine [27]. It is attractive to speculate that the lysine- swap mutant of McdA decreases its voracious ATPase activity, causing it to remain associated with McdB-bound carboxysomes for a longer period and adopting a "stick-and-move" mode of carboxysomes positioning over the nucleoid, similar to the P1 plasmid partition reaction described above. While I am currently unable to purify these McdA variants, a future direction will be to determine their ATPase activities compared with wild-type McdA to directly test this proposal. Why does McdA have such a greater ATPase rate compared with classical ParA-type ATPases? We believe the answer lies in the difference in cargo copy-number in the cell. ParA-based DNA segregation systems are typically found on bacterial chromosomes and large low-copy plasmids. In both cases, the DNA is replicated and the sister copies are then segregated to opposing halves of the cell prior to division. Carboxysome copy number, on the other hand, can be significantly higher and varies depending on growth conditions. For example, when grown with high-light intensity, a single *S. elongatus* cell can contain up to a dozen carboxysomes [55]. I propose that for high-copy-number cargos, an increased ATPase activity is required to compensate for the decreased nearest-neighbor distance between adjacent cargos sharing the same nucleoid matrix. The increased ATPase rate would make the McdA gradient on the nucleoid more sensitive to carboxysome movements over these smaller spatial scales.

## 3.5 Materials and Methods

### 3.5.1 Construct design

All constructs were made using Gibson assembly [56] from PCR fragments or synthesized dsDNA (Integrated DNA Technologies) and verified by Sanger sequencing (Table 3.2). For *mcdB* deletion and native fluorescent fusion gene insertions into the *S. elongatus* genome, constructs were made as previously described [27]. For fluorescent McdA mutants, the fluorescent protein mNG was inserted upstream of the mutated *mcdA* coding sequence with a GSGSGS linker. A 700-bp region upstream and downstream of the *mcdA* coding sequence was chosen as the homology regions required for replacing the native *mcdA* with mNG-tagged McdA mutants. A duplicate *mcdA* promoter and kanamycin resistance cassette were inserted upstream of the native *mcdA* promoter to prevent operon disruption. A second copy of the *rbcS* promoter and gene, tagged at the 3′ end with the fluorescent protein mTQ with a GSGSGS linker, was inserted at NS1 to serve as the carboxysome reporter gene. For *mcdB* deletion lines, a 700-bp region downstream of the *mcdB* coding region was chosen as the downstream homology region for insertion of fluorescent McdA mutants under its native promoter.

### 3.5.2 Growth conditions and transformations

All *S. elongatus* (ATCC 33912) strains were grown in 125-ml baffled flasks (Corning) in 50 ml BG-11 medium (Sigma), pH 8.3, buffered with 1 g/l HEPES. Cells were cultured in a Minitron incubation system (Infors-HT) with the following growth conditions: 60 μmol $m^{-2}$ $s^{-1}$ continuous LED 5600 K light, 32°C, 2% $CO_2$, and shaking at 130 RPM. Plasmids were cloned in chemically competent One Shot TOP10 *E. coli* cells (Thermo Fisher Scientific) in standard manipulation and

| ***Synechococcus elongatus* PCC 7942 Strain Name** | **Description/Genotype** | **Source** |
|---|---|---|
| JSM-206 | *ΔmcdA::mNG-mcdA* (*KmR*), NS1::RbcS-mTQ (*CmR*) | MacCready *et al*., 2018 |
| AH-5 | *ΔmcdA::mNG-mcdA*[K15A] (*KmR*), NS1::RbcS-mTQ (*CmR*) | This study |
| AH-6 | *ΔmcdA::mNG-mcdA*[K15Q] (*KmR*), NS1::RbcS-mTQ (*CmR*) | This study |
| AH-7 | *ΔmcdA::mNG-mcdA*[G11V] (*KmR*), NS1::RbcS-mTQ (*CmR*) | This study |
| AH-8 | *ΔmcdA::mNG-mcdA*[D39A] (*KmR*), NS1::RbcS-mTQ (*CmR*) | This study |
| AH-9 | *ΔmcdA::mNG-mcdA*[K15R] (*KmR*), NS1::RbcS-mTQ (*CmR*) | This study |
| AH-10 | *ΔmcdA::mNG-mcdA*[K151A] (*KmR*), NS1::RbcS-mTQ (*CmR*) | This study |
| AH-11 | *ΔmcdA::mNG-mcdA*[K151S] (*KmR*), NS1::RbcS-mTQ (*CmR*) | This study |
| AH-12 | *ΔmcdA::mNG-mcdA*[S10K,K151S] (*KmR*), NS1::RbcS-mTQ (*CmR*) | This study |
| AH-13 | *ΔmcdAB::mNG-mcdA*[K15R] (*KmR*), NS1::RbcS-mTQ (*CmR*) | This study |
| RR-1 | Δ*mcdA* (*KmR*), NS1::RbcS-mTQ (*CmR*) | Rillema *et al*., 2021 |

Table 3.2. **Cyanobacterial strains used in this study.** Construction of strains are detailed in Methods and Materials.

culture conditions [57]. Transformations of *S. elongatus* cells were performed as previously described [40]. Transformant cells were plated on BG-11 agar with 12.5 μg/ml kanamycin, 12.5 μg/ml chloramphenicol, or 25 μg/ml spectinomycin. Single colonies were picked and transferred into 96-well plates containing BG-11 medium with corresponding antibiotic concentrations. Complete gene insertions and absence of the wild-type gene were verified via PCR, and cultures were removed from antibiotic selection by three series of back dilution prior to imaging.

### 3.5.3 Ciprofloxacin treatment and nucleoid visualization

To induce nucleoid compaction, *S. elongatus* cells were incubated with 50 μM ciprofloxacin overnight under normal growth conditions. To visualize the compacted nucleoid region, ciprofloxacin-treated *S. elongatus* cells were harvested by centrifugation at 13,000 x g for 1 min. The pelleted cells were then washed and resuspended in 100 μl of phosphate-buffered saline (pH 7.2). DAPI (8 μl from a 20 μg/ml stock concentration) was added to the cell suspension followed by 20-min incubation in the dark at 30°C. DAPI-stained cells were washed twice with 1 ml H2O and then resuspended in 100 μl H2O prior to visualization using the DAPI channel.

### 3.5.4 Fluorescence and time-lapse microscopy

Exponentially growing cells (2 ml of cells at $OD_{750} \sim 0.7$) were harvested and spun down at 4000 x g for 1 min and resuspended in 200 μl fresh BG-11, and 2 μl were then transferred to a 1.5% UltraPure agarose (Invitrogen) + BG-11 square pad on a 35-mm glass-bottom dish (MatTek Life Sciences). All fluorescence and phase-contrast imaging were performed using a Nikon Ti2-E motorized inverted microscope controlled by NIS Elements software with a SOLA 365 LED light source, a 100× objective lens (Oil CFI Plan Apochromat DM Lambda Series for Phase Contrast), and a Photometrics Prime 95B back-illuminated sCMOS camera or Hamamatsu Orca-Flash 4.0 LTS camera. mNG-McdA variants were imaged using a "YFP" filter set (C-FL YFP, Hard Coat, High Signal-to-Noise, Zero Shift, Excitation: 500/20 nm [490–510 nm], Emission: 535/30 nm [520–550 nm], Dichroic Mirror: 515 nm). RbcS-mTQ-labeled carboxysomes were imaged using a "CFP" filter set (C-FL CFP, Hard Coat, High Signal-toNoise, Zero Shift, Excitation: 436/20 nm [426–446 nm], Emission: 480/40 nm [460-500 nm], Dichroic Mirror: 455 nm). DAPI fluorescence was imaged using a standard "DAPI" filter set (C-FL DAPI, Hard Coat, High Signal-to-Noise,

Zero Shift, Excitation: 350/50 nm [325–375 nm], Emission: 460/50 nm [435–485 nm], Dichroic Mirror: 400 nm). For multigenerational time-lapse microscopy of mNG-McdA and mNG-McdA[K15R] strains, 2 μl of exponentially growing cells were spotted on 1.5% UltraPure agarose + BG-11 round pads cast in a 35-mm glass-bottom dish already preincubated at 30°C in 5% CO2 for at least 24 h. To sustain photosynthetic growth of *S. elongatus* cells on the microscope stage top, cells were constantly illuminated by the microscope's SOLA LED light source fitted with a 515-nm longpass filter. Temperature, humidity, and $CO_2$ concentrations were controlled with a Tokai Hit Incubation System. NIS Elements software with JOBS acquisition upgrade was used to synchronize control of shutter for growth light and image acquisition. Cells were acclimated to stage top growth conditions (32°C, 5% $CO_2$, 60 μmol $m^{-2}$ $s^{-1}$ light) for at least 30 min before image acquisition. Videos were taken at one frame per hour for a duration of 22 h.

### 3.5.5 Image analysis

Image analysis including cell segmentation, quantification of cell length, foci number, intensity, and spacing were performed using Fiji plugin MicrobeJ 5.13I [58], [59]. Cell perimeter detection and segmentation were done using the rod-shaped descriptor with default threshold settings. Carboxysome detection was performed using the smoothed foci function with tolerance of 50 and Z-score of 30. PCC values for merged signals were calculated using Fiji plugin JACoP (Just Another Colocalization Plugin) 2.1.1 [60]. Data were exported, further tabulated, graphed, and analyzed using GraphPad Prism 9.0.1 for macOS (GraphPad Software, San Diego, CA, www.graphpad.com).

### 3.5.6 B2H and β-galactosidase activity assay

N-terminal T18 and T25 fusions of McdA, all McdA mutant variants, and McdB were constructed using the plasmids pKT25 and pUT18C. Plasmids were sequence-verified and cotransformed into *E. coli* BTH101 in both pairwise combinations [61]. Several colonies of T18/T25 cotransformants were cultured in LB medium with 100 mg/ml ampicillin, 50 mg/ml kanamycin, and 0.5 mM IPTG overnight at 30°C with 225 rpm shaking. Overnight cultures were spotted on indicator LB X-gal plates supplemented with 100 mg/ml ampicillin, 50 mg/ml kanamycin, and 0.5 mM IPTG. Plates were incubated in the dark at 30°C up to 48 h before imaging. To quantify the interactions between hybrid proteins (Miller 1972), β-galactosidase activity measurements were performed as previously described [62] with slight modifications. Two hundred microliters of the overnight cultures were transferred into glass tubes containing 800 µl of Z buffer (45 mM $Na_2HPO_4.12H_2O$, 45 mM $NaH_2PO_4.H_2O$, 10 mM KCl, 1 mM $MgSO_4.7H_2O$, 38.5 mM β-mercaptoethanol). A drop of 0.01% SDS and two drops of chloroform were added, followed by 10 s of vigorous and thorough shaking to facilitate cell permeabilization. Once chloroform settled to the bottom (~15 s after mixing), 50 µl of the reaction mix were transferred into a 96-well flat-bottom microplate filled with 150 µl Z buffer already pre-equilibrated at 28°C in a SpectraMax iD3 microplate reader (Molecular Devices). To start the reaction, 40 µl 0.4% o-nitrophenyl-β-dgalactoside was added and measurements at $OD_{420}$ were taken every 2 min for 1 h at 28°C using the microplate reader. Concurrently, 50 µl of the overnight cultures were added to a well plate containing 150 µl LB for OD600 measurement in the microplate reader. β-galactosidase enzymatic activities, in Miller Units (MU), were calculated using the formula MU = A420/(incubation time in minutes x culture volume in milliliters x $OD_{600}$).

### 3.5.7 Total protein and immunoblot analyses

For total protein analysis in *E. coli*, a 0.2-ml aliquot was lysed using a Qsonica sonication system (20 cycles - 30 s on, 10 s off at 30% power) and centrifuged at 10,000 x g for 1 min at 4 °C. The protein content in the supernatant was measured using a Bradford assay kit (catalogue number 5000006; Bio-Rad Laboratories). Immunoblot samples from *E. coli* cells were prepared by adding an equal volume of 4x Laemmli sample buffer to cultures prior to boiling for 20 min. For immunoblot analyses of *S. elongatus* strains, cultures were concentrated to an $OD_{750}$ of 3 when harvesting. Immunoblot samples were generated by lysing cells with a Qsonica sonication system (20 cycles - 30 s on, 10 s off at 30% power) in 0.5 ml RuBisCO extraction buffer (50 mM EPPS at pH 8.1, 1% PVPP, 526 1 mM EDTA, 10 mM dithiothreitol (DTT), 0.1% Triton, and Sigma protease inhibitor). An equal volume of 2x Laemmli sample buffer was added to cell lysates and boiled for 20 min. Samples (55 µl) were loaded on a 4-12% Bis-Tris NuPAGE gel with wedge wells (Invitrogen). Gels were transferred onto a mini-size polyvinylidene difluoride membrane (Bio-Rad) using a Trans-Blot Turbo system (Bio-Rad). The membrane was immunoprobed using a mouse monoclonal antibody raised against amino acids 1-400 of *Bordetella pertussis* adenylate cyclase toxin origin (Santa Cruz Biotechnology), Cya A (1:1000), or a rabbit polyclonal antisera against McdA (1:1000) (New England Peptide). The membrane was then incubated with the goat antiMouse IgG Secondary Antibody IRDye 800 CW (LI-COR) or the HRP–conjugated anti-Rabbit IgG secondary antibody (Milipore Sigma). Membrane signals were developed with 508 Femto Maximum Sensitivity Substrate (Thermo Scientific) and visualized and quantified using LI-COR Image Studio. The McdA signal was normalized to a nonspecific band as indicated in Fig 3.3A.

### 3.5.8 Expression and purification of *Ct*McdA and *Ct*McdA[D38A]

Both *Ct*McdA and *Ct*McdA[D38A] were expressed and purified in a similar manner. For protein production, the expression plasmids for these constructs [6] were transformed into *E. coli* C41(DE3) cells (Lucigen). Transformants were grown at 37°C and 225 rpm until an $OD_{600}$ of 0.4–0.6 was reached. The culture flasks were rapidly cooled down to 15°C on and protein expression was then induced with the addition of 1 mM IPTG. After overnight induction, the cells were pelleted, flash-frozen in liquid nitrogen and stored at –80°C. Harvested cells were resuspended in Buffer A (25 mM Tris-HCl, pH 7.5, 300 mM NaCl, 10% glycerol, 0.5 mM BME, 50 mg/ml lysozyme, 1.25 kU benzonase, 2 protease inhibitor cocktail tablets) and lysed using a probe sonicator with 15 s on, 15 s off pulsation for 8 min. The lysate was cleared by centrifugation at 12,000 × g at 4 °C for 40 min in a Fiberlite TM F15-8 × 50 cy Fixed Angle Rotor (Thermo Fisher Scientific). The resulting lysate was filtered through a 0.45-µm syringe filter and loaded onto a 5-ml HiTrap TALON Crude cassette (GE) and eluted with a 0 to 400 mM imidazole gradient. Peak fractions were pooled and concentrated using an Amicon Ultra Centrifugal Device (10 KD MWCO). The concentrated protein sample was passed through a HiPrep 26/10 Desalting Column (GE) equilibrated in Q-Buffer (25 mM Tris-HCl, pH 7.5, 150 mM NaCl, 10% glycerol, 1 mM EDTA, 1 mM DTT). The sample was then immediately loaded onto a HiTrap Q HP 5 ml cassette (GE) equilibrated in Q-Buffer. The protein was eluted with a 150 mM to 2 M NaCl gradient. Peak fractions were concentrated to no more than 70 mM and flash-frozen aliquots were kept at –80°C.

### 3.5.9 DNA-binding assay

EMSAs were performed in a final reaction volume of 10 µl in a buffer containing 50 mM HEPES (pH 7.6), 5 mM MgCl2, and 100 mM KCl with 10 nM pUC19 plasmid (2.8 kb) as the supercoiled

DNA substrate. At the concentrations indicated, His-*Ct*McdA and His-*Ct*McdA[D38A] were incubated for 30 min at 23°C with or without ATP (1 mM). Reactions were then mixed with 1 µl 80% glycerol, run on 1% agarose gel in 1× TAE at 110V for 45 min, and stained with ethidium bromide prior to imaging.

### 3.5.10 Protein structure visualization and prediction

Molecular graphics and analyses of protein structures were performed with UCSF Chimera, developed by the Resource for Biocomputing, Visualization and Informatics at the University of California, San Francisco, with support from National Institutes of Health P41-GM103311 (Pettersen et al., 2004). Prediction of *Se*McdA structure was performed with Phyre2 [63].

## 3.6 Acknowledgments

We thank Joshua MacCready, Kiyoshi Mizuuchi, Maria Schumacher, and David Savage for helpful discussions. The pET15b expression vectors used for *Ct*McdA and *Ct*McdA[D38A] were kind gifts from Maria Schumacher. This work is supported by the National Science Foundation to A.G.V. (Award No. 1817478 and CAREER Award No. 1941966), Rackham Graduate Research Grant to P.H., Rackham Professional Development Grant to P.H., American Society for Microbiology Research Capstone Fellowship to P.H., Margaret Dow Towsley Scholarship to P.H., and by a research initiation fund to A.G.V. provided by the MCDB department, University of Michigan.

## 3.7 References

[1] J. Lutkenhaus, "The ParA/MinD family puts things in their place," *Trends Microbiol*, vol. 20, no. 9, pp. 411–418, 2012, doi: 10.1016/j.tim.2012.05.002.

[2] A. G. Vecchiarelli, K. Mizuuchi, and B. E. Funnell, “Surfing biological surfaces: exploiting the nucleoid for partition and transport in bacteria,” *Mol Microbiol*, vol. 86, no. 3, pp. 513–523, 2012, doi: 10.1111/mmi.12017.

[3] D. Kiekebusch and M. Thanbichler, “Plasmid segregation by a moving ATPase gradient,” *Proc National Acad Sci*, vol. 111, no. 13, pp. 4741–4742, 2014, doi: 10.1073/pnas.1402867111.

[4] E. V. Koonin, “A Superfamily of ATPases with Diverse Functions Containing Either Classical or Deviant ATP-binding Motif,” *J Mol Biol*, vol. 229, no. 4, pp. 1165–1174, 1993, doi: 10.1006/jmbi.1993.1115.

[5] M. A. Schumacher, Q. Ye, M. T. Barge, M. Zampini, D. Barillà, and F. Hayes, “Structural Mechanism of ATP-induced Polymerization of the Partition Factor ParF IMPLICATIONS FOR DNA SEGREGATION*,” *J Biol Chem*, vol. 287, no. 31, pp. 26146–26154, 2012, doi: 10.1074/jbc.m112.373696.

[6] M. A. Schumacher, M. Henderson, and H. Zhang, “Structures of maintenance of carboxysome distribution Walker-box McdA and McdB adaptor homologs.,” *Nucleic Acids Res*, vol. 47, no. 11, pp. 5950–5962, 2019, doi: 10.1093/nar/gkz314.

[7] H. Zhang and M. A. Schumacher, “Structures of partition protein ParA with nonspecific DNA and ParB effector reveal molecular insights into principles governing Walker-box DNA segregation.,” *Gene Dev*, vol. 31, no. 5, pp. 481–492, 2017, doi: 10.1101/gad.296319.117.

[8] T. D. Dunham, W. Xu, B. E. Funnell, and M. A. Schumacher, “Structural basis for ADP-mediated transcriptional regulation by P1 and P7 ParA,” *Embo J*, vol. 28, no. 12, pp. 1792–1802, 2009, doi: 10.1038/emboj.2009.120.

[9] J. C. Baxter and B. E. Funnell, “Plasmid Partition Mechanisms,” *Microbiol Spectr*, vol. 2, no. 6, 2014, doi: 10.1128/microbiolspec.plas-0023-2014.

[10] A. Badrinarayanan, T. B. K. Le, and M. T. Laub, “Bacterial Chromosome Organization and Segregation,” *Annu Rev Cell Dev Bi*, vol. 31, no. 1, pp. 171–199, 2015, doi: 10.1146/annurev-cellbio-100814-125211.

[11] A. S. B. Jalal and T. B. K. Le, “Bacterial chromosome segregation by the ParABS system,” *Open Biology*, vol. 10, no. 6, 2020, doi: 10.1098/rsob.200097.

[12] M. J. Davey and B. E. Funnell, “Modulation of the P1 Plasmid Partition Protein ParA by ATP, ADP, and P1 ParB,” *J Biol Chem*, vol. 272, no. 24, pp. 15286–15292, 1997, doi: 10.1074/jbc.272.24.15286.

[13] C. M. Hester and J. Lutkenhaus, “Soj (ParA) DNA binding is mediated by conserved arginines and is essential for plasmid segregation,” *Proc National Acad Sci*, vol. 104, no. 51, pp. 20326–20331, 2007, doi: 10.1073/pnas.0705196105.

[14] J. Castaing, J. Bouet, and D. Lane, “F plasmid partition depends on interaction of SopA with non-specific DNA,” *Mol Microbiol*, vol. 70, no. 4, pp. 1000–1011, 2008, doi: 10.1111/j.1365-2958.2008.06465.x.

[15] A. G. Vecchiarelli *et al.*, “ATP control of dynamic P1 ParA–DNA interactions: a key role for the nucleoid in plasmid partition,” *Mol Microbiol*, vol. 78, no. 1, pp. 78–91, 2010, doi: 10.1111/j.1365-2958.2010.07314.x.

[16] F. Pratto, A. Cicek, W. A. Weihofen, R. Lurz, W. Saenger, and J. C. Alonso, “Streptococcus pyogenes pSM19035 requires dynamic assembly of ATP-bound ParA and ParB on parS DNA during plasmid segregation,” *Nucleic Acids Res*, vol. 36, no. 11, pp. 3676–3689, 2008, doi: 10.1093/nar/gkn170.

[17] A. Sanchez *et al.*, "Stochastic Self-Assembly of ParB Proteins Builds the Bacterial DNA Segregation Apparatus," *Cell Syst*, vol. 1, no. 2, pp. 163–173, 2015, doi: 10.1016/j.cels.2015.07.013.
[18] B. E. Funnell, "ParB Partition Proteins: Complex Formation and Spreading at Bacterial and Plasmid Centromeres," *Frontiers Mol Biosci*, vol. 3, p. 44, 2016, doi: 10.3389/fmolb.2016.00044.
[19] L. C. Hwang *et al.*, "ParA-mediated plasmid partition driven by protein pattern self-organization," *Embo J*, vol. 32, no. 9, pp. 1238–1249, 2013, doi: 10.1038/emboj.2013.34.
[20] A. G. Vecchiarelli, J. C. Havey, L. L. Ing, E. O. Y. Wong, W. G. Waples, and B. E. Funnell, "Dissection of the ATPase Active Site of P1 ParA Reveals Multiple Active Forms Essential for Plasmid Partition," *J Biol Chem*, vol. 288, no. 24, pp. 17823–17831, 2013, doi: 10.1074/jbc.m113.469981.
[21] A. Volante and J. C. Alonso, "Molecular Anatomy of ParA-ParA and ParA-ParB Interactions during Plasmid Partitioning*," *J Biol Chem*, vol. 290, no. 30, pp. 18782–18795, 2015, doi: 10.1074/jbc.m115.649632.
[22] A. G. Vecchiarelli, K. C. Neuman, and K. Mizuuchi, "A propagating ATPase gradient drives transport of surface-confined cellular cargo," *Proc National Acad Sci*, vol. 111, no. 13, pp. 4880–4885, 2014, doi: 10.1073/pnas.1401025111.
[23] A. Turmo, C. R. Gonzalez-Esquer, and C. A. Kerfeld, "Carboxysomes: metabolic modules for CO2 fixation.," *Fems Microbiol Lett*, vol. 364, no. 18, 2017, doi: 10.1093/femsle/fnx176.
[24] C. Yehuda and G. Michael, "The Cyanobacteria—Ecology, Physiology and Molecular Genetics," New York, NY: Springer US, 2006, pp. 1074–1098. doi: 10.1007/0-387-30744-3_39.
[25] C. A. Kerfeld, C. Aussignargues, J. Zarzycki, F. Cai, and M. Sutter, "Bacterial microcompartments," *Nat Rev Microbiol*, vol. 16, no. 5, pp. 277–290, 2018, doi: 10.1038/nrmicro.2018.10.
[26] D. F. Savage, B. Afonso, A. H. Chen, and P. A. Silver, "Spatially Ordered Dynamics of the Bacterial Carbon Fixation Machinery," *Science*, vol. 327, no. 5970, pp. 1258–1261, 2010, doi: 10.1126/science.1186090.
[27] J. S. MacCready *et al.*, "Protein gradients on the nucleoid position the carbon-fixing organelles of cyanobacteria," *Elife*, vol. 7, p. e39723, 2018, doi: 10.7554/elife.39723.
[28] Y. Ah-Seng, F. Lopez, F. Pasta, D. Lane, and J.-Y. Bouet, "Dual Role of DNA in Regulating ATP Hydrolysis by the SopA Partition Protein*," *J Biol Chem*, vol. 284, no. 44, pp. 30067–30075, 2009, doi: 10.1074/jbc.m109.044800.
[29] E. Fung, J. Bouet, and B. E. Funnell, "Probing the ATP-binding site of P1 ParA: partition and repression have different requirements for ATP binding and hydrolysis," *Embo J*, vol. 20, no. 17, pp. 4901–4911, 2001, doi: 10.1093/emboj/20.17.4901.
[30] V. Libante, L. Thion, and D. Lane, "Role of the ATP-binding site of SopA protein in partition of the F plasmid," *J Mol Biol*, vol. 314, no. 3, pp. 387–399, 2001, doi: 10.1006/jmbi.2001.5158.
[31] D. Barillà, M. F. Rosenberg, U. Nobbmann, and F. Hayes, "Bacterial DNA segregation dynamics mediated by the polymerizing protein ParF," *Embo J*, vol. 24, no. 7, pp. 1453–1464, 2005, doi: 10.1038/sj.emboj.7600619.

[32] T. A. Leonard, P. J. Butler, and J. Lowe, “Bacterial chromosome segregation: structure and DNA binding of the Soj dimer - a conserved biological switch,” *Embo J*, vol. 24, no. 2, pp. 270–282, 2005, doi: 10.1038/sj.emboj.7600530.
[33] J. Lutkenhaus and M. Sundaramoorthy, “MinD and role of the deviant Walker A motif, dimerization and membrane binding in oscillation,” *Mol Microbiol*, vol. 48, no. 2, pp. 295–303, 2003, doi: 10.1046/j.1365-2958.2003.03427.x.
[34] D. Kiekebusch, K. A. Michie, L.-O. Essen, J. Löwe, and M. Thanbichler, “Localized Dimerization and Nucleoid Binding Drive Gradient Formation by the Bacterial Cell Division Inhibitor MipZ,” *Mol Cell*, vol. 46, no. 3, pp. 245–259, 2012, doi: 10.1016/j.molcel.2012.03.004.
[35] D. Schumacher *et al.*, “The PomXYZ Proteins Self-Organize on the Bacterial Nucleoid to Stimulate Cell Division,” *Dev Cell*, vol. 41, no. 3, pp. 299-314.e13, 2017, doi: 10.1016/j.devcel.2017.04.011.
[36] H. Ono, A. Takashima, H. Hirata, M. Homma, and S. Kojima, “The MinD homolog FlhG regulates the synthesis of the single polar flagellum of Vibrio alginolyticus,” *Mol Microbiol*, vol. 98, no. 1, pp. 130–141, 2015, doi: 10.1111/mmi.13109.
[37] J. S. Schuhmacher *et al.*, “MinD-like ATPase FlhG effects location and number of bacterial flagella during C-ring assembly,” *Proc National Acad Sci*, vol. 112, no. 10, pp. 3092–3097, 2015, doi: 10.1073/pnas.1419388112.
[38] M. A. J. Roberts, G. H. Wadhams, K. A. Hadfield, S. Tickner, and J. P. Armitage, “ParA-like protein uses nonspecific chromosomal DNA binding to partition protein complexes,” *Proc National Acad Sci*, vol. 109, no. 17, pp. 6698–6703, 2012, doi: 10.1073/pnas.1114000109.
[39] S. Ringgaard, M. Zepeda-Rivera, X. Wu, K. Schirner, B. M. Davis, and M. K. Waldor, “ParP prevents dissociation of CheA from chemotactic signaling arrays and tethers them to a polar anchor,” *Proc National Acad Sci*, vol. 111, no. 2, pp. E255–E264, 2014, doi: 10.1073/pnas.1315722111.
[40] E. M. Clerico, J. L. Ditty, and S. S. Golden, “Circadian Rhythms, Methods and Protocols,” *Methods Mol Biology*, pp. 155–171, 2007, doi: 10.1007/978-1-59745-257-1_11.
[41] N. C. Shaner *et al.*, “A bright monomeric green fluorescent protein derived from Branchiostoma lanceolatum,” *Nat Methods*, vol. 10, no. 5, pp. 407–409, 2013, doi: 10.1038/nmeth.2413.
[42] R. Rillema, Y. Hoang, J. S. MacCready, and A. G. Vecchiarelli, “Carboxysome Mispositioning Alters Growth, Morphology, and Rubisco Level of the Cyanobacterium Synechococcus elongatus PCC 7942,” *Mbio*, vol. 12, no. 4, pp. e02696-20, 2021, doi: 10.1128/mbio.02696-20.
[43] S. Ringgaard, J. van Zon, M. Howard, and K. Gerdes, “Movement and equipositioning of plasmids by ParA filament disassembly,” *Proc National Acad Sci*, vol. 106, no. 46, pp. 19369–19374, 2009, doi: 10.1073/pnas.0908347106.
[44] C. Planchenault *et al.*, “Intracellular positioning systems limit the entropic eviction of secondary replicons toward the nucleoid edges in bacterial cells,” *J Mol Biol*, 2020, doi: 10.1016/j.jmb.2019.11.027.
[45] I. Brännudd, E. Karlsson, G. Nordblom, M. Sjögren, L. S. Näslund, and J. Stevrell, “Unravelling the Mechanisms of Multifunctional Antibiotic Drugs,” 2020.

[46] J. Adler and I. Parmryd, “Quantifying colocalization by correlation: The Pearson correlation coefficient is superior to the Mander’s overlap coefficient,” *Cytom Part A*, vol. 77A, no. 8, pp. 733–742, 2010, doi: 10.1002/cyto.a.20896.
[47] B. Youngren and S. Austin, “Altered ParA partition proteins of plasmid P1 act via the partition site to block plasmid propagation,” *Mol Microbiol*, vol. 25, no. 6, pp. 1023–1030, 1997, doi: 10.1046/j.1365-2958.1997.4761842.x.
[48] J. S. MacCready, J. L. Basalla, and A. G. Vecchiarelli, “Origin and Evolution of Carboxysome Positioning Systems in Cyanobacteria,” *Mol Biol Evol*, 2020, doi: 10.1093/molbev/msz308.
[49] J. S. MacCready, L. Tran, J. L. Basalla, P. Hakim, and A. G. Vecchiarelli, “The McdAB system positions α-carboxysomes in proteobacteria,” *Mol Microbiol*, 2021, doi: 10.1111/mmi.14708.
[50] A. A. Rangarajan, N. M. Koropatkin, and J. S. Biteen, “Nutrient-dependent morphological variability of Bacteroides thetaiotaomicron,” *Microbiology+*, vol. 166, no. 7, pp. 624–628, 2020, doi: 10.1099/mic.0.000924.
[51] B. R. Parry, I. V. Surovtsev, M. T. Cabeen, C. S. O’Hern, E. R. Dufresne, and C. Jacobs-Wagner, “The Bacterial Cytoplasm Has Glass-like Properties and Is Fluidized by Metabolic Activity,” *Cell*, vol. 156, no. 1–2, pp. 183–194, 2014, doi: 10.1016/j.cell.2013.11.028.
[52] N. Erdmann, T. Petroff, and B. E. Funnell, “Intracellular localization of P1 ParB protein depends on ParA and parS,” *Proc National Acad Sci*, vol. 96, no. 26, pp. 14905–14910, 1999, doi: 10.1073/pnas.96.26.14905.
[53] M. Sengupta, H. J. Nielsen, B. Youngren, and S. Austin, “P1 Plasmid Segregation: Accurate Redistribution by Dynamic Plasmid Pairing and Separation ▿ †,” *J Bacteriol*, vol. 192, no. 5, pp. 1175–1183, 2010, doi: 10.1128/jb.01245-09.
[54] T. Hatano and H. Niki, “Partitioning of P1 plasmids by gradual distribution of the ATPase ParA,” *Mol Microbiol*, vol. 78, no. 5, pp. 1182–1198, 2010, doi: 10.1111/j.1365-2958.2010.07398.x.
[55] Y. Sun *et al.*, “Light Modulates the Biosynthesis and Organization of Cyanobacterial Carbon Fixation Machinery through Photosynthetic Electron Flow,” *Plant Physiol*, vol. 171, no. 1, pp. 530–541, 2016, doi: 10.1104/pp.16.00107.
[56] D. G. Gibson, L. Young, R.-Y. Chuang, J. C. Venter, C. A. Hutchison, and H. O. Smith, “Enzymatic assembly of DNA molecules up to several hundred kilobases,” *Nat Methods*, vol. 6, no. 5, pp. 343–345, 2009, doi: 10.1038/nmeth.1318.
[57] G. MR and S. J, *Molecular Cloning: A Laboratory Manual, Fourth Edition*. New York: Cold Spring Harbor Laboratory Press., 2012.
[58] J. Schindelin *et al.*, “Fiji: an open-source platform for biological-image analysis,” *Nat Methods*, vol. 9, no. 7, pp. 676–682, 2012, doi: 10.1038/nmeth.2019.
[59] A. Ducret, E. M. Quardokus, and Y. V. Brun, “MicrobeJ, a tool for high throughput bacterial cell detection and quantitative analysis,” *Nat Microbiol*, vol. 1, no. 7, p. 16077, 2016, doi: 10.1038/nmicrobiol.2016.77.
[60] S. Bolte and F. P. Cordelières, “A guided tour into subcellular colocalization analysis in light microscopy,” *J Microsc-oxford*, vol. 224, no. 3, pp. 213–232, 2006, doi: 10.1111/j.1365-2818.2006.01706.x.
[61] G. Karimova, J. Pidoux, A. Ullmann, and D. Ladant, “A bacterial two-hybrid system based on a reconstituted signal transduction pathway,” *Proc National Acad Sci*, vol. 95, no. 10, pp. 5752–5756, 1998, doi: 10.1073/pnas.95.10.5752.

[62] A. Battesti and E. Bouveret, “The bacterial two-hybrid system based on adenylate cyclase reconstitution in Escherichia coli,” *Methods*, vol. 58, no. 4, pp. 325–334, 2012, doi: 10.1016/j.ymeth.2012.07.018.
[63] L. A. Kelley, S. Mezulis, C. M. Yates, M. N. Wass, and M. J. E. Sternberg, “The Phyre2 web portal for protein modeling, prediction and analysis,” *Nat Protoc*, vol. 10, no. 6, pp. 845–858, 2015, doi: 10.1038/nprot.2015.053.

# CHAPTER IV

## Multi-Generational Live-Cell Imaging of *S. elongatus* as A Powerful Tool For The Study Of Carboxysome Positioning And Inheritance

### 4.1 Abstract

The dynamic process of carboxysome biogenesis, trafficking, and homeostasis involve a complex series of protein self-assembly and self-organization in cyanobacteria. Multiple studies have outlined the sequential and stepwise assembly of carboxysomes during biogenesis and budding events. Due to the multilayered constraints of long-term imaging of cyanobacteria, many reports are limited to capturing still snapshots of these slow growing bacteria and over short periods. To further our understanding of McdAB-based carboxysome positioning and inheritance during cellular growth and division, the development and optimization of long term and multi-generational fluorescence imaging is required. Here, I establish a workflow that overcomes the challenges associated with the long-term imaging on cyanobacteria. The method allows us to now determine how the McdAB system functions throughout the entire cell cycle of *S. elongatus*, and study how the positioning reaction is influenced by cell division, diurnal growth, and circadian rhythms.

## 4.2 Introduction

Bacteria have served as pivotal model systems for the study of cellular and biochemical mechanisms and functions. The discovery of cytokinetic Z ring formation upon cell division by the polymerization of a bacterial tubulin homolog, FtsZ, was one of the earliest key pieces of evidence that like eukaryotes, bacteria employ dynamic subcellular protein organization as a means to regulate their growth and metabolic processes [133]. With the rapid advancements of fluorescence microscopy techniques in recent years, the field of prokaryotic cell biology has benefited greatly from the growing number of spatiotemporally characterized proteins, and our understanding of bacterial cell architecture and organization continues to expand.

Genome sequencing and microbial genetic tools have proven to be instrumental in studying the relationship between genotypes and phenotypes, but these approaches are not capable of elucidating the underlying molecular mechanism of protein interactions and their cellular functions. Imaging key protein players of a molecular event in their native cellular environment can address the "how, where and when" questions that we continually ask in our pursuit to bridge the gap between the wealth of bacterial genetic information the prokaryotic biology field has amassed and the puzzles of bacterial cellular functions we are still trying to solve.

Studies involving live-cell imaging of cyanobacteria have provided the field with an invaluable insight into how a mesoscale proteinaceous complex such as the carboxysome is formed and spatially organized in the cell. By fluorescently labelling the large subunit of Rubisco and a carboxysome shell protein, CcmK4, Savage and team [53] were able to initially report on the equidistant positioning of carboxysomes in *S. elongatus* and tracked the unequal carboxysome inheritance that occurs when *mcdA* is deleted. Indeed, long term imaging of cyanobacterial cells devoid of inherited carboxysomes showed delayed division time, thus underscoring the important

relationship between proper carboxysome maintenance and cell fitness [2]. Subsequently, the work of Cameron and colleagues in 2013 [33] successfully visualized the sequential dynamics of carboxysome formation and showed for the first time that new carboxysomes bud off from preexisting procarboxyomes. And more recently, long term imaging of *Synechococcu*s sp. PCC 7002 allowed individual carboxysomes to be tracked and visualized for more than 60 continuous hours, giving researchers a detailed glimpse on how carboxysomes are inherited, maintained and eventually become polarly-localized just prior to undergoing disassembly [134].

Unfortunately, multi-generational microscopy of cyanobacteria is made difficult by their biological properties. The photosynthetic apparatus needed to convert harvested light energy to usable chemical energy in cyanobacteria is localized to a network of internal thylakoid membranes [135]. Localized inside these membranes are photopigments responsible for light harvesting as well as for photoprotection by the route of non-photochemical quenching [136]. Most cyanobacteria, *S. elongatus* included, carry (i) the photopigments chlorophyll *a*; (ii) the red-shifted phycobiliproteins phycocyanin, allophycocyanin and allophycocyanin-B, and (iii) a wide variety of carotenoids such as β-carotene and zeaxanthin [136], [137]. By mapping the individual fluorescent emission spectra of these classes of pigments, one can fully appreciate the breadth of endogenous background signals present in photosynthetic cyanobacteria across the visible light spectrum (Fig. 4.1A) [138]. This biological property is especially striking when compared to non-photosynthetic bacteria like *E. coli*, which displays minimal endogenous fluorescence when imagined in the red and green fluorescence channels (Fig. 4.1B).

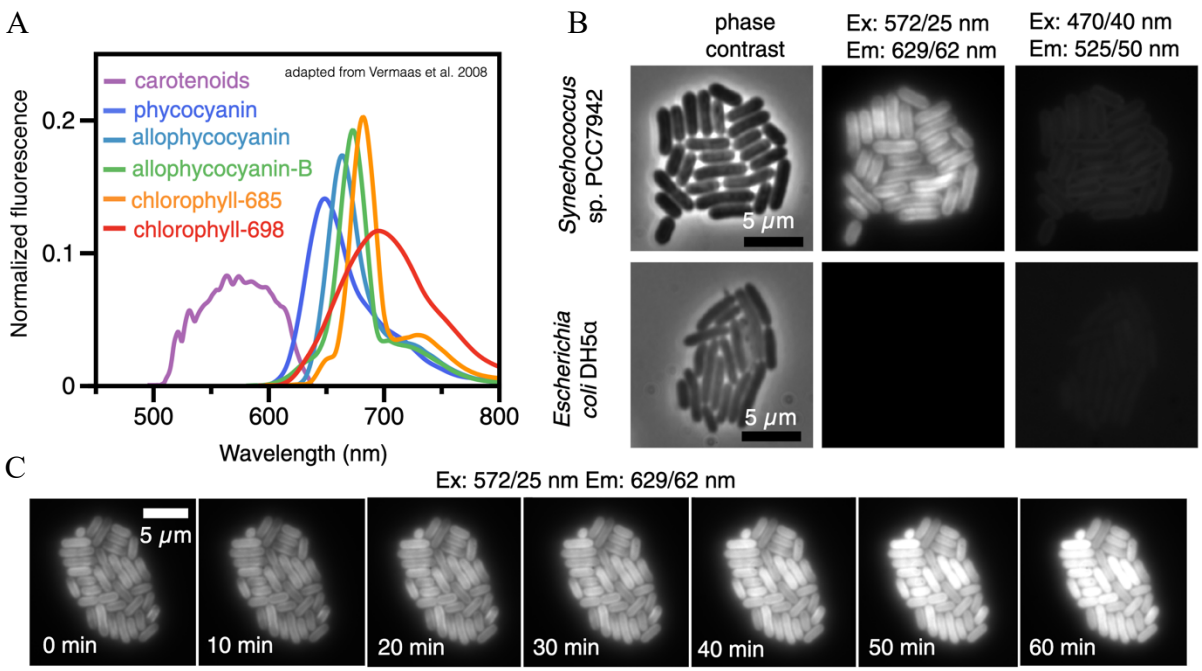


Figure 4.1: **Cyanobacteria possess endogenous fluorescence due to the presence of photopigments.** A. Spectral emission of live *Synechocystis* sp. PCC6803 cells, adapted from [8]. B. Endogenous fluorescence of *S. elongatus* in comparison to *E. coli* DH5a using typical RFP (572ex/629em) and GFP (470ex/525em) filter sets. C. Fluorescent imaging of *S. elongatus* in the red channel leads to photosystem saturation and consequently, increased background fluorescent signal. Reprinted with permission from [9].

During the light dependent stage of photosynthesis, captured photons are passed from the light gathering antenna system to the reaction centers; with the end goal for the excited photons to return to ground state [139]. This electron transfer flux is limited in its functional capacity, specifically under excess illumination [140]. Because of this biological limitation, continuous fluorescence imaging of cyanobacteria is particularly challenging due to the markedly increased fluorescence background signal observed over time (Fig. 4.1C).

The myriad of photopigments present in cyanobacteria reemit collected photons in the 600 nm region and beyond (Fig. 4.1C). With this in mind, the choice of fluorophores, especially for two color imaging, that can be used in cyanobacteria are limited (Fig. 4.2). The use of any red fluorophores such as mCherry would overlap significantly with cyanobacterial background

emission. *S. elongatus* strains carrying fluorescent fusions engineered in the lab typically pairs monomeric NeonGreen (mNG; yellow shifted) and monomeric Turqoise2 (mTQ; blue shifted). But exposing growing cyanobacteria to blue light for an extended amount of time can lead to cellular phototoxicity due to an imbalanced energy transfer between their two photosystems, ultimately leading to photosynthetic inefficiency [141]. There is a need to develop and optimize fluorescence imaging workflows for cyanobacteria, as a means to understand subcellular organization as it relates to the entire bacterial cell cycle and environmental influence.

Our previous study implicated the oscillating ParA-like ATPase McdA to be responsible in modulating the spatial distribution of McdB-bound carboxysomes along the longitudal axis of *S. elongatus* cells [31]. In this study, I found that McdA is a voracious ATPase, displaying ATPase activity that is more than 200-fold higher than other canonical ParA family members (Chapter II, [31]). A few questions naturally arise from the study: (i) Is there still a biological need to actively maintain equidistant carboxysome positioning by burning ATP to sustain McdA oscillations at night when carbon fixation is not occuring? (ii) How does the rhythmic nature of cellular ATP levels in *S. elongatus* influence McdA oscillation throughout the course of a 24-hour day? (iii) How is the oscillating McdA population inherited in dividing *S. elongatus* cells? If cells inherit the McdA pool asymmetrically, how is this imbalance rectified after division? Establishing a multi-generational live-cell imaging approach that is tailored to slow-growing *S. elongatus* cells will provide a means to answer these and other open questions regarding cyanobacterial cell biology, which is a largely untapped field of research.

To carry out long term microscopy of cyanobacteria, the imaging setup will have to sustain multi-day photosynthetic growth while simultaneously keeping drifts of the region of interest and phototoxicity-induced growth defects to a minimum. In this chapter, I outline the workflow I have

established to successfully carry out multi-generational imaging of *S. elongatus*. As outlined below, this technique will allow us to determine the effects of cell division, day/night cycle, and circadian rhythms on carboxysome positioning by the McdAB system in cyanobacteria.

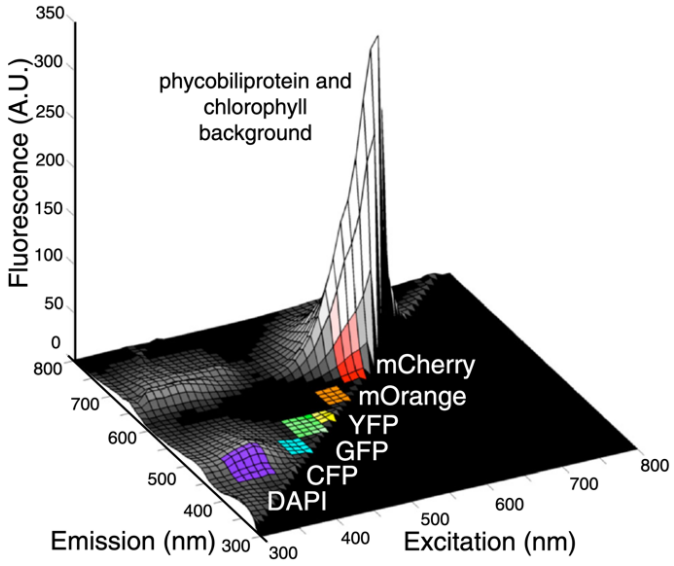


Figure 4.2: **Excitation and emission scan of *S. elongatus* cells plotted with commercially available fluorophore filter set from Carl Zeiss.** z-axis (fluorescence) is in arbitrary units. Reprinted with permission from [9].

## 4.3 Results

### 4.3.1 McdA continues to oscillate during division, which results in an McdA imbalance between daughter cells

To capture multi-generational time lapse images of *S. elongatus*, cells were immobilized on a 1.5% BG-11 agarose pad that was cast in a glass bottom dish (detailed in Material and Methods section in Chapter III). This mounting technique allows for free gaseous exchange to occur while minimizing dehydration. I used the transilluminating light emitting diode (LED) source on the microscope fitted with a 515-nm longpass filter as the light source to sustain photosynthetic growth

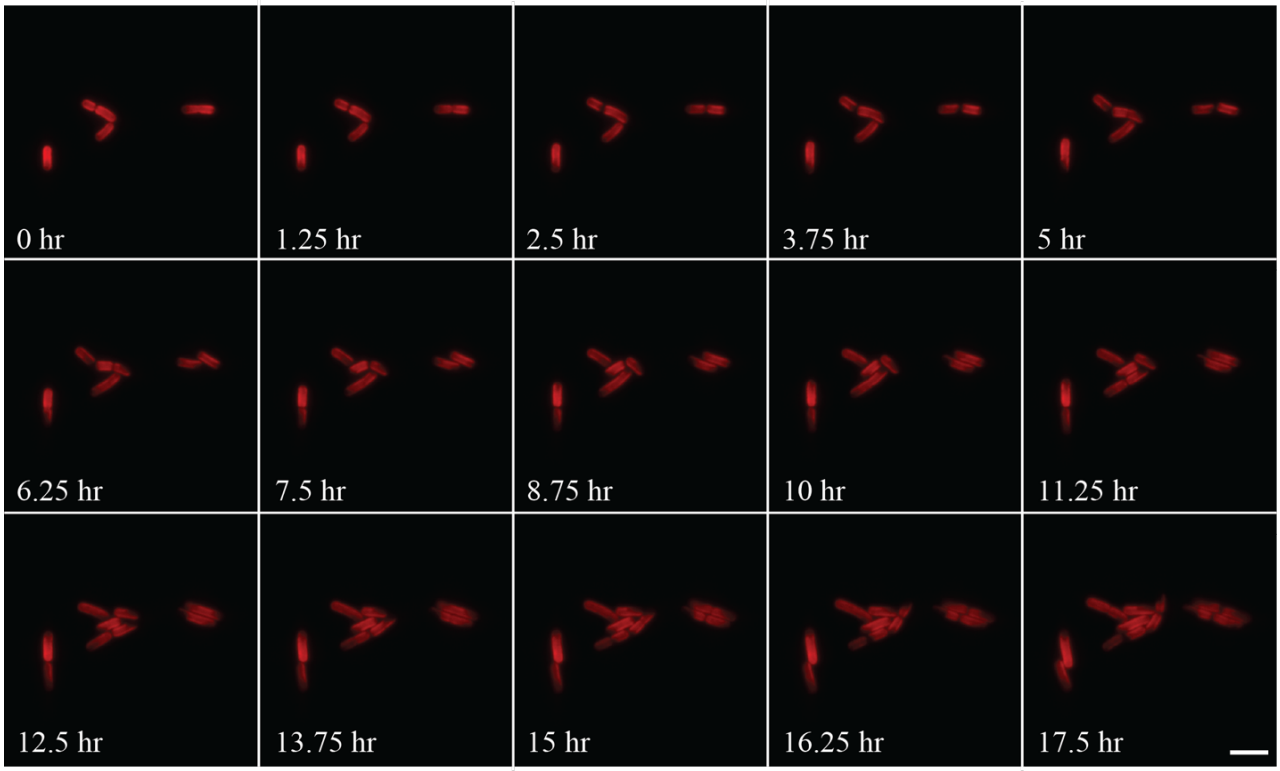


Figure 4.3: **Long-term imaging of *S. elongatus* cells.** Time course showing *S. elongatus* cell growth under constant illumination by the microscope's LED light source (> 515 nm wavelength) at 60 µmol $m^{-2}$ $s^{-1}$ light intensity, 32°C and 5% $CO_2$. Signal shown here is of chlorophyll in the thylakoid membrane imaged in red channel as cell outlines. Scale bars: 5 µm. Time-lapse video: Movie 4.1.

of *S. elongatus* cells. Temperature, humidity, and $CO_2$ control were all provided via the use of a stage-top incubator system.

With the described setup and abiotic conditions, growth of *S. elongatus* colonies could be sustained for up to 2 days with a doubling time of roughly 5-6 hours, which is consistent with previously recording double times of *S. elongatus* when grown in liquid culture [142] (Fig. 4.3, Movie 4.1). Chlorophyll fluorescence in the thylakoid membrane was used to determine cell perimeter and growth rate.

The McdAB system actively distributes carboxysomes allowing for faithful inheritance in newly formed daughter cells [31], [53]. In dividing *S. elongatus* cells, mNG-McdA displayed

robust oscillatory dynamics through the invaginating septum during the early stages of cytokinesis (Figure 4.4). While I observed an McdAB system-mediated equal carboxysome distribution between the resulting daughter cyanobacterial cells post-division, one cell ultimately inherited all of the McdA pool due to its slow oscillation period (~11 minutes) (Fig. 4.4, last panel). How *S. elongatus* cells actively sense and regulate cellular McdA concentrations is a subject of future studies using this long term imaging approach.

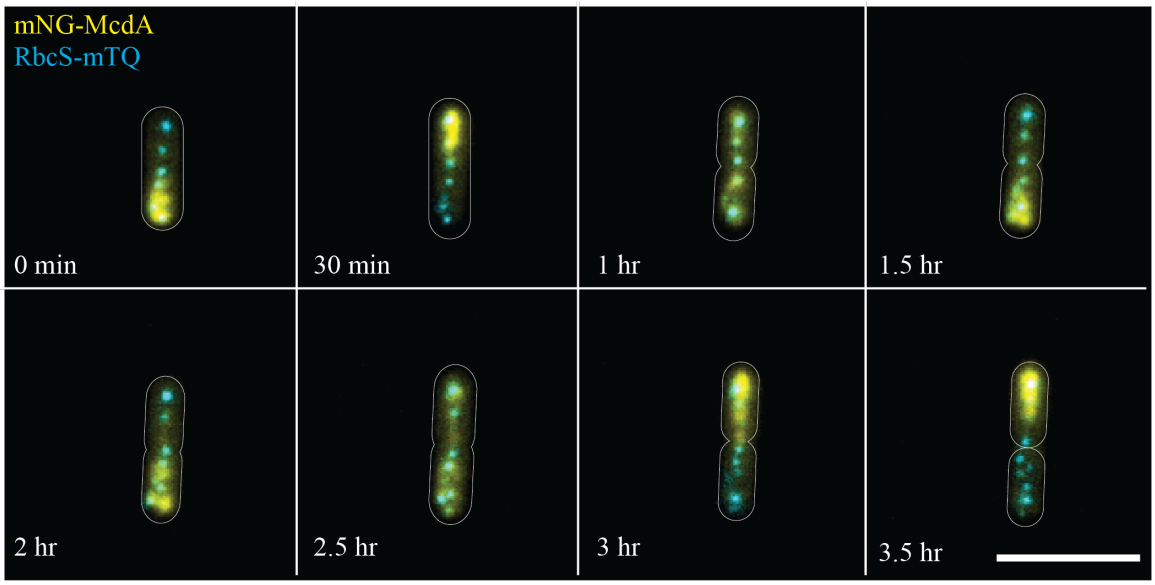


Figure 4.4: **McdA oscillatory patterning remains robust throughout cell cycle and division.** Time course images showing merged mNG-McdA (yellow) and carboxysome foci (cyan) signals during cytokinesis. Cell outlines in fluorescent channels are based on chlorophyll fluorescence in the thylakoid membrane imaged in red channel. Scale bars: 5 μm.

### 4.3.2 Entrained *S. elongatus* cells undergo light-dependent growth and division

Cyanobacterial global gene expression, growth, cell division and cellular processes are regulated by its circadian rhythm [143]. *S. elongatus* has long been employed as the main model organism for the study of a prokaryotic circadian oscillator. Cyanobacterial cells grown in constant illumination in a laboratory setting can be entrained so that their endogenous circadian rhythm is synchronized with an external 12 hr light: 12 hr dark cycle [144]. The entrainment process involves

maintaining the cyanobacterial cultures in an active growing environment by constant dilution of batch cultures to maintain a constant cell density during light/dark growth [145]. It is currently unknown if and how day/night cycles and the circadian clock influences carboxysome positioning by the McdAB system.

I have successfully optimized a workflow for sustaining photosynthetic growth of entrained *S. elongatus* cells on the microscope by synchronizing the timing of the LED transilluminator shutter with the light exposure setting of our photosynthetic incubators where batch liquid cultures are grown. Consistent with previous reports [142], [145], [146], I was able to capture diurnal cycle-dependent cell growth and division in entrained *S. elongatus* cells by maintaining day/night light exposure on the microscope (Fig. 4.5, Movie 4.2). Entrained *S. elongatus* cells showed cellular growth and division events only during the relative day period. During the relative night, cells halted growth and division.

It has been shown that entrained *S. elongatus* cells have a period of slowed cell division rates consistent with the onset of early relative night period [145]. Additionally, cell division occurs exclusively in the presence of light and uncoupled from circadian rhythm regulation [145]. In contrast, the circadian clock is also capable of inhibiting cell division when light is present, in a phenomenon termed circadian gating [145]. The biological phenomenon takes place when cells are synchronized in diurnal cycles and subsequently released into constant light. As *S. elongatus* cells anticipate the impending dark periods (termed subjective night), the onset of cell division is inhibited during the initial 4-6 hour window [142]. This multifaceted regulatory mechanism of *S. elongatus* circadian-controlled cellular processes highlights the importance of unravelling how environmental cues affects the dynamics of McdAB system in ensuring proper carboxysome trafficking, homeostasis, and inheritance.

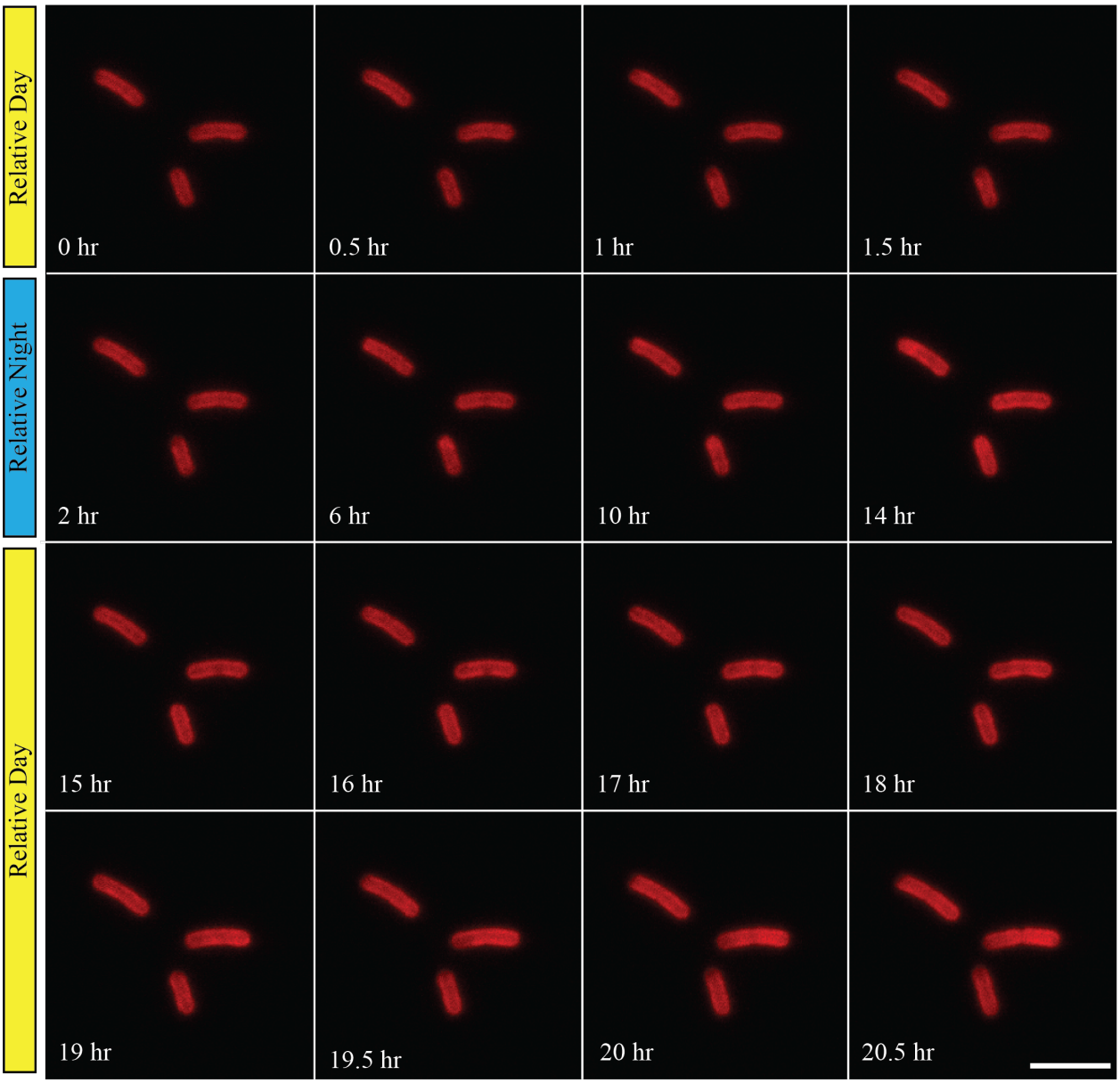


Figure 4.5: **Entrained *S. elongatus* cells displayed diurnal-dependent cell growth and division patterns.** Time course images showing *S. elongatus* cellular elongation and division coinciding with relative day and night periods (indicated in the left panel). Signal shown is of thylakoid membrane imaged in red channel as cell outlines. Scale bars: 5 μm. Time-lapse video: Movie 4.2.

### 4.3.3 McdA oscillatory dynamics, carboxysome biogenesis and positioning in entrained *S. elongatus* cells persist throughout growth in light/dark cycles

My previous work has established that McdA is a unique member of the ParA/MinD family, possessing an uncharacteristically high ATPase activity [31], [147]. The temporal separation between photosynthesis during diurnal growth and energy utilization in the dark phase inevitably causes changes in ATP/ADP ratios. In *S. elongatus*, ATP levels were observed to steeply decrease within the first 2 min after the shift into dark phase [148], [149], followed by a gradual decrease to 50% of the pre-dark ATP level and subsequent rapid recovery when the cells are exposed to light again [150]. Given the unusually high ATPase activity of McdA compared to other ParA/MinD family ATPases, I next set out to determine if McdA oscillation and carboxysome dynamics are affected during light-dependent cellular growth and division in entrained *S. elongatus* cells.

As shown previously, mNG-McdA displays pole-to-pole oscillations while actively positioning newly formed and already present carboxysomes in the presence of light (Fig. 4.6, top and last rows; Movie 4.3). Surprisingly, during the dark cycle, mNG-McdA oscillations persisted and carboxysome distribution was maintained in these entrained *S. elongatus* cells (Fig. 4.6, two middle rows; Movie 4.3). This finding suggests that despite the high energy expenditure *S. elongatus* cells incur to maintain McdA oscillation during the dark cycle with decreased ATP levels present, the benefits of distributing carboxysomes outweigh the cost of cellular energy expenditure.

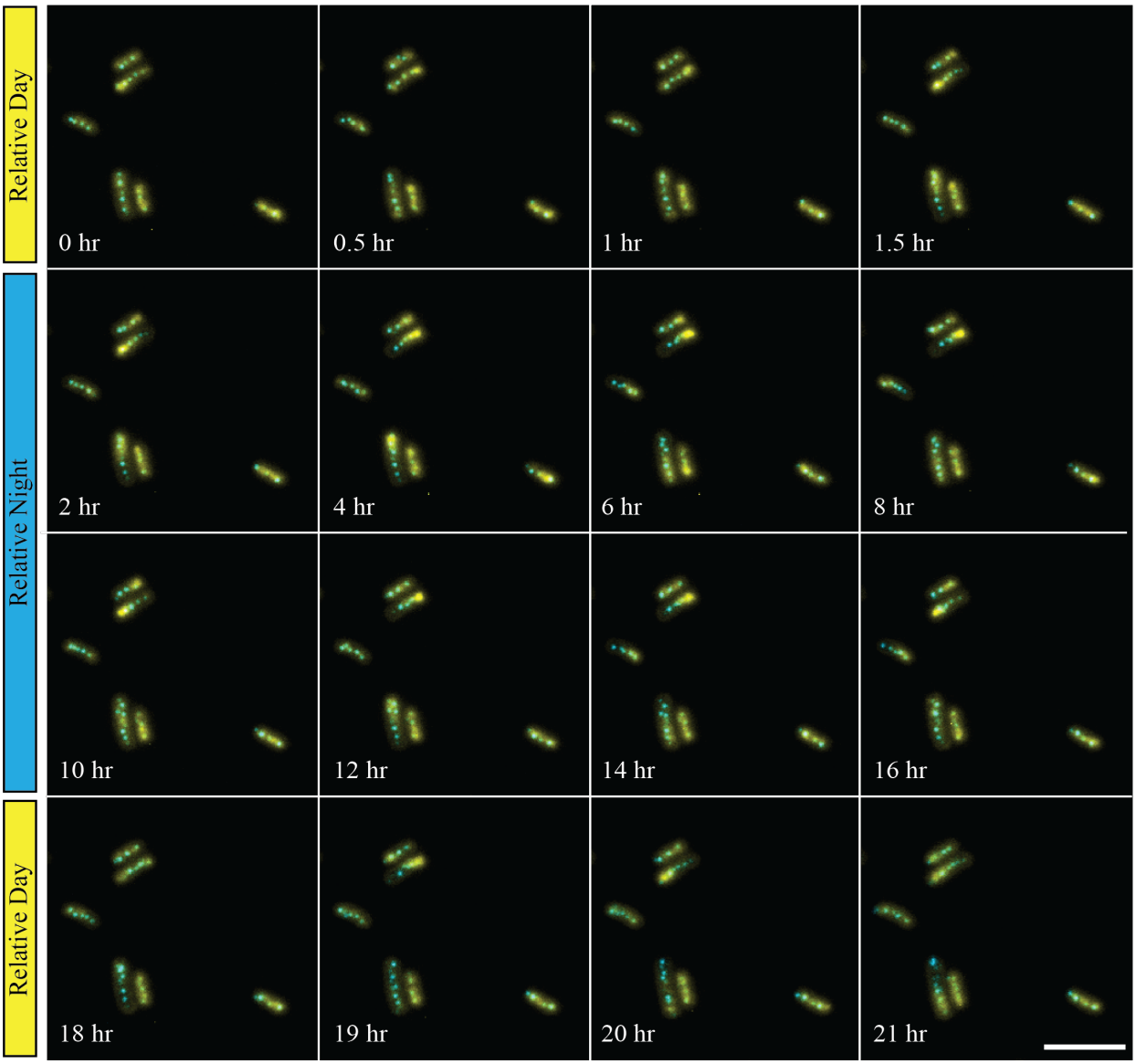


Figure 4.6: **McdA oscillatory patterning maintains carboxysome positioning in entrained *S. elongatus* cells throughout diurnal growth**. Time course images showing merged mNG-McdA (yellow) and carboxysome foci (cyan) signals during growth in light/dark diel cycles (indicated in the left panel). Scale bars: 5 μm. Time-lapse video: Movie 4.3.

## 4.4 Discussion

Long term and multi-generational fluorescent imaging of cyanobacterial cells has been challenging due to multiple constraints presented by these microorganisms' inherent physical and biological properties [54]. To establish an efficient workflow for long term imaging of *S. elongatus* cells, I

first had to reconfigure the existing imaging hardware on the microscope to sustain photosynthetic growth on the microscope stage. With the use of a highly sensitive and tunable stage top incubator system, I was able to control and maintain optimal humidity, temperature, and $CO_2$ concentration surrounding the agarose pad harboring immobilized *S. elongatus* cells. Humidity control was required to limit drift that occurs as the agar pad dehydrates over long-term imaging. Temperature control and maintenance is critical for imaging photosynthetic growth on the stage top because of the heat generated from near continuous light exposure. Finally, high $CO_2$ (5%) is required to boost the growth rate of *S. elongatus* to obtain experimentally feasible doubling times (~ 6 hrs in high $CO_2$ compared to ~15 hrs in ambient $CO_2$). Finally, I had to balance acquisition parameters to minimize phototoxicity-induced growth defects and fluorophore photobleaching. Taken together, I was able to overcome these limitations and establish a roadmap for successful long term and multi-generational cyanobacterial cell imaging in the lab.

Overall, this newly established imaging workflow enabled me to observe mNG-McdA and fluorescent carboxysome inheritance and dynamics during long term growth as well as during cell division. I found that mNG-McdA maintains its pole-to-pole oscillation through forming septa during cell division (Fig. 4.4) and during dark cycles in entrained *S. elongatus* cells (Fig. 4.6, Movie 4.3). We initially hypothesized that *S. elongatus* would halt or potentially dampen its McdA oscillatory patterning at night as a response to depleting cellular concentrations of ATP [148]–[150]. Strikingly, I observed continued mNG-McdA oscillation in entrained *S. elongatus* cells throughout the light/dark cycles.

Based on my results, this persistent mNG-McdA oscillation is imperative in maintaining proper carboxysome positioning. Intriguingly, I found that new carboxysomes were still being assembled and positioned during the dark cycles (Fig. 4.6, Movie 4.3). Sun and colleagues [151]

have reported that carboxysome abundance, dynamics, and carbon fixation activities are modulated in *S. elongatus* cells as a response to the metabolic changes that happen during diurnal growth, with carboxysomes assuming a more polar localization during the dark period. Reports have also shown that procarboxysomes and inactivated carboxysomes are more polarly located [33], [151]. It is possible that there might be an unknown, McdAB-mediated mechanism involved that would sequester this subset of carboxysomes into the polar regions transiently during the dark cycle while maintaining normal cellular distribution for other functionally mature carboxysomes. This could explain why *S. elongatus* cells would still invest in the cellular energy expenditure needed to maintain McdA oscillation in the dark despite falling ATP storage.

We have previously reported that *mcdA* overexpression causes a collapse of its oscillatory patterning meanwhile overexpression of *mcdB* led to the formation of bar carboxysomes with altered ultrastructure as seen in their fluorescent and TEM images [31]. Additionally, similarly elongated carboxysome signals were observed in Δ*ccmL* mutant strains of *S. elongatus*, presumably due to a failure in shell closure and thus, incomplete dissociation of new carboxysomes budding from preexisting procarboxysomes [33]. Visualizing the sequential biogenesis events leading to these abnormal carboxysome phenotypes via long term and multigenerational imaging of *S. elongatus* cells could answer pertinent questions in the field, especially ones centering on how McdAB stoichiometry imbalance could cause such dramatic changes to McdA function as well as carboxysome size, ultrastructure, and homeostasis in the cell.

## 4.5 Materials and Methods

### 4.5.1 Culture growth conditions and entrainment

All *S. elongatus* culture growth conditions are as described in Chapter III (page 75). To synchronize cellular growth phase during entrainment [17], *S. elongatus* batch cultures were grown in a 12 hr light: 12 hr dark cycles with continuous dilution in order to maintain a maximal $OD_{750}$ of 0.1 for three consecutive days. Batch cultures were kept in this light/dark cycles until cells are ready to be imaged.

### 4.5.2 Fluorescence and time-lapse microscopy

Visualization methods are as described in Chapter III (page 77). Videos were taken at one frame every 15 min for a duration of up to 42 hours.

## 4.6 References

[1] E. Bi and J. Lutkenhaus, "FtsZ ring structure associated with division in Escherichia coli," *Nature*, vol. 354, no. 6349, pp. 161–164, 1991, doi: 10.1038/354161a0.
[2] D. F. Savage, B. Afonso, A. H. Chen, and P. A. Silver, "Spatially Ordered Dynamics of the Bacterial Carbon Fixation Machinery," *Science*, vol. 327, no. 5970, pp. 1258–1261, 2010, doi: 10.1126/science.1186090.
[3] J. C. Cameron, S. C. Wilson, S. L. Bernstein, and C. A. Kerfeld, "Biogenesis of a Bacterial Organelle: The Carboxysome Assembly Pathway," *Cell*, vol. 155, no. 5, pp. 1131–1140, 2013, doi: 10.1016/j.cell.2013.10.044.
[4] N. C. Hill, J. W. Tay, S. Altus, D. M. Bortz, and J. C. Cameron, "Life cycle of a cyanobacterial carboxysome," *Sci Adv*, vol. 6, no. 19, p. eaba1269, 2020, doi: 10.1126/sciadv.aba1269.
[5] J. Mareš, O. Strunecký, L. Bučinská, and J. Wiedermannová, "Evolutionary Patterns of Thylakoid Architecture in Cyanobacteria," *Front Microbiol*, vol. 10, p. 277, 2019, doi: 10.3389/fmicb.2019.00277.
[6] Y. Sun, F. Huang, and L.-N. Liu, "Microbial Photosynthesis," pp. 319–343, 2020, doi: 10.1007/978-981-15-3110-1_15.
[7] A. R. Grossman, D. Bhaya, K. E. Apt, and D. M. Kehoe, "Light-Harvesting Complexes in Oxygenic Photosynthesis: Diversity, Control, and Evolution," *Annu Rev Genet*, vol. 29, no. 1, pp. 231–288, 1995, doi: 10.1146/annurev.ge.29.120195.001311.
[8] W. F. J. Vermaas *et al.*, "In vivo hyperspectral confocal fluorescence imaging to determine pigment localization and distribution in cyanobacterial cells," *Proc National Acad Sci*, vol. 105, no. 10, pp. 4050–4055, 2008, doi: 10.1073/pnas.0708090105.

[9] R. Yokoo, R. D. Hood, and D. F. Savage, “Live-cell imaging of cyanobacteria,” *Photosynth Res*, vol. 126, no. 1, pp. 33–46, 2015, doi: 10.1007/s11120-014-0049-x.
[10] D. Campbell, V. Hurry, A. K. Clarke, P. Gustafsson, and G. Öquist, “Chlorophyll Fluorescence Analysis of Cyanobacterial Photosynthesis and Acclimation,” *Microbiol Mol Biol R*, vol. 62, no. 3, pp. 667–683, 1998, doi: 10.1128/mmbr.62.3.667-683.1998.
[11] G. H. Krause and E. Weis, “Chlorophyll Fluorescence and Photosynthesis: The Basics,” *Annu Rev Plant Phys*, vol. 42, no. 1, pp. 313–349, 1991, doi: 10.1146/annurev.pp.42.060191.001525.
[12] V. M. Luimstra, J. M. Schuurmans, A. M. Verschoor, K. J. Hellingwerf, J. Huisman, and H. C. P. Matthijs, “Blue light reduces photosynthetic efficiency of cyanobacteria through an imbalance between photosystems I and II,” *Photosynth Res*, vol. 138, no. 2, pp. 177–189, 2018, doi: 10.1007/s11120-018-0561-5.
[13] J. S. MacCready *et al.*, “Protein gradients on the nucleoid position the carbon-fixing organelles of cyanobacteria,” *Elife*, vol. 7, p. e39723, 2018, doi: 10.7554/elife.39723.
[14] T. Mori and C. H. Johnson, “Independence of Circadian Timing from Cell Division in Cyanobacteria,” *J Bacteriol*, vol. 183, no. 8, pp. 2439–2444, 2001, doi: 10.1128/jb.183.8.2439-2444.2001.
[15] J. S. MacCready *et al.*, “Supplement: Protein gradients on the nucleoid position the carbon-fixing organelles of cyanobacteria.,” *Elife*, vol. 7, p. e39723, 2018, doi: 10.7554/elife.39723.
[16] S. E. Cohen and S. S. Golden, “Circadian Rhythms in Cyanobacteria,” *Microbiol Mol Biol R*, vol. 79, no. 4, pp. 373–385, 2015, doi: 10.1128/mmbr.00036-15.
[17] S. E. Cohen *et al.*, “Dynamic Localization of the Cyanobacterial Circadian Clock Proteins,” *Curr Biol*, vol. 24, no. 16, pp. 1836–1844, 2014, doi: 10.1016/j.cub.2014.07.036.
[18] T. Mori, B. Binder, and C. H. Johnson, “Circadian gating of cell division in cyanobacteria growing with average doubling times of less than 24 hours,” *Proc National Acad Sci*, vol. 93, no. 19, pp. 10183–10188, 1996, doi: 10.1073/pnas.93.19.10183.
[19] B. M. C. Martins, A. K. Tooke, P. Thomas, and J. C. W. Locke, “Cell size control driven by the circadian clock and environment in cyanobacteria,” *Proc National Acad Sci*, vol. 115, no. 48, p. 201811309, 2018, doi: 10.1073/pnas.1811309115.
[20] P. Hakim, Y. Hoang, and A. G. Vecchiarelli, “Dissection of the ATPase active site of McdA reveals the sequential steps essential for carboxysome distribution,” *Mol Biol Cell*, p. mbc.E21-03-0151, 2021, doi: 10.1091/mbc.e21-03-0151.
[21] S. Takano, J. Tomita, K. Sonoike, and H. Iwasaki, “The initiation of nocturnal dormancy in Synechococcus as an active process,” *Bmc Biol*, vol. 13, no. 1, p. 36, 2015, doi: 10.1186/s12915-015-0144-2.
[22] M. J. A. Ihlenfeldt and J. Gibson, “CO2 fixation and its regulation in Anacystis nidulans (Synechococcus),” *Arch Microbiol*, vol. 102, no. 1, pp. 13–21, 1975, doi: 10.1007/bf00428339.
[23] M. J. Rust, S. S. Golden, and E. K. O’Shea, “Light-Driven Changes in Energy Metabolism Directly Entrain the Cyanobacterial Circadian Oscillator,” *Science*, vol. 331, no. 6014, pp. 220–223, 2011, doi: 10.1126/science.1197243.
[24] D. M. Raskin and P. A. J. de Boer, “Rapid pole-to-pole oscillation of a protein required for directing division to the middle of Escherichia coli,” *Proc National Acad Sci*, vol. 96, no. 9, pp. 4971–4976, 1999, doi: 10.1073/pnas.96.9.4971.
[25] Y. Sun, F. Huang, G. F. Dykes, and L.-N. Liu, “Diurnal Regulation of In Vivo Localization and CO2-Fixing Activity of Carboxysomes in Synechococcus elongatus PCC 7942,” *Life*, vol. 10, no. 9, p. 169, 2020, doi: 10.3390/life10090169.

# CHAPTER V

## Discussions and Concluding Remarks

### 5.1 Discussions

The experimental framework outlined in Chapter IV provides a long-term and multi-generational imaging approach for *S. elongatus* in an effort to visualize protein self-organization during phototrophic growth and division. Self-organization in bacteria has been extensively studied in model organisms, such as *E. coli* [1] and *B. subtilis* [2], [3]. The two best studied is cell division positioning by the MinCDE system [4], [5] and DNA segregation by the ParABS system [6]–[8]. Here my findings extend the field into the trafficking of protein-based bacterial organelles by the McdAB system in non-model photosynthetic bacteria. Investigating dynamic protein organization in non-model organisms such as cyanobacteria is important for understanding the mechanisms driving subcellular pattern formation and the resulting mode of transport and positioning that uses dynamic protein gradients [8]–[12], as opposed to traditional filament-based mechanisms [13]–[16]. Here I summarize my findings and suggest future directions in the study of carboxysome positioning by the McdAB system in cyanobacteria. I specifically focus on what I think will be two key biological influencers on carboxysome positioning: (1) circadian rhythms, and (2) the compaction state of the nucleoid, which I propose should not be considered as a benign matrix in the carboxysome positioning mechanism.

### 5.1.1 Circadian rhythm brings about transcriptomic and proteomic changes to carbon-concentrating mechanism components in *S. elongatus*

Cyanobacteria are the only prokaryotic organisms capable of oxygenic photosynthesis and rely on an intrinsic circadian clock that faithfully maintains a 24-hr periodicity [17]–[19]. Cyanobacteria naturally predict, adapt, and respond to daily light/dark cycles by rendering environmental cue inputs into regulated gene expression outputs [20]. The molecular control and underlying mechanisms of circadian timekeeping have been studied extensively in *S. elongatus* The *S. elongatus* circadian oscillator consists of proteins KaiA, KaiB and the central player KaiC, a hexameric ATPase that possesses autokinase and autophosphatase activities [21], [22]. The cyclic nature of KaiC phosphorylation and ATPase activities are mediated by KaiA and KaiB. During the period of subjective day, KaiC undergoes sequential autophosphorylation induced by KaiA binding [23]. Conversely, KaiB sequesters KaiA away from KaiC, activating KaiC intrinsic autophosphatase activity during the relative night period [23], [24].

This rhythmic process of KaiC phosphorylation cycles relies on environmental cues channeled by KaiA, the histidine kinase CikA [25], [26] and light-dependent iron-sulfur protein LdpA [27]. KaiA and CikA binding to oxidized quinone, which rapidly accumulates in darkness [28], target these proteins for degradation and allows for dephosphorylation of KaiC [29]. LdpA modulates periods in circadian rhythms by sensing light-dependent changes in electron transport and CikA cytosolic pool [27], [30]. Additionally, KaiC can sense the cellular ATP/ADP ratio that changes dramatically throughout the day, particularly due to the temporal separation of photosynthesis and catabolism [31]–[33]. The redox state, ATP pool, and environmental light sensing mechanisms cooperatively set the rhythm of circadian oscillation in *S. elongatus*.

The cellular output of the circadian rhythm in *S. elongatus* is mediated by a two-component system consisting of histidine kinase SasA and transcriptional response regulator RpaA [34], [35]. SasA interaction with KaiC stimulates its autophosphorylation and in turn, phosphorylates RpaA. In its phosphorylated form, RpaA binds to promoters of ~170 genes on the chromosome, including genes implicated in the regulation of metabolism, the circadian clock, nucleoid topology, cellular division, and growth [36]. During day/night cyanobacterial growth, the circadian clock drives the expression of two distinct gene classes. Expression of Class I genes, which is under the regulation of phosphorylated RpaA (P-RpaA), peak at early subjective night [36] meanwhile Class II genes show maximum expression during subjective dawn [37]. Δ*rpaA* mutants are arrested in Class II expression dawn-like state and do not display any rhythmic gene expression, emphasizing its central role in mediating circadian outputs [34]. The far-reaching implications of circadian oscillator regulation can be seen across global gene expression [38], [39], cellular division [17], [18], nucleoid compaction [40], [41] and metabolite compartmentalization [42], [43]. Intriguingly, this faithful timekeeping mechanism of the *S. elongatus* circadian oscillator can be reconstituted *in vitro* in the presence of KaiA, KaiB, KaiC, SasA, CikA, RpaA, and DNA encoding for clock-controlled promoters [44], [45].

*mcdA* and *mcdB* genes have been implicated as direct targets of RpaA. Along with genes encoding for carboxysome components, *mcdA* and *mcdB* genes are categorized as dawn-peaking Class II genes [36], [46]. This classification is consistent with the critical role carboxysomes play in the light-dependent carbon-fixation step of oxygenic photosynthesis in *S. elongatus*. It is highly likely that McdA and McdB levels are tightly modulated throughout the course of the *S. elongatus* life cycle; for example, maintaining relative and absolute protein levels of McdA and McdB in the cell. Our previous data suggests this balance is crucial as McdB overexpression leads to the

formation of massive bar carboxysomes, whereas McdA overexpression leads to small and misshaped carboxysomes [47]. Given the drastic changes to carboxysome ultrastructure in response to McdA and McdB imbalances, it is attractive to speculate that environmental cues provide input via the circadian clock to regulate McdAB levels, which could influence carboxysome size, number, and/or distribution in the cell.

Transcriptomic analyses have suggested that Rubisco genes and the *ccm* operon (encoding for CcmK2, CcmL, CcmM, CcmN and CcmO; Fig 1.2) all possess photosynthesis-related rhythmic expression, peaking around subjective dawn [48], [49]. Conversely however, proteomic studies indicated that cellular Rubisco levels undergo only modest changes throughout light/dark cycles [50], [51]. This inconsistency could be attributed to cellular localization/sequestration (inside vs outside of carboxysomes) or post-translational modification of Rubisco that could be photosynthesis- or light cycle-dependent [52]. Indeed, β-carboxysomes have been reported to undergo light-mediated changes in their size, copy number, composition, spatial positioning and mobility [53]. Moreover, the inside-out assembly approach observed during *de novo* carboxysome biogenesis favors dense Rubisco arrangement and packing to maximize the enzyme's concentration in carboxysome lumen [54]. This dense Rubisco core organization has been implicated to serve as a foundation for maintaining carboxysome structural integrity [54], [55]. By co-labeling a shell protein that is known to be recruited in the later stages of the carboxysome assembly process (such as CcmO or CcmL) along with Rubisco in an *S. elongatus* strain grown in light/dark cycles on the microscope stage, one could begin to dissect how circadian rhythms affect the efficiency of Rubisco packaging into carboxysomes and in turn, carboxysome size. It is plausible that McdB may be playing a terminal role in the carboxysome assembly process by

rendering a properly-sized and completely-assembled carboxysome as “mature” and licenses it to be “picked up” by the McdA oscillation for proper cellular distribution and positioning.

### 5.1.2 Nucleoid compaction and the polyploidy of *S. elongatus*: Is the nucleoid really just a benign matrix for McdA gradient formation and carboxysome positioning?

We have provided multiple line of evidence that McdA forms dynamic oscillatory gradients on the nucleoid for distributing carboxysomes down the cell length [47], [56]. Currently not considered in our models, however, is the fact that *S. elongatus* cells can carry anywhere between one to ten identical copies of its chromosome at any time [57]. Also, chromosome copy number as well as compaction state are both influenced by circadian rhythms [40], [41]. Nearing the end of the subjective day, *S. elongatus* chromosomes stop replicating and become compacted into distinct “nucleoid islands” [40]. Going forward, it is important to refine our diffusion-ratchet mechanism of carboxysome positioning by taking into account the potential influence of chromosome copy number and nucleoid expansion/compaction.

I have observed that mNG-McdA is capable of maintaining its oscillatory dynamics over highly-compacted nucleoids in ciprofloxacin-treated cells (Movie 3.2) as well as during the transition between light and dark cycles in entrained *S. elongatus* cells (Fig. 4.6). These preliminary finding suggest that McdA oscillation and carboxysome positioning continues regardless of the compaction state of the nucleoid. The positioning of cyanobacterial chromosomes and carboxysomes are mutually exclusive [58], with chromosomes being replicated independent of cell division but instead correlated with cell length [59]. Strikingly, despite their high copy number in the cell, *S. elongatus* chromosomes are segregated in a non-random manner, which is speculated to be the result of a cellular event that transiently aligns the replicated chromosomes

just prior to cell division to ensure proper inheritance of chromosome copies to daughter cells [58], [59]. Taking circadian rhythm-mediated chromosome compaction/relaxtion cycles into consideration, disentangling the relationship between this transient pre-division chromosome arrangement and spatial distribution of carboxysomes occupying the nucleoid space could further our understanding on the influences that nucleoid dynamics potentially have on the McdAB system throughout the cell cycle.

Despite the dramatic variation in genome copy number within an *S. elongatus* population, protein concentration has been shown to remain relatively constant across all cells in a population, with cellular volume and total protein displaying a linear and positively-correlated relationship with genome copy number [60]. We previously found that McdB must be bound to carboxysomes to generate McdA oscillations on the nucleoid. Without carboxysomes, McdA coated the nucleoid and McdB was diffuse in the cytoplasm [47]. These results suggest that to establish McdA pole-to-pole oscillatory dynamics, McdB must not only be present, but it must be concentrated or localized on assembled carboxysomes [47]. Several fundamental questions arise from these findings: iii) How do different cell and nucleoid morphologies (rod vs spherical) and cell states (unicellular vs filamentous) affect McdAB dynamics, carboxysome positioning, and homeostasis? iv) How does McdB associate with the carboxysome and how does this interaction influence carboxysome ultrastructure? Answering these questions will provide valuable insight into understanding the connection between circadian rhythms, changes in nutrient availability, biophysical cellular constraints and carboxysome maintenance in cyanobacteria.

## 5.2 Summary of Findings

In Chapter II, I showed that McdA from *S. elongatus* is a unique member for the ParA/MinD family of ATPases; all of which encode for a deviant Walker-A motif required for ATP-binding and –hydrolysis. I found that like other ParAs involved in chromosome segregation and plasmid partition, McdA can bind nonspecifically bind to DNA *in vitro*, which translates into binding the nucleoid *in vivo* (Fig 2.2). But *in vivo*, McdA does not just coat the nucleoid. Instead, it forms dynamic pole-to-pole oscillations. This self-organized oscillation is dependent upon a protein we identified in the Vecchiarelli lab, we called McdB. I showed that McdB is capable of stimulating McdA ATPase activity and its release from the nucleoid (Fig 2.4). I also found that McdB associates with the carboxysome via a number of interactions with shell proteins. The interaction between carboxysome-localized McdB and nucleoid-bound McdA results in: (i) an McdA depletion zone on the nucleoid in the vicinity of carboxysomes, (ii) a global break in McdA symmetry along the nucleoid, (iii) carboxysomes chasing regions of increased McdA concentration, and (iv) emergence of a pole-to-pole McdA oscillation (Fig 1.4A, Movie 1.1). This set of observations suggested that instead of a cytoskeletal model, the McdAB system is employing a Brownian-Ratchet mechanism of motion, with carboxysomes being positioned in a directed and persistent manner towards increasing amount of McdA on the nucleoid [11], [47], [61], [62].

In Chapter III, by strategically introducing amino acid substitutions in the McdA ATP-binding pocket, I was able to sequentially trap McdA at specific steps in its ATP cycle. This allowed me to map out critical events in the ATPase cycle of McdA that allows it to bind ATP, dimerize, change its conformation into a DNA-binding state, interact with McdB-bound carboxysomes, hydrolyze ATP, and release from the nucleoid. Additionally, I showed that McdA is a unique and unstudied member of ParA family ATPases as it employs a previously

uncharacterized signature lysine in the C-terminal half of the protein instead of one in the Walker A box (Fig 3.7A). I have also identified an ATP-trapped McdA mutant (McdA[K15R]) that locks McdB-bound carboxysomes onto the nucleoid, but no longer oscillates (Fig. 3.5). It would be interesting to see how carboxysomes locked onto the nucleoid affects the rhythmic nucleoid rearrangement and compaction/relaxation cycles in entrained *S. elongatus* cells, as well as the impact it might have on DNA-related processes such replication, chromosome segregation and transcription.

In Chapter IV, I provide an experimental framework for long-term, multi-generational, and real-time visualization of fluorescent components in *S. elongatus* cells grown in constant light or diurnal cycles. By overcoming many imaging- and growth-condition issues specific to cyanobacteria, I was able to image growing *S. elongatus* cells for up to two days without compromising growth rates or detecting any phenotypic defects in carboxysome positioning. My findings showed that McdA oscillations persist during cell division, resulting in an asymmetric inheritance of the McdA pool. Further investigation is required to determine how daughter cells lacking McdA rapidly respond to this depletion and what effect this transient McdA depletion has on carboxysome distributions in the cell. I also observed persistent McdA oscillations in the dark cycle. This is an intriguing finding given that carbon-fixation, the main function of carboxysomes, does not occur during the subjective night period. This leads to the question, why and how are carboxysomes being positioned at night over highly condensed nucleoids. Exploring this fundamental question would enrich our understanding of the robust nature of the McdAB system and the need for maintaining proper carboxysome distribution independent of active carbon fixation.

## 5.3 Future Directions

My findings in Chapter II provide the biochemical underpinnings for the molecular mechanism of the McdAB system in *S. elongatus.* With the use of a DNA-carpeted flowcell, we were able to show that McdA is able to associate with DNA without the formation of cytoskeletal filaments, as subscribed by models previous to my work and the work of others in the Vecchiarelli lab [47]. Going forward, using this powerful cell-free reconstitution approach, we can probe further into McdA interaction, movement, and residence time on the DNA carpet to determine binding, exchange, and dissociation rates. These biochemical parameters are critical to *in silico* modelling of the diffusion-ratchet model we proposed. The long-term goal using this cell-free reconstitution approach is to visualize the entire carboxysome positioning system *in vitro*, which would consist of fluorescent McdA, McdB, and carboxysomes on a DNA carpet that serves as a nucleoid biomimetic. This powerful approach would allow for systematic and rigorous control over experimental conditions and various components of the carboxysome and its positioning system. This cell-free approach will allow us to answer the following questions : i) How does McdA discriminate between free and carboxysome-localized McdB? ii) What amount of McdB must be present on a carboxysome before McdA recognizes it as a 'mature' cargo ready to be positioned? This bottom-up reconstitution approach would provide significant insights into the molecular interactions driving carboxysome distributions in the cell, without the major limitations and complexity associated with studying this specific self-organizing system in a cyanobacteria cell.

Using fluorescently-tagged carboxysome components and genetic knockout strains, two reports have shown that *S. elongatus* cells first assemble a "procarboxysome", which forms from the inside-out. Rubisco associates with linker proteins to form the interior matrix followed by shell

encapsulation. Following the formation of a procarboxysome, subsequent carboxysomes were assembled using the procarboxysome as a template - budding off and then distributing down the cell length [47], [63], [64]. Our past study has implicated McdB as a determinant for carboxysome size and ultrastructure through a mechanism we have not fully investigated [47]. By systematically labelling each carboxysome component along with McdB in the same strain we will be able to image carboxysome assembly and budding events, and determine where and how McdB fits in during the carboxysome assembly sequence.

In Chapter II and III, I have put forth multiple lines of evidence that McdA oscillatory dynamics and subsequently, carboxysome spatial distribution is highly dependent upon nucleoid topology in *S. elongatus*. What is not yet clear is how carboxysome trafficking is affected by rhythmic nucleoid compaction/relaxation [40], [41] and nucleoid dynamics during cell division. To address these issues, one requires a stable nucleoid marker for polyploid *S. elongatus* cells; DAPI staining would not be sufficient. One could however, fluorescently label a nucleoid-associated proteins such as the HU homolog in *S. elongatus* [65], [66]. Additionally, as McdAB concentration and ratios in *S. elongatus* cells are independent of their genome copy-number, the emergent dynamics of McdA is largely influenced by the geometry, topology and/or availability of the surface area upon which they are scaffolding on, which in this case is the nucleoid. It would be interesting to see how the McdAB system would behave in other morphologically different cyanobacterial cells, but with differing chromosome number.

## 5.4 Concluding remarks

My thesis work has begun to answer many questions pertaining to the new field of organelle trafficking in bacteria. Current studies on bacterial organelles, like BMCs, are almost entirely

centered on the biogenesis and synthetic application of these self-assembling compartments. My work is among the first to examine the molecular mechanism of protein-based microcompartment trafficking within a bacterial cell. My findings will inform current efforts in understanding carboxysome biogenesis, positioning, trafficking and homeostasis, and hopefully will serve as a bridge to narrow the current gap in knowledge in utilizing carboxysomes for synthetic biology applications and for understanding BMC inheritance in general.

## 5.5 References


[1] B. Ramm, T. Heermann, and P. Schwille, "The E. coli MinCDE system in the regulation of protein patterns and gradients," *Cell Mol Life Sci*, vol. 76, no. 21, pp. 4245–4273, 2019, doi: 10.1007/s00018-019-03218-x.

[2] F. Dempwolff, C. Reimold, M. Reth, and P. L. Graumann, "Bacillus subtilis MreB Orthologs Self-Organize into Filamentous Structures underneath the Cell Membrane in a Heterologous Cell System," *Plos One*, vol. 6, no. 11, p. e27035, 2011, doi: 10.1371/journal.pone.0027035.

[3] H. Xu, J. Dauparas, D. Das, E. Lauga, and Y. Wu, "Self-organization of swimmers drives long-range fluid transport in bacterial colonies," *Nat Commun*, vol. 10, no. 1, p. 1792, 2019, doi: 10.1038/s41467-019-09818-2.

[4] J. Lutkenhaus, "Assembly Dynamics of the Bacterial MinCDE System and Spatial Regulation of the Z Ring," *Biochemistry-us*, vol. 76, no. 1, pp. 539–562, 2007, doi: 10.1146/annurev.biochem.75.103004.142652.

[5] J. Lutkenhaus, "Escherichia coli cell division," *Curr Opin Genet Dev*, vol. 3, no. 5, pp. 783–788, 1993, doi: 10.1016/s0959-437x(05)80099-1.

[6] J. C. Baxter and B. E. Funnell, "Plasmid Partition Mechanisms," *Microbiol Spectr*, vol. 2, no. 6, 2014, doi: 10.1128/microbiolspec.plas-0023-2014.

[7] J. Lutkenhaus, "The ParA/MinD family puts things in their place," *Trends Microbiol*, vol. 20, no. 9, pp. 411–418, 2012, doi: 10.1016/j.tim.2012.05.002.

[8] A. G. Vecchiarelli, K. Mizuuchi, and B. E. Funnell, "Surfing biological surfaces: exploiting the nucleoid for partition and transport in bacteria," *Mol Microbiol*, vol. 86, no. 3, pp. 513–523, 2012, doi: 10.1111/mmi.12017.

[9] A. G. Vecchiarelli, Y. Seol, K. C. Neuman, and K. Mizuuchi, "A moving ParA gradient on the nucleoid directs subcellular cargo transport via a chemophoresis force.," *Bioarchitecture*, vol. 4, no. 4–5, pp. 154–9, 2014, doi: 10.4161/19490992.2014.987581.

[10] A. G. Vecchiarelli, K. C. Neuman, and K. Mizuuchi, "A propagating ATPase gradient drives transport of surface-confined cellular cargo," *Proc National Acad Sci*, vol. 111, no. 13, pp. 4880–4885, 2014, doi: 10.1073/pnas.1401025111.

[11] L. Hu, A. G. Vecchiarelli, K. Mizuuchi, K. C. Neuman, and J. Liu, "Directed and persistent movement arises from mechanochemistry of the ParA/ParB system," *Proc National Acad Sci*, vol. 112, no. 51, pp. E7055–E7064, 2015, doi: 10.1073/pnas.1505147112.
[12] L. C. Hwang *et al.*, "ParA-mediated plasmid partition driven by protein pattern self-organization," *Embo J*, vol. 32, no. 9, pp. 1238–1249, 2013, doi: 10.1038/emboj.2013.34.
[13] J. Lutkenhaus, "Another Cytoskeleton in the Closet," *Cell*, vol. 115, no. 6, pp. 648–650, 2003, doi: 10.1016/s0092-8674(03)00977-2.
[14] T. A. Leonard, P. J. Butler, and J. Lowe, "Bacterial chromosome segregation: structure and DNA binding of the Soj dimer - a conserved biological switch," *Embo J*, vol. 24, no. 2, pp. 270–282, 2005, doi: 10.1038/sj.emboj.7600530.
[15] L. Lin, M. O. Valeriano, A. Harms, L. Søgaard-Andersen, and M. Thanbichler, "Bactofilin-mediated organization of the ParABS chromosome segregation system in Myxococcus xanthus," *Nat Commun*, vol. 8, no. 1, p. 1817, 2017, doi: 10.1038/s41467-017-02015-z.
[16] S. Ringgaard, J. van Zon, M. Howard, and K. Gerdes, "Movement and equipositioning of plasmids by ParA filament disassembly," *Proc National Acad Sci*, vol. 106, no. 46, pp. 19369–19374, 2009, doi: 10.1073/pnas.0908347106.
[17] T. Mori and C. H. Johnson, "Independence of Circadian Timing from Cell Division in Cyanobacteria," *J Bacteriol*, vol. 183, no. 8, pp. 2439–2444, 2001, doi: 10.1128/jb.183.8.2439-2444.2001.
[18] T. Mori, B. Binder, and C. H. Johnson, "Circadian gating of cell division in cyanobacteria growing with average doubling times of less than 24 hours," *Proc National Acad Sci*, vol. 93, no. 19, pp. 10183–10188, 1996, doi: 10.1073/pnas.93.19.10183.
[19] T. Kondo, T. Mori, N. V. Lebedeva, S. Aoki, M. Ishiura, and S. S. Golden, "Circadian Rhythms in Rapidly Dividing Cyanobacteria," *Science*, vol. 275, no. 5297, pp. 224–227, 1997, doi: 10.1126/science.275.5297.224.
[20] S. E. Cohen and S. S. Golden, "Circadian Rhythms in Cyanobacteria," *Microbiol Mol Biol R*, vol. 79, no. 4, pp. 373–385, 2015, doi: 10.1128/mmbr.00036-15.
[21] Y. Xu, T. Mori, R. Pattanayek, S. Pattanayek, M. Egli, and C. H. Johnson, "Identification of key phosphorylation sites in the circadian clock protein KaiC by crystallographic and mutagenetic analyses," *P Natl Acad Sci Usa*, vol. 101, no. 38, pp. 13933–13938, 2004, doi: 10.1073/pnas.0404768101.
[22] T. Nishiwaki *et al.*, "Role of KaiC phosphorylation in the circadian clock system of Synechococcus elongatus PCC 7942," *P Natl Acad Sci Usa*, vol. 101, no. 38, pp. 13927–13932, 2004, doi: 10.1073/pnas.0403906101.
[23] Y.-I. Kim, G. Dong, C. W. Carruthers, S. S. Golden, and A. LiWang, "The day/night switch in KaiC, a central oscillator component of the circadian clock of cyanobacteria," *Proc National Acad Sci*, vol. 105, no. 35, pp. 12825–12830, 2008, doi: 10.1073/pnas.0800526105.
[24] Y.-G. Chang, R. Tseng, N.-W. Kuo, and A. LiWang, "Rhythmic ring–ring stacking drives the circadian oscillator clockwise," *Proc National Acad Sci*, vol. 109, no. 42, pp. 16847–16851, 2012, doi: 10.1073/pnas.1211508109.
[25] O. Schmitz, M. Katayama, S. B. Williams, T. Kondo, and S. S. Golden, "CikA, a Bacteriophytochrome That Resets the Cyanobacterial Circadian Clock," *Science*, vol. 289, no. 5480, pp. 765–768, 2000, doi: 10.1126/science.289.5480.765.
[26] S. Miyagishima, C. P. Wolk, and K. W. Osteryoung, "Identification of cyanobacterial cell division genes by comparative and mutational analyses," *Mol Microbiol*, vol. 56, no. 1, pp. 126–143, 2005, doi: 10.1111/j.1365-2958.2005.04548.x.

[27] N. B. Ivleva, M. R. Bramlett, P. A. Lindahl, and S. S. Golden, “LdpA: a component of the circadian clock senses redox state of the cell,” *Embo J*, vol. 24, no. 6, pp. 1202–1210, 2005, doi: 10.1038/sj.emboj.7600606.
[28] Y.-I. Kim, D. J. Vinyard, G. M. Ananyev, G. C. Dismukes, and S. S. Golden, “Oxidized quinones signal onset of darkness directly to the cyanobacterial circadian oscillator,” *Proc National Acad Sci*, vol. 109, no. 44, pp. 17765–17769, 2012, doi: 10.1073/pnas.1216401109.
[29] N. B. Ivleva, T. Gao, A. C. LiWang, and S. S. Golden, “Quinone sensing by the circadian input kinase of the cyanobacterial circadian clock,” *Proc National Acad Sci*, vol. 103, no. 46, pp. 17468–17473, 2006, doi: 10.1073/pnas.0606639103.
[30] M. Katayama, T. Kondo, J. Xiong, and S. S. Golden, “ldpA Encodes an Iron-Sulfur Protein Involved in Light-Dependent Modulation of the Circadian Period in the Cyanobacterium Synechococcus elongatus PCC 7942,” *J Bacteriol*, vol. 185, no. 4, pp. 1415–1422, 2003, doi: 10.1128/jb.185.4.1415-1422.2003.
[31] M. J. Rust, S. S. Golden, and E. K. O’Shea, “Light-Driven Changes in Energy Metabolism Directly Entrain the Cyanobacterial Circadian Oscillator,” *Science*, vol. 331, no. 6014, pp. 220–223, 2011, doi: 10.1126/science.1197243.
[32] G. Dong *et al.*, “Elevated ATPase Activity of KaiC Applies a Circadian Checkpoint on Cell Division in Synechococcus elongatus,” *Cell*, vol. 140, no. 4, pp. 529–539, 2010, doi: 10.1016/j.cell.2009.12.042.
[33] K. Terauchi *et al.*, “ATPase activity of KaiC determines the basic timing for circadian clock of cyanobacteria,” *Proc National Acad Sci*, vol. 104, no. 41, pp. 16377–16381, 2007, doi: 10.1073/pnas.0706292104.
[34] N. Takai *et al.*, “A KaiC-associating SasA–RpaA two-component regulatory system as a major circadian timing mediator in cyanobacteria,” *Proc National Acad Sci*, vol. 103, no. 32, pp. 12109–12114, 2006, doi: 10.1073/pnas.0602955103.
[35] H. Iwasaki, S. B. Williams, Y. Kitayama, M. Ishiura, S. S. Golden, and T. Kondo, “A KaiC-Interacting Sensory Histidine Kinase, SasA, Necessary to Sustain Robust Circadian Oscillation in Cyanobacteria,” *Cell*, vol. 101, no. 2, pp. 223–233, 2000, doi: 10.1016/s0092-8674(00)80832-6.
[36] J. S. Markson, J. R. Piechura, A. M. Puszynska, and E. K. O’Shea, “Circadian Control of Global Gene Expression by the Cyanobacterial Master Regulator RpaA,” *Cell*, vol. 155, no. 6, pp. 1396–1408, 2013, doi: 10.1016/j.cell.2013.11.005.
[37] M. L. Paddock, J. S. Boyd, D. M. Adin, and S. S. Golden, “Active output state of the Synechococcus Kai circadian oscillator,” *Proc National Acad Sci*, vol. 110, no. 40, pp. E3849–E3857, 2013, doi: 10.1073/pnas.1315170110.
[38] T. Kondo, N. F. Tsinoremas, S. S. Golden, C. H. Johnson, S. Kutsuna, and M. Ishiura, “Circadian Clock Mutants of Cyanobacteria,” *Science*, vol. 266, no. 5188, pp. 1233–1236, 1994, doi: 10.1126/science.7973706.
[39] T. Kondo *et al.*, “Circadian rhythms in prokaryotes: luciferase as a reporter of circadian gene expression in cyanobacteria,” *Proc National Acad Sci*, vol. 90, no. 12, pp. 5672–5676, 1993, doi: 10.1073/pnas.90.12.5672.
[40] R. M. Smith and S. B. Williams, “Circadian rhythms in gene transcription imparted by chromosome compaction in the cyanobacterium Synechococcus elongatus,” *Proc National Acad Sci*, vol. 103, no. 22, pp. 8564–8569, 2006, doi: 10.1073/pnas.0508696103.
[41] M. A. Woelfle, Y. Xu, X. Qin, and C. H. Johnson, “Circadian rhythms of superhelical status of DNA in cyanobacteria,” *Proc National Acad Sci*, vol. 104, no. 47, pp. 18819–18824, 2007, doi: 10.1073/pnas.0706069104.

[42] S. Diamond, D. Jun, B. E. Rubin, and S. S. Golden, “The circadian oscillator in Synechococcus elongatus controls metabolite partitioning during diurnal growth,” *Proc National Acad Sci*, vol. 112, no. 15, pp. E1916–E1925, 2015, doi: 10.1073/pnas.1504576112.
[43] G. K. Pattanayak, C. Phong, and M. J. Rust, “Rhythms in Energy Storage Control the Ability of the Cyanobacterial Circadian Clock to Reset,” *Curr Biol*, vol. 24, no. 16, pp. 1934–1938, 2014, doi: 10.1016/j.cub.2014.07.022.
[44] M. Nakajima *et al.*, “Reconstitution of Circadian Oscillation of Cyanobacterial KaiC Phosphorylation in Vitro,” *Science*, vol. 308, no. 5720, pp. 414–415, 2005, doi: 10.1126/science.1108451.
[45] A. G. Chavan *et al.*, “Reconstitution of an intact clock reveals mechanisms of circadian timekeeping,” *Science*, vol. 374, no. 6564, p. eabd4453, 2021, doi: 10.1126/science.abd4453.
[46] D. G. Welkie *et al.*, “Genome-wide fitness assessment during diurnal growth reveals an expanded role of the cyanobacterial circadian clock protein KaiA,” *Proc National Acad Sci*, vol. 115, no. 30, p. 201802940, 2018, doi: 10.1073/pnas.1802940115.
[47] J. S. MacCready *et al.*, “Protein gradients on the nucleoid position the carbon-fixing organelles of cyanobacteria,” *Elife*, vol. 7, p. e39723, 2018, doi: 10.7554/elife.39723.
[48] H. Ito *et al.*, “Cyanobacterial daily life with Kai-based circadian and diurnal genome-wide transcriptional control in Synechococcus elongatus,” *Proc National Acad Sci*, vol. 106, no. 33, pp. 14168–14173, 2009, doi: 10.1073/pnas.0902587106.
[49] V. Vijayan, I. H. Jain, and E. K. O’Shea, “A high resolution map of a cyanobacterial transcriptome,” *Genome Biol*, vol. 12, no. 5, p. R47, 2011, doi: 10.1186/gb-2011-12-5-r47.
[50] J. R. Waldbauer, S. Rodrigue, M. L. Coleman, and S. W. Chisholm, “Transcriptome and Proteome Dynamics of a Light-Dark Synchronized Bacterial Cell Cycle,” *Plos One*, vol. 7, no. 8, p. e43432, 2012, doi: 10.1371/journal.pone.0043432.
[51] A. C. L. Guerreiro *et al.*, “Daily Rhythms in the Cyanobacterium Synechococcus elongatus Probed by High-resolution Mass Spectrometry–based Proteomics Reveals a Small Defined Set of Cyclic Proteins*,” *Mol Cell Proteomics*, vol. 13, no. 8, pp. 2042–2055, 2014, doi: 10.1074/mcp.m113.035840.
[52] N. Nassoury, L. Fritz, and D. Morse, “Circadian Changes in Ribulose-1,5-Bisphosphate Carboxylase/Oxygenase Distribution Inside Individual Chloroplasts Can Account for the Rhythm in Dinoflagellate Carbon Fixation,” *Plant Cell*, vol. 13, no. 4, pp. 923–934, 2001, doi: 10.1105/tpc.13.4.923.
[53] Y. Sun, A. Wollman, F. Huang, M. Leake, and L. Liu, “Single-organelle quantification reveals the stoichiometric and structural variability of carboxysomes dependent on the environment,” *Plant Cell*, vol. 31, no. 7, p. tpc.00787.2018, 2019, doi: 10.1105/tpc.18.00787.
[54] B. D. Rae, B. M. Long, M. R. Badger, and G. D. Price, “Functions, Compositions, and Evolution of the Two Types of Carboxysomes: Polyhedral Microcompartments That Facilitate CO2 Fixation in Cyanobacteria and Some Proteobacteria,” *Microbiol Mol Biol R*, vol. 77, no. 3, pp. 357–379, 2013, doi: 10.1128/mmbr.00061-12.
[55] C. A. Kerfeld and M. R. Melnicki, “Assembly, function and evolution of cyanobacterial carboxysomes,” *Curr Opin Plant Biol*, vol. 31, pp. 66–75, 2016, doi: 10.1016/j.pbi.2016.03.009.
[56] P. Hakim, Y. Hoang, and A. G. Vecchiarelli, “Dissection of the ATPase active site of McdA reveals the sequential steps essential for carboxysome distribution,” *Mol Biol Cell*, p. mbc.E21-03-0151, 2021, doi: 10.1091/mbc.e21-03-0151.
[57] M. Griese, C. Lange, and J. Soppa, “Ploidy in cyanobacteria,” *Fems Microbiol Lett*, vol. 323, no. 2, pp. 124–131, 2011, doi: 10.1111/j.1574-6968.2011.02368.x.

[58] I. H. Jain, V. Vijayan, and E. K. O'Shea, "Spatial ordering of chromosomes enhances the fidelity of chromosome partitioning in cyanobacteria," *P Natl Acad Sci Usa*, vol. 109, no. 34, pp. 13638–43, 2012, doi: 10.1073/pnas.1211144109.
[59] A. H. Chen, B. Afonso, P. A. Silver, and D. F. Savage, "Spatial and Temporal Organization of Chromosome Duplication and Segregation in the Cyanobacterium Synechococcus elongatus PCC 7942," *Plos One*, vol. 7, no. 10, p. e47837, 2012, doi: 10.1371/journal.pone.0047837.
[60] X. Zheng and E. K. O'Shea, "Cyanobacteria Maintain Constant Protein Concentration despite Genome Copy-Number Variation," *Cell Reports*, vol. 19, no. 3, pp. 497–504, 2017, doi: 10.1016/j.celrep.2017.03.067.
[61] L. Hu, A. G. Vecchiarelli, K. Mizuuchi, K. C. Neuman, and J. Liu, "Brownian ratchet mechanisms of ParA-mediated partitioning," *Plasmid*, vol. 92, pp. 12–16, 2017, doi: 10.1016/j.plasmid.2017.05.002.
[62] L. Hu, A. G. Vecchiarelli, K. Mizuuchi, K. C. Neuman, and J. Liu, "Brownian Ratchet Mechanism for Faithful Segregation of Low-Copy-Number Plasmids," *Biophys J*, vol. 112, no. 7, pp. 1489–1502, 2017, doi: 10.1016/j.bpj.2017.02.039.
[63] A. H. Chen, A. Robinson-Mosher, D. F. Savage, P. A. Silver, and J. K. Polka, "The Bacterial Carbon-Fixing Organelle Is Formed by Shell Envelopment of Preassembled Cargo," *Plos One*, vol. 8, no. 9, p. e76127, 2013, doi: 10.1371/journal.pone.0076127.
[64] J. C. Cameron, S. C. Wilson, S. L. Bernstein, and C. A. Kerfeld, "Biogenesis of a Bacterial Organelle: The Carboxysome Assembly Pathway," *Cell*, vol. 155, no. 5, pp. 1131–1140, 2013, doi: 10.1016/j.cell.2013.10.044.
[65] F. Wu, E. V. Rijn, B. G. C. V. Schie, J. E. Keymer, and C. Dekker, "Multi-color imaging of the bacterial nucleoid and division proteins with blue, orange, and near-infrared fluorescent proteins," *Front Microbiol*, vol. 6, p. 607, 2015, doi: 10.3389/fmicb.2015.00607.
[66] M. Wery, C. L. Woldringh, and J. Rouviere-Yaniv, "HU-GFP and DAPI co-localize on the Escherichia coli nucleoid," *Biochimie*, vol. 83, no. 2, pp. 193–200, 2001, doi: 10.1016/s0300-9084(01)01254-8.

# APPENDIX

# APPENDIX A

## Supplemental Movie Legend

Movie 1.1: Oscillation of mNG-McdA (magenta) occurs while carboxysomes (blue) are fluorescently labeled. Video 3 from [1] (: https://creativecommons.org/licenses/by/4.0/).

Movie 3.1: Live-cell fluorescence microscopy of mNG-McdA variants of *S. elongatus*. (Top Left) Wildtype mNG-McdA oscillated (magenta) and uniformly distributed carboxysomes (cyan). All McdA mutants no longer oscillated and carboxysomes were mispositioned. Movies were taken at 30 seconds per frame for 30 minutes. Playback at 20 frames per second (600x real time). Movie S1 from [2] (https://creativecommons.org/licenses/by-nc-sa/3.0/).

Movie 3.2: Live-cell fluorescence microscopy of *S. elongatus* cells treated with ciprofloxacin. mNGMcdA (magenta) continued to oscillate on ciprofloxacin-compacted nucleoids (DAPI, green) and carboxysomes (cyan) were still distributed across the compacted nucleoid. Movie was taken at one frame per minute for 30 min. Playback at 20 frames per second (1200x real-time). Movie S2 from [2] (https://creativecommons.org/licenses/by-nc-sa/3.0/).

Movie 3.3: Multi-generational time-lapse microscopy of mNG-McdA (top row) and mNG-McdA[K15R] strains (bottom row). Wildtype mNG-McdA oscillated (magenta) and uniformly distributed carboxysomes (cyan). mNG-McdA[K15R] formed foci that colocalized with carboxysome aggregates (cyan). Chlorophyll (red) in the thylakoid membranes were used to quantify cell growth rate and doubling times presented in Fig. 3.5K and 3.5L. Movies were taken at one frame per hour for 22 hours. Playback at 5 fps (18000x real-time). Movie S3 from [2] (https://creativecommons.org/licenses/by-nc-sa/3.0/).

Movie 4.1: Multi-generational time-lapse microscopy of wildtype *S. elongatus* cells showing *S. elongatus* cell growth under constant illumination by the microscope's LED light source. Time stamp is in hour:min. Chlorophyll (red) in the thylakoid membranes were imaged to visualize cell outlines. Movie was taken at one frame per 15 min for 17.5 hours. Playback at 5 fps (4500x real-time).

Movie 4.2: Multi-generational time-lapse microscopy of wildtype *S. elongatus* cells showing *S. elongatus* cell growth under 12 hour light: 12 hour dark cycle. Labels on top left corner depict relatve day or night cycle. Movie was taken at one frame per 30 min for 21 hours. Playback at 5 fps (4500x real-time).

Movie 4.3: Multi-generational time-lapse microscopy of showing merged mNG-McdA (yellow) and carboxysome foci (cyan) signals during *S. elongatus* growth in light/dark diel cycles. Labels

on top left corner depict relatve day or night cycle. Movie was taken at one frame per 15 min for 21 hours. Playback at 5 fps (4500x real-time).

**References**

[1] J. S. MacCready *et al.*, "Protein gradients on the nucleoid position the carbon-fixing organelles of cyanobacteria," *Elife*, vol. 7, p. e39723, 2018, doi: 10.7554/elife.39723.
[2] P. Hakim, Y. Hoang, and A. G. Vecchiarelli, "Dissection of the ATPase active site of McdA reveals the sequential steps essential for carboxysome distribution," *Mol Biol Cell*, p. mbc.E21-03-0151, 2021, doi: 10.1091/mbc.e21-03-0151.